Optimization of shunt damped composite structures using negative capacitances

From the Department of Mechanical Engineering

at the Technische Universität Darmstadt

to obtain the academic degree of

Doctor of Engineering (Dr.-Ing.)

Approved

Thesis presented by

M.Sc. Rogério Salloum

From Franca, Brazil

Examiner: Prof. Dr.-Ing. Tobias Melz

Co-Examiner: Prof. Dr.-Ing. Stephan Rinderknecht

Submitted on the 19th October 2015

Defended on the 24th February 2016

Darmstadt 2016

D17

TECHNISCHE UNIVERSITÄT DARMSTADT

Fraunhofer LBF

Abstract

Vibrations in modern machines such as cars, airplanes and bridges constitute a real issue that can cause undesirable noise, damages and even catastrophic failures. In order to reduce this harmful effect, passive vibration attenuation measures have been extensively used, but can no longer cope with the increasing complexity of engineering systems. In this sense, novel smart structures have been created to efficiently suppress vibration without notable adverse effects. A well-known technique consists in coupling a piezoceramic transducer to a mechanical structure and then connecting it to a shunt circuit.

In this thesis, a novel approach to deal with the application of shunted piezoceramics in lightweight composite structures for vibration attenuation is proposed. It is based on the simultaneous optimization of different sub-systems of the smart structure, i.e. host structure, transducers and electronics, so that a set of technical requirements can be met. Instead of being considered as an add-on solution, the shunted piezoceramics are regarded as additional design variables. In this sense, passive structural mass is substituted by active material in an intelligent way, which can potentially reduce overall weight and at the same time improve the dynamic response of the smart structure. To show the potential of this approach, a carbon fiber control arm will be considered as a realistic case study after the development steps described below.

In the first part of this work, a study on the physical integration of piezoceramic transducers within laminate composites is carried out. The maximization of the generalized electromechanical coupling coefficient is proposed, since it dictates the damping effectiveness in shunt applications. The influences of the stacking sequence and the geometric integration pattern are numerically and experimentally analyzed using glass and carbon fiber test coupons.

In the second part, the optimization process is taken from the coupon level to the sub-component level. Numerical and experimental analyses are carried out using a scale model of the control arm. It consists of a cantilever carbon fiber beam with I-shaped cross-section, controlled by the use of piezoceramics. Vibration attenuation is achieved through an *RL*-shunt circuit connected in series with a negative capacitance, which is built through a synthetic circuit based on an operational amplifier. The classical sequential approach is first introduced, in which the piezoceramics are applied onto the surface of the beam. Then, it is compared to the novel approach, in which the beam, now with integrated piezoceramics, is fully optimized taking into account its geometry, the stacking sequence, the transducer dimensions and the shunt circuit components. Thanks to the simultaneous approach, not only the mechanical requirements of the structure, such as mass, global stiffness and dynamic behavior can be respected, but also the electrical characteristics of the shunt circuit.

In the third part, a novel tuning technique for shunt damping with a negative capacitance is proposed. It is based on the measured electromechanical impedance of a smart structure, which is represented through an equivalent electrical circuit. A numerical optimization permits for the first time the correct choice of all electric components in the shunt circuit, since all mechanical quantities are analyzed in a purely electrical form.

In the last part, the acquired knowledge is applied to the control arm. It is redesigned according to the methodology validated with the sub-component to show that high vibration attenuation using shunt damping and high mass saving can be simultaneously attained.

Zusammenfassung

Schwingungen sind in den meisten technischen Anlagen und Maschinen unerwünscht und können zu störenden Geräuschen, Schäden oder frühzeitigem Versagen führen. Um dem zu begegnen, werden meist passive Maßnahmen zur Schwingungsminderung eingesetzt, die aber den steigenden Anforderungen und der zunehmenden Komplexität technischer Systeme nicht mehr gerecht werden. Daher wurden neuartige adaptive Strukturen entwickelt, um effizient Schwingungen zu mindern, ohne nennenswerte Nachteile zu erzeugen.

In dieser Dissertation wird eine neuartige Methode zur Anwendung von semi-aktiver Dämpfung mit Piezowandlern in Leichtbauverbundstrukturen zur Schwingungsminderung untersucht. Diese Methode basiert auf der gleichzeitigen Optimierung der verschiedenen Teilsysteme der adaptiven Struktur, nämlich der mechanischen Grundstruktur, dem Wandler und der Elektronik, sodass die Anforderungen an die adaptive Struktur besser erfüllt werden können. Der Piezowandler wird dabei anders als bisher nicht als Zusatzmodul betrachtet, sondern als komplementäre Designvariable berücksichtigt. Dadurch kann passive Masse der mechanischen Grundstruktur durch aktives Material ersetzt werden, was das Gesamtgewicht verringert und gleichzeitig die Schwingung der Struktur mindern kann. Um die Wirksamkeit dieser Methode zu zeigen, wird ein Querlenker aus Kohlefaser als realitätsnahes Beispielsystem nach den unten beschriebenen Entwicklungsschritten betrachtet.

Im ersten Teil dieser Arbeit wird eine Untersuchung über die Integration von Piezowandlern in Verbundwerkstoffe durchgeführt. Dabei wird der elektromechanische Kopplungskoeffizient maximiert, da dieser das Dämpfungspotential bestimmt. Die Einflüsse der unterschiedlichen Lagenanordnungen und des geometrischen Musters im Verbundwerkstoff werden numerisch und experimentell mit Glas- und Kohlefaserproben analysiert.

Im zweiten Teil wird ein numerischer und experimenteller Optimierungsprozess mit einem vereinfachten Querlenker durchgeführt, der aus einem Kragbalken aus Kohlefasern mit einem I-Profil besteht. Um Schwingungen zu reduzieren, werden auf der Balkenoberfläche applizierte bzw. in den Balken integrierte Piezowandler mit einem *RL*-Schwingkreis in Reihe mit einer negativen Kapazität verbunden. Bei der klassischen sequentiellen Methode werden die Piezowandler auf den Balken appliziert. Diese Methode wird mit dem neuen Vorgehen verglichen, bei dem der Balken mit integrierten Piezowandlern optimiert wird. Hierbei werden die Geometrie des Balkens, die Lagenanordnung, die Wandlergeometrie und die Elektronik im Optimierungsprozess berücksichtigt. Somit können neben den mechanischen Anforderungen an die Struktur, wie Masse, Steifigkeit und dynamisches Verhalten, auch die elektrischen Eigenschaften der semi-aktiven Schaltung berücksichtig werden.

Im dritten Teil wird eine neuartige Abstimmungsmethode für die semi-aktive Dämpfung mit einer negativen Kapazität vorgestellt. Diese basiert auf der gemessenen elektromechanischen Impedanz einer adaptiven Struktur, die durch einen elektrischen Schwingkreis in einem Simulationsmodell dargestellt wird. Eine numerische Optimierung ermöglicht zum ersten Mal die systematische Auswahl aller elektrischen Komponenten in der Elektronik, da alle mechanischen Größen in einer rein elektrischen Form analysiert werden.

Im letzten Teil wird die Methode auf den Querlenker angewendet, um zu zeigen, dass eine hohe Schwingungsdämpfung mit der semi-aktiven Methode und eine hohe Massenreduzierung gleichzeitig erreicht werden können.

"If at first the idea is not absurd, then there is no hope for it."

— Albert Einstein

Acknowledgements

The study presented in this thesis is the result of my scientific activities as an employee for 3 years of the Division Smart Structures at the Fraunhofer Institute for Structural Durability and System Reliability LBF in Darmstadt, Germany. I am very thankful for having worked in this state-of-the-art facility with excellent working conditions. The research work has been conducted within the Initial Training Network GRESIMO (Best Training for Green and Silent Mobility), which was funded under the FP7 Marie Skłodowska-Curie Program of the European Commission. This financial support is gratefully acknowledged.

This written thesis is the conclusion of a demanding yet rewarding work that could not have been achieved without the helpful contribution of several people.

First of all, I would like to thank Prof. Tobias Melz and Prof. Stephan Rinderknecht for the interest in this work and for having accepted the difficult task of examiner. I am also very thankful to Prof. Thilo Bein for having offered me the opportunity to work at LBF in 2012.

I would also like to acknowledge the continuous support, kindness and patience of my mentor Dirk Mayer, whose outstanding knowledge and scientific expertise in all topics have been extremely valuable. I could not have finished this work in time without his inspiring guidance throughout these years.

Moreover, I gratefully acknowledge the collaboration of Oliver Heuss, who has enormously contributed to the success of this work. His suggestions and technical discussions have broadened my knowledge of smart structures. I also want to thank Benedict Götz for the teamwork and fruitful discussions and my student Robert Messer who contributed with his work to some results presented in this thesis.

I want to thank all the numerous colleagues working at LBF, in particular Chris, Georg and Max, and also all the GRESIMO fellows, for the warm welcome, the good time spent together, the friendly coffee breaks and their help in all matters.

My sincere thanks also go to the company Karl Mayer and the employees Tilman Richers, Andreas Bleier and Ralf Rickert, who have made real my composite structures.

Finally, no words can express my deepest gratitude to my parents, who have always believed in me and supported me with reassurance to follow my dreams during all these years. They provide me inspiration for living and I will be forever thankful for their encouragement.

Table of contents

List of figures

List of tables

1 Introduction

Since the 1990s, there has been an enormous growth in smart structures technology. Several fields of study benefit from this development, such as space vehicles, aircrafts, railway, marine and automotive systems, civil structures, robots, heavy machinery, electronic and medical equipment. A wide range of applications include noise and vibration suppression, damping increase, structural health monitoring, active shape change and energy harvesting. A smart, intelligent or adaptive structure [1] typically consists of a host structure, actuators and sensors, a microprocessor that analyzes the signals, a control law to change the characteristics of the structure and integrated power electronics. More importantly, it has the ability to adapt its performance according to environmental stimuli in a controlled manner.

Regarding the automotive industry, modern passenger cars are increasingly restrained to improve energy efficiency and to reduce CO_2 emissions. This challenge must be met by introducing advanced powertrain technologies on the one hand, and by significantly reducing the weight of vehicles on the other. In order to accomplish the latter, the replacement of metals by lightweight composite materials is a viable solution, but this can significantly change the noise and vibration behavior of the vehicle. The conflicting demand of comfort increase and weight reduction requires hence novel design and optimization techniques. In this sense, the smart structures field is a promising technology that plays a major role in the development of future lightweight transportation systems.

Among the numerous possibilities to reduce vibrations, one well-known technique uses shunted piezoelectric transducers, which are applied to a mechanical structure and connected to an electronic circuit. When correctly designed, the shunt can significantly attenuate the vibration of the system without excessive mass addition. Much research has been done in the last decades to analyze various types of shunts in terms of their potentials and characteristics. Nonetheless, they are not yet integrated in many technical structures, not only because of high costs, but also due to the high effort required to design the electronics effectively together with the mechanical structure and transducer.

As a promising area of research, this work presents a novel methodology for a full design of a smart structure, where its different sub-systems, i.e. host structure, transducers and electronics, are simultaneously optimized to meet target requirements. The design optimization focuses on numerical and experimental analyses of a composite part with piezoceramic transducers connected to a semi-active shunt network, more precisely a resistor, an inductor and a negative capacitance in series. In particular, the piezoceramic transducers are embedded inside the composite material and, for the first time, the electromechanical coupling is investigated for different geometric integration patterns. To achieve a maximum damping, a novel tuning technique for shunt damping with a negative capacitance is proposed, based on the measured electromechanical impedance and a numerical optimization. In order to show the advantages of shunted systems, a carbon fiber control arm is used as an application example. To validate the vibration attenuation, a fiber-reinforced piezoelectric module is developed and is shown to be a major breakthrough in helping to spread the shunt damping technique to lightweight composite structures.

1.1 Piezoelectric shunt damping

When dealing with mechanical systems, several problems can appear related to high vibration levels, such as diminished durability, unwanted noise, health hazards and safety issues. In the context of lightweight composite structures, high vibrations are mainly due to the low mass and damping inherent to this class of materials, associated with an insufficient design.

In order to attenuate these undesirable effects, passive methods can be used. These include e.g. the application of layers of viscoelastic polymers or even dispersed piezoceramic particles inside a laminate composite, as investigated in [2]. An alternative solution consists in applying mechanical vibration absorbers [3], but they are often associated with a high mass added to the structure. Complementary to passive damping methods, different active techniques exist [4] and are capable of effectively attenuating vibrations thus increasing comfort and durability. In this case, however, there is always the need for actuation power and relatively high demand for computational controller performance.

Between these two techniques are situated the semi-passive [5] and the semi-active methods [6], which benefit from low cost components and a simple controller design. These methods consist in coupling a piezoceramic transducer to a mechanical structure and then connecting it to a shunt circuit. This can be very effective, since piezoelectric ceramics exhibit a strong electromechanical coupling and are capable of converting mechanical into electrical energy and vice versa. It is hence possible to introduce actuation forces to the host structure and to change the mechanical properties of the system due to the interaction of piezoceramics and shunt circuit without the need of any sensor information. Among different strategies, one possibility is that the circuit dissipates the electrical energy converted by the piezoelectric material in the form of Joule heating. Therefore, the shunt removes vibration energy from the mechanical system and the damping increases. It has already been shown that active control is able to achieve better attenuation results than both semi-passive [7] and semi-active techniques [8], [9]. Nevertheless, if optimally designed, the shunt circuit can highly attenuate vibrations in a certain frequency range.

Various types of shunts have already been developed and tested regarding their potentials and characteristics in vibration control. However, they are not yet integrated in many technical structures, due to the high effort required to design a semi-active device, since there are many correlated parameters that have to be optimized in order to get an applicable solution. One of the most important parameters is the generalized electromechanical coupling coefficient, which represents the mechanical energy converted into electrical energy in the transducer. It also defines the damping effectiveness in shunt techniques and its maximization represents a real challenge in the design. In order to overcome this, several issues still have to be investigated. Although excellent damping can be achieved with shunt circuits, they usually require a very accurate and sensitive tuning. The knowledge of the structure is therefore required and several variables can degrade the performance, such as the temperature and even the vibration level of the structure, due to the non-linear behavior of the piezoelectric material and possible overloads in the shunt circuit. Moreover, since most shunt circuits are based on operational amplifiers, which possess an inherent feedback loop, stability is not granted and thorough analyses must be carried out during the design process. At last, shunt circuits usually require external electrical energy that is needed for the active components and should not be mistaken for the energy injected into the structure.

1.2 Embedded piezoceramics in fiber-reinforced plastics

In the last decades, piezoceramics became the major type of actuator being investigated for smart structures. A piezoceramic has no moving parts and its displacement is based on solid-state dynamics. It shows hence almost no wear, a fact that makes it suitable for dynamic applications where reliability is of major concern. The most common types are monolithic plate transducers and stack actuators. Generally, the specific power density of piezoceramics is higher than conventional actuators, like electromagnetic or hydraulic. Moreover, piezoceramics require less space and present faster response time and broader frequency bandwidth.

In the context of smart structures, lightweight composite materials are often a reasonable choice, since they present excellent properties that cannot be achieved by conventional materials, such as stiffness to weight ratio and resistance to fatigue. More recently, fiber-reinforced plastics have allowed more possibilities than commonly used materials for smart functional integration and their custom-designed nature offers a unique opportunity to minimize weight and improve dynamic behavior.

At the same time, much research has been done on trying to efficiently design together metal structures and surface-bonded actuators, but few technical applications can be found where piezoceramic materials are embedded in composite structures. When shunt damping techniques are to be used, in order to maximize vibration attenuation, there is a need to maximize the electromechanical coupling, as demonstrated in [10]. Compared to conventional surface-bonded transducers, the functional integration of active material provides direct coupling of the transducers to the structure.

Furthermore, by embedding the piezoceramics inside a laminate composite, it is possible to design both structure and transducer simultaneously in order to improve the dynamic performance. If the transducer is part of the structure, it is also used as a load carrying element, which can lead to an overall mass reduction by finding a compromise between structure and transducer regarding stiffness and mass. Further advantages of this integration are the preserved outer surface of the structure and the protection of the transducer from the external environment, which leads to an extended lifetime. Nevertheless, the manufacturing of such components can be very challenging and the end-of-life recycling has a negative environmental impact, since most transducers are lead-containing. Besides, there is a concern about the durability of the composite material and the integrity of the transducer, since it becomes inaccessible for inspection or repairs.

1.3 State-of-the-art techniques

To show the latest technological advances, the fields present in this thesis have been divided into three main subjects: Piezoelectric shunt damping, functional integration using piezoceramics and simultaneous optimization of smart structures.

1.3.1 Piezoelectric shunt damping

Piezoelectric structures have been intensively investigated over the past decades and shunted piezoceramics have been a promising technique to reduce structural vibrations in various applications. This technique has been first introduced in [11] to dampen optical structures and has been later analytically formulated in [5] for passive shunts. Most of the recent work has focused on the investigation of numerous shunt circuits and techniques and an overview of possible applications has been extensively discussed in [12]. In order to maximize vibration attenuation, shunt circuits must be correctly tuned to the piezoceramics and the host structure they are connected to. Several tuning methods can be found in the literature covering most of the shunt techniques. In the case of an *RL*-shunt for a single-mode vibration, the optimal resistance and inductance values, for which the electrical energy dissipation is maximized, and therefore the mechanical displacement is minimized, have been derived in [5] and further analyzed in [13] and [14]. Moreover, [15] has introduced a method for online tuning of the shunt parameters using a synthetic impedance and an adaptive feedback. [16] has developed a new numerical method to optimize the electrical components of an *RL*-shunt applied to multi-modal vibration suppression. [17] has presented a new approach that optimizes several shunt circuits to attenuate the vibration of a multi-modal system.

One of the newest and most promising techniques in piezoelectric shunt damping, however, is the inclusion of a negative capacitance. This component is usually built through a synthetic circuit based on an operational amplifier. This concept has been first patented in [18] and has been later applied in [19] in the context of shunt damping. In [6] and [20], the effect of a negative capacitance has been theoretically studied and experimentally validated, proving that it has a broadband effect in terms of vibration attenuation. [21] has investigated the effect of shunted piezoceramics with negative capacitance in comparison to a classical tuned mass damper. [22] has shown that a negative capacitance can highly improve sound isolation when connected to a piezoelectric polymer film. [23] has shown several negative capacitance implementations using an operational amplifier and different feedback schemes. [24] has presented the impedance equation for the negative capacitance circuit in the Laplace domain and, for the first time, together with [25], has derived design guidelines to assure stability for the circuit considering the complete electromechanical system. [26] has published an approach to optimize the parameters of a negative capacitance circuit, which uses the concept of strain-induced voltage and minimizes the velocity response of a structure, while assuring stability, based on experimental measurements. [27] has shown that the passive components of the negative capacitance circuit have to be chosen correctly, so as to improve power output and efficiency of the operational amplifier. In order to avoid high-voltage issues, [28] recently suggested a novel negative impedance circuit design, in which a high-voltage operational amplifier would not be necessary.

As it will be shown later in this thesis, if a negative capacitance is inserted into a resonant *RL*-shunt, several advantages become noticeable. As for other shunt techniques, the negative capacitance shunt also requires an optimal tuning for maximized damping. The mostly known analytical derivations have been originally presented in [13] and later reformulated in [14] for a single-mode vibration, in the case of connecting the negative capacitance to an *RL*-shunt. Even though several studies have been published using the negative capacitance circuit alone, a thorough understanding and a practical application of this technique together with the *RL*-shunt are yet to be validated, especially in the context of composite structures.

Despite high efforts to develop real shunt damping applications, the majority of the published works remains as ongoing research using elementary structures. Few cases can be found using real-life structures, for example in [29], where the damping enhancement for a space structure using shunted piezoceramics has been investigated, in [30], where the potential benefits of an *RL*-shunt have been shown by attenuating a dominant vibration mode of a vehicle subframe, in [8], where the use of a negative capacitance in a truss structure has reduced the vibration response, in [14], where the application of shunted piezoceramics to a disk brake has been shown to suppress squealing noise, and most recently in [31], where the integration of an array of piezoceramic transducers and several *RL*-shunts into a rotationally periodic structure has been successfully achieved.

1.3.2 Functional integration

While conventional shunt damping techniques are based on bonded transducers, the state-of-the-art technologies for functional integration of piezoceramics into smart structures are numerous. With respect to metallic structures, [32] has investigated different types of actuators in an aluminum sandwich beam and [33] has discussed a technology to manufacture metal sheets with integrated piezoceramic fibers in micro-cavities used for sensing purposes.

On the other hand, the first work related to piezoceramic transducers embedded in laminate composite structures has been published in [34], where glass and carbon fiber specimens have been manufactured, tested and compared to analytical models in regard to their dynamic behavior. The manufacturing techniques have also been developed and static tests of the specimens have concluded that, although the elastic modulus of the composite is not affected, its ultimate strength is reduced by the presence of the actuator. In the context of adaptive structures, the advantages of multi-functional integration in lightweight composites have been discussed in [35], where the new role of sensors and actuators has been made noticeable. Later in [36], different aspects related to the integration of piezoceramic actuators into laminate composite structures for aerospace applications have been discussed, such as different integration patterns and methods for non-destructive testing. In regard to cyclic mechanical loads, [37] investigated the fatigue response of the host structure with an embedded device, whereas [38] investigated the fatigue response of the embedded transducer itself for different load scenarios. In [39], a manufacturing method for integrating a thin flexible layer of a piezoceramic network inside a carbon fiber laminate composite structure has been developed, which has been used to demonstrate structural health monitoring techniques. In [40], piezoceramic sensors and actuators have been embedded in a laminate carbon fiber beam with optimized depth to the surface, in order to minimize the dynamic response. In [41] and [42], multi-layer piezoceramic actuators using the d_{33}-effect have been embedded in a glass fiber tunable vibration absorber, which has been optimized for durability. The latest trend also explores the possibility of integrating high-voltage power electronics inside piezoelectric actuators, as discussed in [43]. Nevertheless, most applications present in the literature only target active vibration control or sensing applications and do not cover the main issues related to shunt damping techniques, e.g. the maximization of the electromechanical coupling.

With the aim to create adaptive composite structures for real industrial applications, concepts of piezoelectric modules have been investigated in the early 1990s at Active Control eXperts, Inc. and in the early 2000s at the German Aerospace Center DLR. The goal was to

develop a robust multi-functional material that combines load carrying capability, sensor and actuator properties. In this sense, packaged piezoceramic systems have been developed and manufactured with mechanical stabilization and electrical contacts and isolation, which led to the patented devices QuickPack™ [44] and DuraAct™ [45] patch transducers. In [46], the latter has been integrated in carbon fiber samples and experimental investigations of the static strength have been carried out. Several modules have also been integrated in a glass fiber train leaf spring, so as to perform and validate an active vibration control approach. Meanwhile, various configurations of patch transducers are commercially available, using different material geometries, piezoelectric effects and electrical connections. Their most relevant properties and applications have been discussed in [47].

Following this idea, [48] has developed a new thermoplastic-compatible piezoceramic module, so that it can be integrated into thermoplastic composite structures for optimal strain transmission, in contrast to bonded transducers with high shear losses in the adhesion. The further work in [49] has presented a robust manufacturing process for composite structures based on the hot pressing technology that allows the integration of these new piezoelectric modules and the operational testing of the produced samples. Another manufacturing technique has been presented in [50], where piezoceramic elements are integrated in glass fiber structures using a multi-fiber injection method, but only for sensing purposes.

In [51], a novel piezoceramic patch transducer with increased pre-stress has been developed, manufactured and tested, making it suitable for the integration into carbon fiber composites where high mechanical loads are expected. This module has been then applied in [52] using a carbon fiber rotor blade, where for the first time the idea of simultaneous optimization of adaptive composite structures has been demonstrated using piezoelectric shunt damping. Nevertheless, only structural parameters and the transducer position are considered as input variables and only the *RL*-shunt technique is taken into account.

1.3.3 Simultaneous optimization

In order to improve vibration control with piezoceramics, [53] has shown that systematic criteria are necessary for optimal sensing and actuation on a smart structure. Within shunt damping techniques, a high coupling of the transducer with the structure is especially desired, since this is the driving parameter that improves the damping performance and avoids instability issues. Different parameters influence this coupling, such as the type, quantity and placement of piezoelectric material [54]. With the growing interest in shunt techniques in the past years, several works that investigate the maximization of the coupling can be found in the literature. In [55], the maximization of the coupling has been investigated by adjusting the thickness of piezoceramic patches using shunted vibration absorbers to reduce noise level in vehicle structures. [56] has presented a detailed analytical model of a plate with embedded piezoceramic transducers, connected to a resonant shunt circuit, in order to maximize the coupling in terms of optimal positioning of the patches. [57] has optimized the vibration damping of a cantilever beam by means of a shunt circuit by varying the position and dimensions of piezoceramic patches. It has also been shown that the mass and stiffness effect of the patches on the vibrations of the structure cannot be neglected. In [58], the effective material properties of a piezoelectric macro-fiber composite with the d_{15}-effect have been analyzed using several geometric parameters, so that the electromechanical coupling coefficient can be

maximized. In [59], the problem of optimal positioning of surface-bonded piezoelectric patches in sandwich plates has been addressed. More recently, [60] has made an analysis of the optimal shape of a piezoceramic transducer in a bending and a longitudinal bimorph. Nevertheless, little work has been done in the context of laminate composite structures. In this case, as has been shown in [61], not only the position of the piezoceramics is relevant for the coupling, but also the orientation of the fibers in the structure play a major role in the achievable damping.

In the context of simultaneous optimization, it has already been discussed in [62] that optimizing an actuator on pre-determined host structures, and vice versa, is little effective. In this sense, a truly optimized adaptive structure is the one where the structure, transducers and electronics have all been simultaneously designed to work in perfect harmony. Nevertheless, little effort has been made in this field to develop a robust methodology.

The first general simultaneous optimization formulation has been published in [63], in which a feedback controller for flexible structures is designed. In [64], piezoelectric sensors and actuators have been designed together with a composite plate. As the understanding of smart structure grows and computational power improves, a number of optimization methods have been published in the last years. [65] and [66] have presented analytical algorithms to simultaneously optimize host structure, location of sensors and controller parameters, as efficiently as possible, even when there are conflicting requirements. Another powerful technique is the topology optimization, which has been used in [67], [68], [69] and [70] to simultaneously consider the best distribution of conventional structural material and active piezoceramic material, so that the most suitable structural or electrical response can be found, e.g. in active vibration control or energy harvesting applications. [71] has presented an optimization approach applied to a laminate composite plate, where first the optimal stacking sequence and then the optimal position of piezoelectric actuators is found, in order to minimize the vibration amplitude. [72] has used a new numerical approach to optimize the structural geometry, the position of piezoceramic actuators and control parameters, in order to suppress structural vibrations.

Numerical models of complex structures typically present differential equations of high order to describe the dynamic behavior. This increases the computational power needed during the simultaneous optimization thus limiting its benefits. An important tool in the design of such structures is the model reduction, which reduces the computational complexity by finding a low-order approximation of the original model. Several techniques have been published [73], e.g. the mode displacement and the Krylov subspace, and are widely used in piezoelectric applications.

When transducers and control variables are included in the optimization of the host structure, the correct method of interaction between simulations has to be chosen. In traditional design methods, structural parameters are first optimized, fixed and only at the very end the optimization of the electronics occur, especially with active control systems. However, several techniques that deal with a true simultaneous optimization have been published, such as the nested approach [74], the layered strategy [75] and the integrated topology [76].

In spite of growing activities, most published works only deal with academic geometries and mostly metallic materials, only active control is considered and no experimental data is used in the design loop whatsoever. In this sense, several considerations still have to be taken into account when designing such systems, such as efficient energy conversion between mechanical

and electrical sub-systems, load carrying capability of transducers, durability of the composite structure and the transducer and reliable manufacturing techniques.

1.4 The control arm in an automotive suspension

In order to show that piezoelectric shunt damping techniques can be applied to technical structures, attention will be given to one very important component in a passenger vehicle: The control arm, commonly named wishbone. It is part of the widely used MacPherson suspension and connects each front wheel to the subframe or directly to the chassis. It usually has a flat triangular shape that pivots in two vertices, whereas one end is connected to the steering knuckle at the wheel, allowing the vertical movement of spring and damper.

Other than assuring maneuverability of the vehicle and holding the wheel during brake or acceleration, the control arm is one of the main transfer paths for vibrations coming from the wheels into the chassis. If not designed correctly, the control arm can have coincidental resonant frequencies with other sub-systems of the vehicle, such as the subframe, the suspension system or even the tires, thus resulting in high vibration levels if excited. The reduction of these vibrations is often a design requirement that is related to the comfort of passengers. For example, when driving through a rough roadway, high frequency vibration and noise are perceived in the range 25-100 Hz, which are defined as harshness. When driving over small obstacles, vibration is perceived in the intermediate range 5-25 Hz, which is defined as shake [77]. Vibrations from the road can be partly isolated by rubber mounts present in the two pivots of the control arm, as long as they have proper orientations and the used materials have suitable stiffness and damping in radial and axial directions. However, whereas soft mounts improve comfort, they degrade drivability and handling of the vehicle. Therefore, in order to achieve better noise and vibration performance, changes in other vehicle parts might be necessary. These include the application of absorbing materials on the chassis or vibration absorbers in the powertrain, which have a high cost in mass and eventually in fuel consumption. This leads to the investigation of an integrated suppression of resonant vibrations inside the structure of the control arm itself.

1.5 Motivation for research

Modern mobile structures are increasingly benefiting from lightweight fiber-reinforced plastics, particularly in the aeronautic industry. Although lighter structures reduce energy consumption, they are susceptible to vibration problems. Smart structures provide nowadays a reasonable choice for vibration attenuation and intense research has been done in the field but, in spite of considerable progress, limited commercial products can be found. Due to low awareness, high costs and reliability concerns, the smart structures technology has not widely penetrated the automotive industry, for example, although some applications start to appear and their performance to be acknowledged, such as active noise control and crash systems [78]. Based on a literature research and the state-of-the-art techniques presented previously, the following needs have been identified at the moment this research began:

1) The damping property of materials is usually not considered early in the design phase of a structure and this fact, together with an insufficient design, can lead to excessive vibration

levels. Up to the present time, shunt damping is considered as an add-on solution, in which the traditional approach consists in applying a piezoceramic transducer to the structure. This consequently results in an unwanted increase in stiffness and weight. In most cases, this also brings difficulties in implementing the electrical circuit and performing damping. It is therefore evident that there is a need for a new design approach that is capable of simultaneously dealing with the structure, transducers and circuit, potentially reducing added weight and increasing functionalities.

2) Much research has focused on the physical integration of piezoelectric transducers inside the host structure during manufacturing, especially within laminate composites. In the context of shunt damping, however, a systematic approach is still needed, especially regarding the maximization of the electromechanical coupling. Together with the simultaneous design, this is the most reasonable way leading to a complete functional integration.

3) When used to perform vibration control, the negative capacitance has to be built through a synthetic circuit that is based on an operational amplifier, a fact that increases the complexity of the interaction between structure, transducer and electronics. Even though the negative capacitance circuit has been extensively investigated, the real circuit implementation diverges most of the time from the theoretical prediction. In the particular case where this circuit is connected in series to a resonant *RL*-shunt, the increased number of variables makes the optimization process of the vibration attenuation very difficult. Therefore, robust circuit design guidelines on how to choose the exact parameters of all circuit elements are still needed.

4) In spite of proven potential of the shunt damping technique, few applications exist for vibration control of load carrying mechanical structures. This is mainly due to complexity of the subject but also to the lack of a convincing methodology to design the system in a reliable way. Therefore, there is still the need to reduce the gap between a laboratory experiment and a ready-to-market product.

1.6 Objectives and approaches

In the framework of this thesis, specific attention is given to the use of piezoceramic transducers in composite structures and their application for adapting the dynamic performance using a resonant negative capacitance shunt circuit.

This thesis is organized using the bottom-up approach: Initially, individual base elements of smart structures are described and thoroughly investigated, namely fiber-reinforced plastics, piezoceramic transducers and the shunt circuit. Then, these elements are linked together with increasing complexity to form larger objects of study. First, the coupling between the piezoceramics and the laminate composite is analyzed in the coupon level. Then, the investigations move forward to the sub-component level, where a simplified smart structure is developed, considering additionally the shunt circuit. Finally, the design is brought to the upper level, where a real component illustrates the benefits of using the shunt damping technique compared to competitive technologies.

In spite of established research, this work presents several novel contributions and attempts to address the aforementioned needs according to the following research objectives:

1) The main purpose of this thesis is to develop a robust methodology to efficiently design a lightweight laminate composite structure together with piezoceramic transducers and a shunt circuit. An optimization process is presented in which several technical requirements are simultaneously taken into account. In the context of semi-active control, the full simultaneous optimization is presented for the first time. To validate the novel approach, a sub-component was chosen so that the simplified behavior of a control arm can be represented. Here, embedded piezoceramics are also considered during the design process of the structure and the optimization of the electromechanical coupling is proposed. Another novelty is that the electrical characteristics and limitations of the shunt circuit are also considered. Due to the complexity of the negative capacitance circuit, the design guidelines take into account not only numerical results, but also measured data. The objective is to show that, once the shunt damping technique is regarded as part of the design space, instead of an add-on solution, undesirable stiffness and mass can be eliminated and the technical requirements can be more easily met, without mechanical or electrical adverse effects.

2) To quantify the effectiveness of embedded piezoceramics in laminate composites, another goal is to investigate different integration patterns. Several geometric distributions of the layered material and of the transducers are considered and their impact on the electromechanical coupling is analyzed. In terms of load carrying structures, this work also starts the discussion on the strength and durability once the transducer is inside the composite material.

3) Additionally to the design of the mechanical structure and transducers, the electrical behavior of the shunt is also investigated. The goal is to find the best combination of parameters of the shunt circuit, so that vibration attenuation can be maximized. Here, an *RL*-shunt circuit connected in series with a negative capacitance is used to dampen only one mechanical eigenfrequency at a time. Due to the sensitive tuning characteristic of the negative capacitance, the parameters of the shunt circuit are optimized using experimental data. The novel contribution consists in considering the mechanical structure and transducers in the electrical domain, facilitating hence the analysis once the shunt circuit is connected.

4) So as to avoid countermeasures against unwanted noise and vibrations in other vehicle parts, which usually have a high cost in mass, the goal of this research is to develop a smart control arm, especially designed with lightweight composite materials, capable of absorbing vibrations through piezoceramic transducers and a shunt circuit. Here in particular, a novel fiber-reinforced piezoelectric module is developed in order to allow a more realistic functional integration. This proposed solution is hence a smart alternative to classical correction measures and will convince that shunt techniques can be applied not only to simple academic beams, but also to technical structures with tight technical requirements.

1.7 Structure of the thesis

This thesis is divided in nine chapters. Chapter 1 consists of the introductory part, where an overview of smart structures is presented and the state-of-the-art techniques in piezoelectric shunt damping, functional integration and simultaneous optimization are described. The research needs and the novel contributions of this work are also emphasized. Then, Chapter 2 collects the theoretical fundamentals needed for this work. Initially, a brief description of fiber-

reinforced plastics is made, followed by the main concepts of piezoelectric transducers, where the constitutive equations and the equivalent electrical circuit of piezoceramics are derived. The principles of piezoelectric shunt damping are also presented and an emphasis is given to the negative capacitance connected to an *RL*-shunt. Afterwards, Chapter 3 points out the different techniques used to obtain a numerical model of the composite structure, the piezoceramic transducer and the shunt circuit. The optimization approach of the coupled system is also described. After presentation of the covered topics and the used tools, Chapter 4 is dedicated to the physical integration of piezoceramic transducers into fiber-reinforced plastics. In-depth numerical and experimental analyses of different coupons are used to investigate the dynamic behavior and to show the advantages of this technique. The acquired knowledge is then applied in Chapter 5, which focuses on the simultaneous optimization of a composite structure with integrated piezoceramics together with the shunt circuit. The proposed novel design approach is investigated using a scale model of a control arm. To experimentally validate the results, Chapter 6 presents a new tuning technique based on the measured electromechanical impedance of a smart structure, so as to maximize the shunt damping performance. In Chapter 7, the developed methods are applied to a more realistic case study: The control arm, which is redesigned for optimal vibration attenuation using shunted piezoceramic transducers. The last part consists of Chapters 8 and 9, where a critical analysis of the presented results is made and the transferability of the developed techniques into more complex engineering problems is discussed.

2 Theory

In this chapter, the basic theory of fiber-reinforced plastics, the fundamentals of piezoelectricity and the principles of piezoelectric shunt damping are presented. Specific attention will be given to the equivalent electrical circuit of a piezoceramic transducer, which will be later exploited in Chapter 6. The advantages of the resonant negative capacitance are shown and an analytical tuning method is briefly described. The complex impedance of the negative impedance converter is also derived, since it is the basic circuit responsible for the increased effectiveness of piezoelectric shunt damping.

2.1 Fiber-reinforced plastics

Several modern technologies require materials with unusual properties that cannot be achieved by conventional metal alloys, ceramics or polymers. This is especially true for applications that require high performance materials, such as aircraft, aerospace, underwater, transportation and high-speed rotating machines. Required characteristics usually include low density, high strength and stiffness, resistance to abrasion, impact and fatigue [79].

In this sense, composite materials have been created to improve the mechanical characteristics of elementary materials through the combination of usually two distinct phases: One is the matrix, which is continuous and surrounds the other phase, called dispersed phase. The most technologically relevant type of dispersed phase is in the form of fibers. The resultant properties of the fiber-reinforced plastic (as from now called simply “FRP”) are a function of the properties of the constituent phases, their relative amounts and the geometry of the fibers. There is hence a clear contribution from the matrix and fibers to the properties of the material: Strength and stiffness are driven by the fibers, whereas the matrix binds the fibers together and acts as the medium by which an externally applied stress is transmitted and distributed to the fibers. Moreover, the matrix protects the fibers from surface damages, increases toughness and dominates thermal conductivity. These basic characteristics allow the extension of property ranges usually necessary for high-end structural components.

More specifically in the automotive industry, where fuel consumption and CO_2 emissions are driven by vehicle weight, the need for lightweight FRPs is substantial. The high specific modulus and specific strength of carbon fiber, for example, make it suitable for high-performance structural components, ultimately leading to a significant weight reduction, performance increase of the final product and reduced manufacturing costs [80].

2.1.1 Manufacturing process

Unlike conventional materials, there is a close relation between the manufacturing of a composite material and its end use. An exhaustive description of all existing processes is neither possible nor desired, since the manufacturing technique is part of the design process. There are some classical methods though, such as compression molding, resin-transfer molding, sheet molding compound, roll-forming process, pultrusion and filament winding, which are capable of dealing with different types of fibers and resins [81]. Details of these manufacturing techniques will not be discussed.

The most widely used composite material form in structural applications, however, is the prepreg. Prepregs are continuous and aligned fibers, unidirectional or woven, embedded in a partially cured polymer resin. Several types of resin can be used, such as epoxy, phenolic and polyimide. Carbon, glass and aramid are the most common fiber sort. At room temperature, the resin undergoes curing reaction; therefore the prepreg is stored at low temperatures.

A laminate composite material is a bonded stack of several layers, or plies, with various orientations, as depicted in **Figure 2.1**. The layers are usually bonded together using a single matrix material.

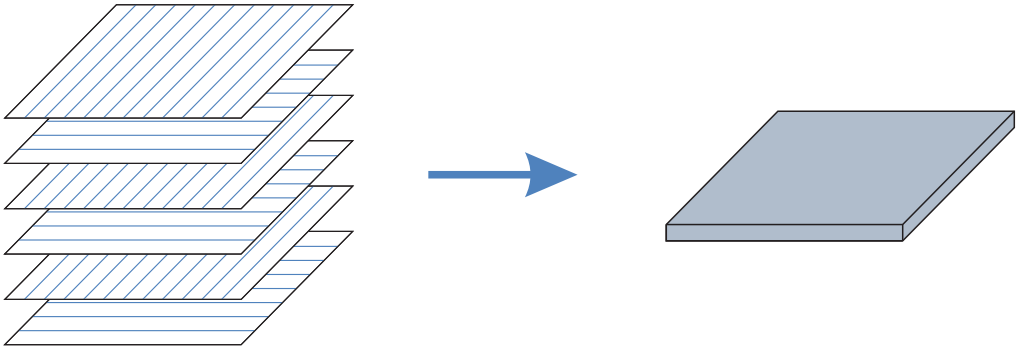

Figure 2.1. Stacking of oriented FRP layers resulting in a laminate composite plate

The actual manufacturing of a laminate begins with the layup, which consists in laying the prepregs onto a tooled surface. The stacking sequence arrangement may be unidirectional, but more often the fiber orientation is alternated. This procedure may be carried out entirely by hand (hand lamination) or by an automated process. Afterwards, by the simultaneous application of heat and pressure, a chemical reaction transforms the matrix into a solid structural material and final curing is accomplished. Curing may last from a few seconds up to several hours depending on applied temperature and resin characteristics.

Different processing techniques exist, in which quality and costs vary [82]: Vacuum bag process, where the laminate is involved by a plastic bag, to which a vacuum pump is connected, and placed inside an oven; autoclave process, where an additional pressure (1-10 bar) is applied; pressure bag process, where an external mold of the laminate is needed and pressure is applied from the inside; hot pressing process, in which a temperature- and force-controlled press compresses the stacked layers inside a metal mold.

2.1.2 Classical laminate theory

The classical laminate theory consists of a collection of material mechanics hypotheses that describe stress and deformation of a composite structure. Using this theory, the structural laminate behavior can be predicted by the characteristics of each constituent layer [83], allowing the computation of forces, moments, strain and stresses.

The basic assumptions are: The layers are perfectly bonded together; material properties of each layer are constant through the thickness; the relation strain-stress presents a linear-elastic behavior; lines originally straight and normal to the mid-plane remain straight and normal in extension and bending; there is a plane stress state; and in-plane strains and curvature are small compared to all other dimensions. These requirements are fulfilled if a relatively thin or moderate thick laminate is assumed, where the thickness is small compared to the other dimensions.

The general behavior of laminate materials is known to be anisotropic. In special cases, however, the analysis might be simplified depending on the nature of each layer and on the symmetry of the stacking sequence in the laminate. Considering a single layer with a three-dimensional orthotropic material property, as it is the case for most prepregs, the Hooke's law can be written as described in Eq. (2.1):

$$\begin{bmatrix} \varepsilon_{xx} \\ \varepsilon_{yy} \\ \varepsilon_{zz} \\ 2\varepsilon_{yz} \\ 2\varepsilon_{xz} \\ 2\varepsilon_{xy} \end{bmatrix} = \begin{bmatrix} 1/E_x & -\nu_{xy}/E_y & -\nu_{xz}/E_z & 0 & 0 & 0 \\ -\nu_{xy}/E_x & 1/E_y & -\nu_{yz}/E_z & 0 & 0 & 0 \\ -\nu_{xz}/E_x & -\nu_{yz}/E_y & 1/E_z & 0 & 0 & 0 \\ 0 & 0 & 0 & 1/G_{yz} & 0 & 0 \\ 0 & 0 & 0 & 0 & 1/G_{xz} & 0 \\ 0 & 0 & 0 & 0 & 0 & 1/G_{xy} \end{bmatrix} \begin{bmatrix} \sigma_{xx} \\ \sigma_{yy} \\ \sigma_{zz} \\ \sigma_{yz} \\ \sigma_{xz} \\ \sigma_{xy} \end{bmatrix} \tag{2.1}$$

where ε is the strain tensor, σ is the stress tensor, E is the Young's modulus, ν is the Poisson's ratio and G is the shear modulus. By having the knowledge of only 9 material parameters, it is possible to describe the elastic behavior of each layer and eventually calculate the compliance matrix of the complete laminate.

2.1.3 Failure and durability

In the design of FRPs, there is a strong need for a simple fracture analysis that is physically representative. Several failure criteria for static mechanical loads can be found in the literature. The simple maximum strain/stress criterion, applicable to isotropic plies, compares the actual strain/stress to the failure limits in the ply coordinate system. In the Tsai-Hill failure criterion, both tensile and compressive strengths are used to determine a quadratic function. In the Hashin criterion, critical tensile or compressive loads in the fiber direction or in the transverse direction are all independently computed.

A well-established and commonly used criterion, though, is the Puck failure criterion, initially published in [84] and further developed in [85]. It considers two distinctive types of failure, one for fiber and another for inter-fiber, because the effects of both fracture phenomena are completely different. The fiber failure takes into account both tensile and compression loads. The inter-fiber failure is based on the brittle behavior of composites and additionally makes distinction between three different fracture modes. In order to calculate the failure condition, a master fracture surface is mathematically calculated using material-dependent constants, such as the fracture resistances and the slope parameters. A simple way to represent the failure condition is through the reserve factor, which is the factor all existing stresses have to be multiplied with in order to achieve fracture. Despite the fact that real excitations on a smart structure are often dynamic, the reserve factor evaluates the permissible static load that can be

applied to a composite part before it fails, enabling to identify weak spots in the structure, leading to a better design and potentially reducing weight.

In regard to durability of FRPs, several factors play a major role, such as humidity, temperature, chemical environment and radiation. When it comes to cyclic mechanical loads, fatigue exhibits a very complex behavior due to the anisotropic characteristics of the material. In this case, different types of damage can occur, such as fiber fracture, matrix cracking, fiber buckling or delamination. Several lifetime prediction methodologies have been published [86] and most of them largely depend on experimental input parameters. An extensive fatigue analysis is outside the scope of this thesis. Nevertheless, some parameters affecting fatigue can be neglected and integrated in the static Puck reserve factor.

2.2 Fundamentals of piezoelectricity

The term piezoelectricity refers to the effect present in many natural crystals that is the generation of electricity under mechanical pressure. The direct piezoelectric effect is defined as an electric polarization of a material produced by a mechanical strain. The inverse piezoelectric effect also exists and is the appearance of a mechanical strain as a result of an applied electric field. The piezoelectric effect is related to the geometric properties of certain crystal categories. If the unit cell of a crystal possesses a certain degree of asymmetry, the separation of positive and negative charges results in a permanent polarization of the material.

2.2.1 History

The direct piezoelectric effect was first observed by the brothers Pierre and Jacques Curie in 1880 when conducting research into a related phenomenon, the pyroelectric effect, which is the generation of electricity as a result of a temperature change. Their first measurements were demonstrated on several natural crystals such as quartz, tourmaline, Rochelle salt, cane sugar and topaz.

The inverse piezoelectric effect was mathematically deduced from fundamental thermodynamic equations by Gabriel Lippmann in 1881 and later experimentally validated by the Curie brothers. For several years, piezoelectricity remained a laboratory curiosity until a comprehensive treatment of the theory was published in the Woldemar Voigt's Textbook on Crystal Physics, in 1910.

It is not before the First World War that the piezoelectric effect found a practical application. Ocean floor exploration and underwater search led to the development of devices for emitting and receiving ultrasonic waves. In 1916, Paul Langevin developed a submarine ultrasonic emitter and detector driven by quartz plates. Several piezoelectric oscillators, resonators, transformers and sensors were subsequently developed during the next decades and are now used in a wide range of applications.

2.2.2 Piezoelectric ceramics

In contrast to natural crystals, synthetic piezoelectric materials exhibit much better properties and are more suitable for technological applications. The most used material is ferroelectric ceramics, or piezoceramics. Since a large scale manufacturing became possible, the domain of applications expanded considerably. Typical materials being used include Barium Titanate ($BaTiO_3$) and Lead Zirconate Titanate ($Pb[Zr_xTi_{1-x}]O_3$), more commonly known as PZT. Recently, new materials with superior performance compared to PZT-based ceramics are being developed and specific attention is given to environmentally friendly lead-free ceramics.

The properties of piezoceramics are a function of their constituents. Among these materials, two categories exist: A "soft" composition, where piezoelectric coefficients are high and the material exhibits high hysteresis, and a "hard" composition, where piezoelectric coefficients are low and the material exhibits low hysteresis. In smart structures applications, soft piezoceramics are preferred due to their large induced strain.

Piezoceramics are polycrystalline materials that do not exhibit the piezoelectric effect in their natural form. The material is manufactured by mixing fine powders of the component metal oxides in specific proportions. It is then heated to around 1000°C and sintered to a desired shape. In the case of the PZT-ceramics, it possesses above the Curie temperature (which is specific to the material composition) a cubic centrosymmetric unit cell. If temperature falls below the Curie temperature, a phase transformation occurs and the unit cells become asymmetric tetragonal. As a result, the unit cell presents a permanent dipole moment. The two different unit cells are schematically represented in **Figure 2.2**.

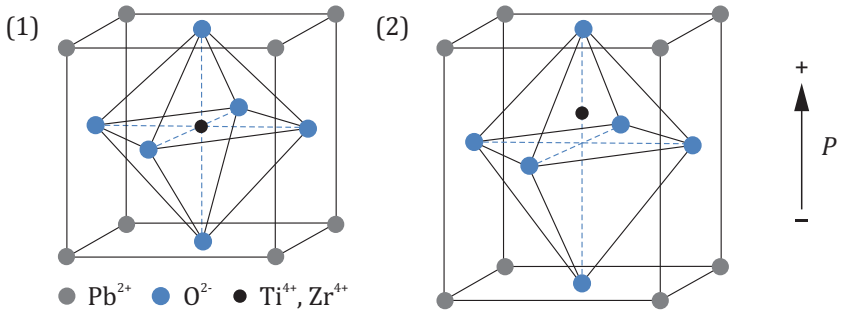

Figure 2.2. PZT unit cell above (1) and below (2) the Curie temperature

A volume of unit cells with the same orientation of dipole moments is called a Weiss domain. Due to the dipole moment in the unit cells, each domain in the material presents a spontaneous polarization, which is responsible for the piezoelectric characteristics of a single domain. In a bulk sample of piezoceramic material, there are many oriented domains that are randomly distributed, so the resultant polarization of the sample is zero and it presents no macroscopic piezoelectric properties.

In order to become piezoelectric, metal electrodes are deposited on appropriate surfaces and the ceramic material is polarized through the application of a strong electric field (typically more than 2 kV/mm). This imposes the realignment of domains in the same direction of the applied field. If the poling electric field is removed, the parallel domain orientation is partially

retained and the ceramic is permanently polarized. The orientations of domains during the poling process are represented in **Figure 2.3**.

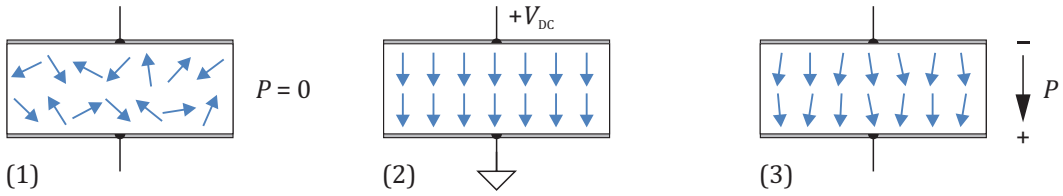

Figure 2.3. Orientations of domains before (1), during (2) and after (3) the poling process

Piezoceramics are commercially available in a variety of materials, of shapes such as disks, plates, rings as well as in the form of assembled actuators and transducers, such as multi-layer stack actuators, preloaded cased actuators and patch transducers. The right choice depends on displacement and force levels required by the application, as well as on the strain, voltage and temperature requirements, among other parameters. Some standard piezoceramic products are shown in **Figure 2.4**.

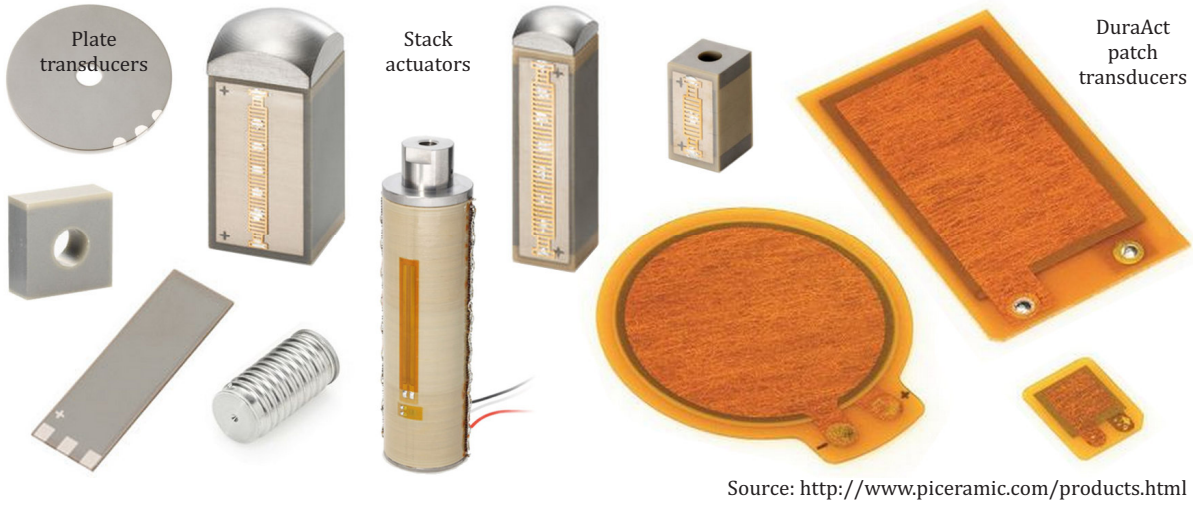

Source: http://www.piceramic.com/products.html

Figure 2.4. Piezoceramic actuators and transducers produced by PI Ceramic GmbH

2.2.3 Electromechanical constitutive equations

The piezoelectric effect can be expressed in terms of a linear constitutive equation that is derived from basic thermodynamic relations. A standardized [87] way of writing this equation is represented in Eq. (2.2):

$$\begin{bmatrix} S \\ D \end{bmatrix} = \begin{bmatrix} S^E & d^{\mathrm{T}} \\ d & \varepsilon^{\mathrm{T}} \end{bmatrix} \begin{bmatrix} T \\ E \end{bmatrix} \tag{2.2}$$

where S is the strain vector, D is the vector of electric displacement, S^E is the compliance matrix with constant electric field, d is the matrix of piezoelectric strain constants, ε^{T} is the relative permittivity matrix with constant mechanical stress, T is the stress vector and E is the vector of applied electric field.

The basic piezoelectric constitutive relations are assumed linear, in which all coefficients are assumed to be constant and independent of applied mechanical stress or electric field. In reality, however, under high mechanical stress or electric field, piezoceramics often present non-linear behavior. Besides, piezoelectric materials exhibit hysteresis, electrical aging, magneto-mechano-electric interactions and dynamic effects.

Figure 2.5 shows the definition of the coordinate system and poling direction of a piezoceramic plate transducer with surface electrodes. Axes 1, 2 and 3 correspond to translation in axes x, y and z, respectively, whereas axes 4, 5 and 6 represent shear around axes x, y and z, respectively.

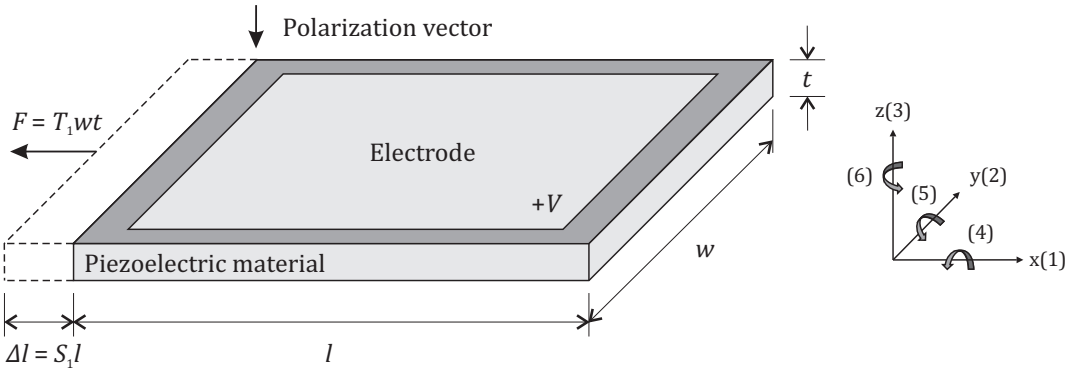

Figure 2.5. Schematic representation of a piezoceramic plate transducer (d_{31}-effect)

Assuming that the piezoceramic is poled along axis 3 and that the material is transversely isotropic, several parameters in the constitutive equations are simplified [88] and Eq. (2.2) can be rewritten in matrix form as shown in Eq. (2.3) and (2.4):

$$\begin{bmatrix} S_1 \\ S_2 \\ S_3 \\ S_4 \\ S_5 \\ S_6 \end{bmatrix} = \begin{bmatrix} S_{11}^E & S_{12}^E & S_{13}^E & 0 & 0 & 0 \\ S_{12}^E & S_{11}^E & S_{13}^E & 0 & 0 & 0 \\ S_{13}^E & S_{13}^E & S_{33}^E & 0 & 0 & 0 \\ 0 & 0 & 0 & S_{44}^E & 0 & 0 \\ 0 & 0 & 0 & 0 & S_{44}^E & 0 \\ 0 & 0 & 0 & 0 & 0 & 2(S_{11}^E - S_{12}^E) \end{bmatrix} \begin{bmatrix} T_1 \\ T_2 \\ T_3 \\ T_{23} \\ T_{31} \\ T_{12} \end{bmatrix} + \begin{bmatrix} 0 & 0 & d_{31} \\ 0 & 0 & d_{31} \\ 0 & 0 & d_{33} \\ 0 & d_{15} & 0 \\ d_{15} & 0 & 0 \\ 0 & 0 & 0 \end{bmatrix} \begin{bmatrix} E_1 \\ E_2 \\ E_3 \end{bmatrix} \tag{2.3}$$

$$\begin{bmatrix} D_1 \\ D_2 \\ D_3 \end{bmatrix} = \begin{bmatrix} 0 & 0 & 0 & 0 & d_{15} & 0 \\ 0 & 0 & 0 & d_{15} & 0 & 0 \\ d_{31} & d_{31} & d_{33} & 0 & 0 & 0 \end{bmatrix} \begin{bmatrix} T_1 \\ T_2 \\ T_3 \\ T_{23} \\ T_{31} \\ T_{12} \end{bmatrix} + \begin{bmatrix} \varepsilon_{11}^{\mathrm{T}} & 0 & 0 \\ 0 & \varepsilon_{11}^{\mathrm{T}} & 0 \\ 0 & 0 & \varepsilon_{33}^{\mathrm{T}} \end{bmatrix} \begin{bmatrix} E_1 \\ E_2 \\ E_3 \end{bmatrix} \tag{2.4}$$

The use of piezoelectric materials in technical applications is usually divided into three effects [89]: The d_{31}-effect applies if the electric field is along the polarization axis, but the strain of interest is that along axis 1 (orthogonal to the polarization axis); the d_{33}-effect applies if electric field, polarization and strain are along the same axis; if an electric field is applied perpendicular to the polarization axis, the material shears and the d_{15}-effect applies.

The piezoelectric constant d_{ij} is the ratio of the strain in the *j*-axis to the electric field applied along the *i*-axis. Considering the d_{31}-effect as depicted in **Figure 2.5**, where the strain exists along the 1-axis caused by a force *F*, the electric charge q that appears on the electrodes can be calculated by Eq. (2.5):

$$q = d_{31} T_1 w t \tag{2.5}$$

Assuming that the stress field only exists along the 1-axis, the capacitance C_p of the plate transducer when it is mechanically free can be determined from Eq. (2.6):

$$C_\mathrm{p} = \frac{q}{V} = \frac{\varepsilon_{33}^\mathrm{T} l w}{t} \tag{2.6}$$

A very important piezoelectric material property is the coupling coefficient k_{ij}, which represents the ability of a piezoceramic material to transform electric energy to mechanical energy and vice versa. The *ij* indices indicate that the strain is in the *j*-axis and the electrodes are perpendicular to the *i*-axis. The coupling coefficient can be calculated by the amount of electrical energy W_e stored in the capacitor when the applied force *F* does a mechanical work W_m. It can also be calculated using other piezoelectric constants, as represented in Eq. (2.7):

$$k_{31}^2 = \frac{W_\mathrm{e}}{W_\mathrm{m}} = \frac{q^2/2C_\mathrm{p}}{F\Delta l/2} = \frac{d_{31}^2}{S_{11}^E \varepsilon_{33}^\mathrm{T}} \tag{2.7}$$

When a force is applied to a piezoceramic transducer, different mechanical stiffnesses are observed depending on whether the electrodes are open or short-circuited. If the electrodes are short-circuited, the electric charges of opposite polarities accumulated on the electrodes cancel each other, no electrical energy can be stored in the piezoelectric capacitor and the material appears to be less stiff.

2.2.4 Equivalent electrical circuit

Piezoceramics electrical characteristics, as well as its structural properties, can be represented in terms of an equivalent electrical circuit. This provides a convenient approach to analyze the piezoceramic when it is connected to an external electrical network. A piezoelectric material behaves predominantly as a capacitor. However, in structural vibration applications, it is essential to have its accurate equivalent electrical circuit model.

Several circuit representations can be found in the literature, each consisting of combinations of basic electrical components, such as resistors, capacitors, inductors and even transformers. The choice of a particular representation depends mainly on the frequency range, material losses and mode of operation.

The equivalent circuit suggested in [87] for a piezoelectric vibrator near a sufficiently isolated resonance is depicted in **Figure 2.6** (1). This so-called Van Dyke model is useful only if vibration amplitudes are low and if the circuit parameters are independent of frequency. In this model, C_0 represents the inherent piezoelectric capacitance and the $R_1L_1C_1$ branch represents the mechanical resonance of the piezoceramic, either when it is in the free condition (unloaded case) or when it is attached to a mechanical structure (loaded case). The values of the components are usually obtained experimentally through the electrical impedance in the Laplace domain, as described in Eq. (2.8):

$$Z_{\text{Van-Dyke}}(s) = \frac{L_1C_1s^2 + R_1C_1s + 1}{L_1C_1C_0s^3 + R_1C_1C_0s^2 + (C_1 + C_0)s} \tag{2.8}$$

When assessing the capacitance of a piezoceramic attached to a resonant mechanical structure, two possible values can be measured, as investigated in [90]. At frequencies higher than the resonance, i.e. $s \to \infty$, the "dynamic" capacitance is obtained, which corresponds to the inherent piezoelectric capacitance of the transducer C_0. At frequencies lower than the resonance, i.e. $s \to 0$, the "static" capacitance is obtained, which corresponds to $C_1 + C_0$.

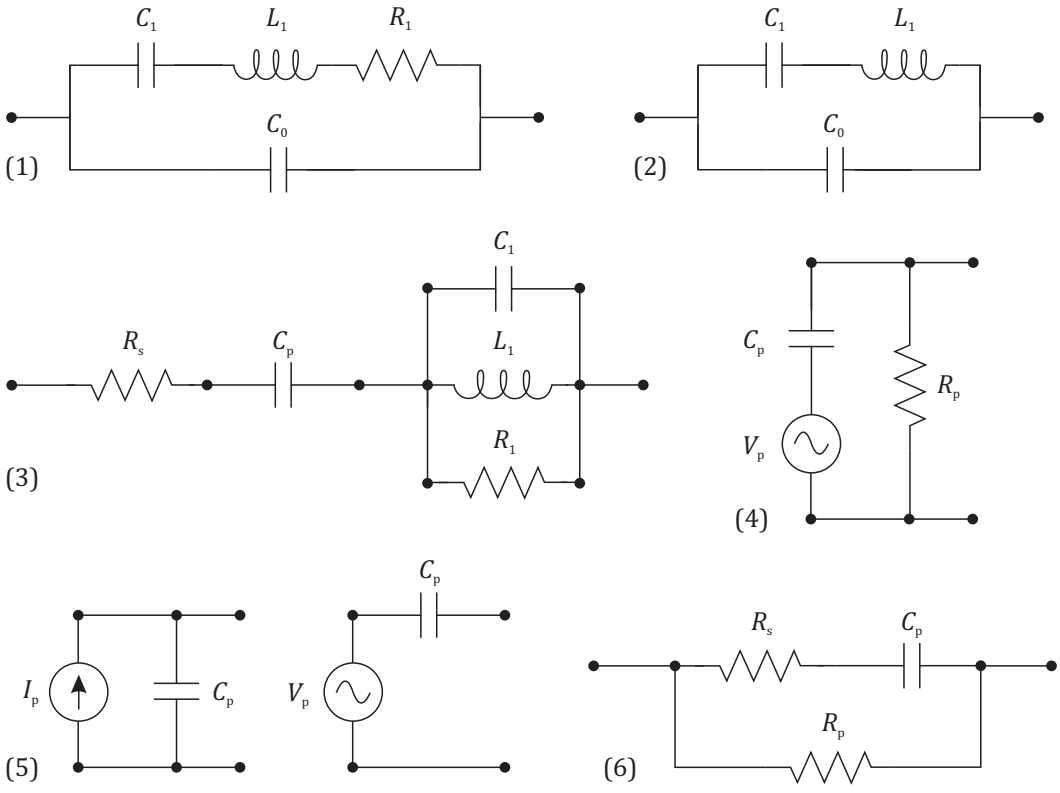

Figure 2.6. Piezoceramics equivalent electrical circuits

In order to deal with piezoelectric materials with high losses, a similar model has been proposed by [91], where the circuit elements C_0, C_1 and L_1 are considered as complex quantities. The piezoelectric loss factor is taken into account by the imaginary part of the impedance, which

is determined by three factors: The dielectric, elastic and piezoelectric losses associated with the material. This model is shown in **Figure 2.6** (2).

A more accurate model has been developed for sensory systems in [92] and can be seen in **Figure 2.6** (3). It consists of a series connection of a resistor, which represents the internal losses, a capacitor, which stands for the inherent capacitance of the piezoelectric material, and a parallel RLC branch. In the loaded case, this resonant branch represents a single degree of freedom mechanical structure, i.e. an ideal mass-spring-damper system. This effective mechanical system is relative to the piezoceramic and already takes into account the electromechanical coupling. The analogy between the mechanical and electrical representations of the system is depicted in **Figure 2.7**.

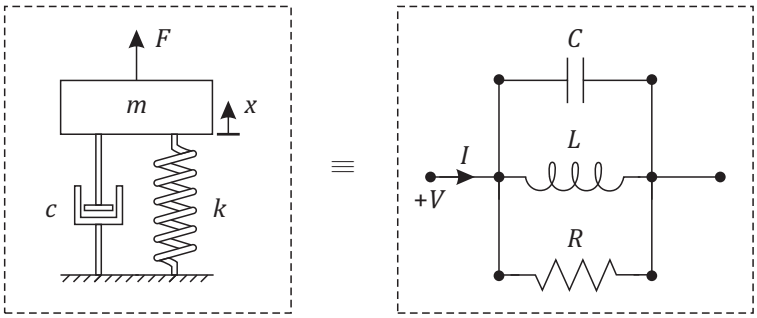

Figure 2.7. Electrical representation of a resonant mechanical structure

The mobility or mechanical admittance Y of a mechanical structure is defined as velocity response per unit force excitation [93]. Eq. (2.9) shows the mechanical admittance of a single degree of freedom mechanical system and the analogous electrical impedance Z of the parallel RLC circuit in the Laplace domain:

$$Y = \frac{xs}{F} = \frac{s}{ms^2 + cs + k} \equiv Z = \frac{V}{I} = \frac{s}{Cs^2 + s/R + 1/L} \tag{2.9}$$

It can be noticed that the effective mechanical mass m is mathematically equivalent to the capacitance C, the effective damping coefficient c, to the inverse of the resistance R, and the effective stiffness k, to the inverse of the inductance L. The advantage of using parallel instead of series RLC branches to represent the resonant modes is that the RLC values are easier determined when several modes are close to each other. The same approach could be applied to a series RLC circuit. In this case, however, the electrical impedance is analogous to the mechanical impedance. The mechanical mass is equivalent to the inductance, the damping coefficient to the resistance, and the stiffness, to the inverse of the capacitance.

In regard to semi-active vibration control applications, [26] proposed a modified piezoelectric model that is directly used with a negative capacitance shunt. It consists of a voltage source in series with a capacitor and in parallel with a resistor, shown in **Figure 2.6** (4). In this case, the resonant part is not directly represented in the circuit, but is taken into account in the voltage source instead.

When used as a sensor, the piezoceramics can be equally represented by a charge generator (current source) in parallel with a capacitor and optionally a resistor (Norton's equivalent), or by a voltage source in series with a capacitor and optionally a resistor (Thévenin's equivalent), as investigated by [94] and shown in **Figure 2.6** (5).

In [95], a parallel and a series resistor are simultaneously modeled, which represent the internal charge leakage of the piezoceramic and the energy dissipation in the hysteresis loop, respectively. This non-resonant model is shown in **Figure 2.6** (6).

2.3 Principles of piezoelectric shunt damping

Semi-passive and semi-active techniques take advantage of electromechanical transducers that are capable of converting mechanical energy into electrical energy and vice versa. In a mechanical structure incorporating transducers such as piezoceramics, its stiffness acts in parallel with the stiffness of the host structure. Hence, by connecting it to an external electrical network, i.e. a shunt circuit, its mechanical impedance can be controlled and the dynamic response can be changed in different ways. This principle is depicted in **Figure 2.8**.

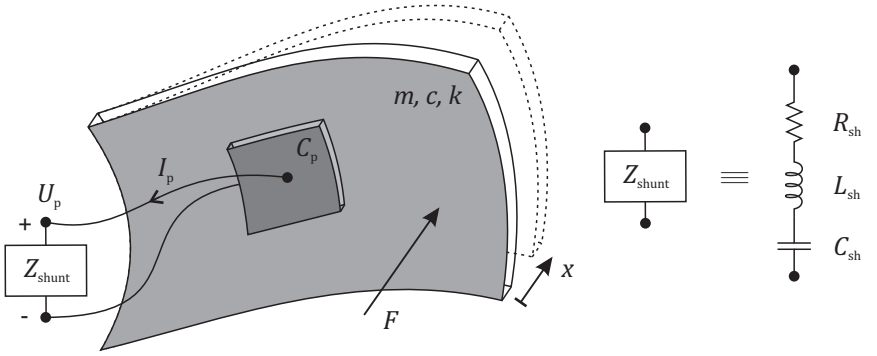

Figure 2.8. Principle of a shunted piezoceramic applied to a mechanical structure

One very important parameter in piezoelectric shunt damping is the generalized electromechanical coupling coefficient (K_{31} in the case of the d_{31}-effect, as from now called simply "GEMCC"). The square of the GEMCC physically describes how much mechanical energy is converted into electrical energy, and vice versa, at a given eigenfrequency of the system. As first introduced by [5], the GEMCC of a mode can be calculated using the piezoelectric material coupling coefficient k_{31}, as calculated in Eq. (2.7), together with the modal stiffness K of the structure and the modal stiffness K_{11}^E of the short-circuited piezoceramic, as shown in Eq. (2.10):

$$K_{31}^2 = \left(\frac{K_{11}^E}{K + K_{11}^E}\right)\left(\frac{k_{31}^2}{1 - k_{31}^2}\right) \tag{2.10}$$

It can be noticed that the GEMCC of the system depends not only on the piezoelectric material, but also on the ratio between the stiffness of the piezoceramic and the stiffness of the

total system. This indicates that a compromise must be found between these two values in order to obtain a sufficiently high GEMCC.

An alternative approach to obtain the GEMCC of a mode consists in considering the eigenfrequency of the structure when the electrodes of the piezoceramics are open ω_{open} and when they are short-circuited ω_{short}, obtained either by numerical or experimental means. The expression for the square of the GEMCC is then simplified and results in Eq. (2.11):

$$K_{31}^2 = \frac{\omega_{\text{open}}^2 - \omega_{\text{short}}^2}{\omega_{\text{short}}^2} \tag{2.11}$$

The GEMCC can also be calculated if an equivalent circuit of the electromechanical structure is available, e.g. the Van Dyke model presented earlier. In order to fulfill Eq. (2.11), the two eigenfrequencies can be indirectly obtained from the equivalent circuit through the impedance equation, e.g. Eq. (2.8). It is stated in [96] that, considering the impedance of the equivalent electrical circuit $Z_{\text{eq-circuit}}$, in the vicinity of the natural frequency of interest, there is a zero that represents the short circuit eigenfrequency ω_{short}, and there is a pole that represents the open circuit eigenfrequency ω_{open}. These eigenfrequencies can be identified on the magnitude and phase plot of the impedance, as depicted in **Figure 2.9**, and are calculated by Eq. (2.12) and Eq. (2.13):

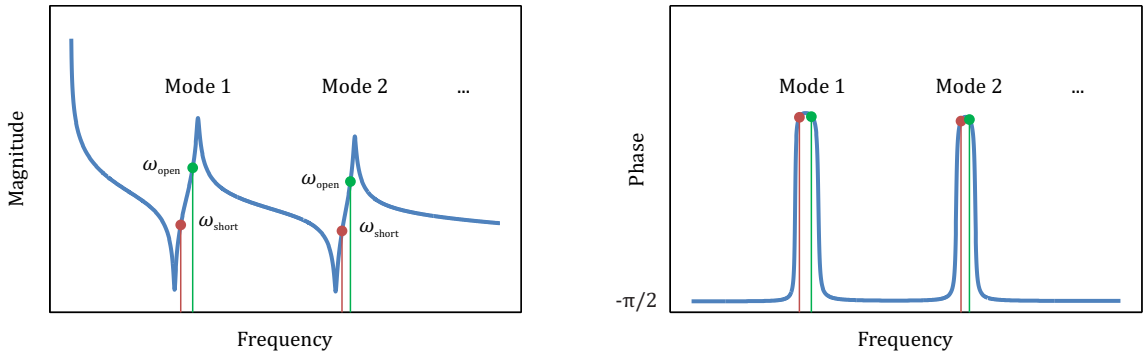

Figure 2.9. Magnitude and phase plot of the impedance of a piezoceramic structure

$$\omega_{\text{short}} = \text{Im}\left[\text{zero}(Z_{\text{eq-circuit}})\right] \tag{2.12}$$

$$\omega_{\text{open}} = \text{Im}\left[\text{pole}(Z_{\text{eq-circuit}})\right] \tag{2.13}$$

In the context of this thesis, the shunt technique will be mostly used to increase damping in systems with low inherent structural damping, hence the shunt damping term. More specifically, focus will be given to basic electrical components connected to the piezoceramic, such as resistors, capacitors and inductors.

The most elementary electrical circuit to reduce vibrations with a shunted system is the purely passive resistive shunt (*R*-shunt). It has been introduced in [5], where the analytical equations for the electromechanical system have been derived.

Additionally, the resistive resonant shunt (*RL*-shunt), in which an inductor and a resistor are connected to the piezoceramic, has been first introduced in [11] and later analytically formulated in [5]. Since the piezoceramic electrically behaves as a capacitor, the resultant *RLC* circuit is a damped resonant system, which can be tuned to a certain frequency, e.g. the eigenfrequency of the mechanical system, and therefore perform similarly to a mechanical tuned mass damper. This technique can be better applied on structures with a clear resonant vibration, since it has narrowband effectiveness. With respect to technical applications, the needed inductance value can be very high, maybe tens or hundreds of Henry. In order to avoid a bulky inductor component, a synthetic impedance has to be used, the so-called gyrator circuit [97], which generates the reciprocal of a passive element present in the circuit. Here, no power for actuation or signal processing is needed, but since the circuit needs a power supply, this technique is defined as semi-passive.

2.3.1 Negative capacitance

A piezoceramic material mainly behaves as a capacitor due to the unbalanced electric charges that appear on its electrodes when a mechanical strain is applied. The reciprocal effect results in an increase in the mechanical stiffness of the material when a charge is present. If a capacitor with a positive capacitance value is connected to the piezoceramic [98], the equivalent capacitance of the resultant parallel connection increases, and so does the mechanical stiffness. In the case of a piezoelectric structure, the resonance frequency can be therefore adjusted between the short circuit and the open circuit eigenfrequency.

In order to counteract this effect, a capacitor with a negative capacitance value can be connected to the transducer and thus reduce the equivalent capacitance. In this case, the negative capacitance behaves as a spring element with a negative stiffness, as evidenced by [99], where the elasticity of piezoelectric polymer films has been adjusted using a variable negative capacitance. The negative capacitance thus reduces the mechanical stiffness and consequently the eigenfrequency. Here, the resonance frequency can be adjusted between the short circuit eigenfrequency and theoretically zero. More precisely, as analytically described in [13], the eigenfrequency ω_{res} can be calculated as a function of the shunt capacitance using Eq. (2.14):

$$\omega_{res} = \omega_{short}\sqrt{\frac{1+\delta+\delta K_{31}^2}{1+\delta}} \tag{2.14}$$

where δ is the ratio between the inherent capacitance of the piezoceramic C_p and the shunt negative capacitance C_sh, as shown in Eq. (2.15):

$$\delta = \frac{C_\mathrm{p}}{C_\mathrm{sh}} \tag{2.15}$$

2.3.2 *RLC*-shunt circuit

In the case of the *RL*-shunt, the maximum attainable vibration reduction highly depends on the GEMCC, as indicated in [13]. A method of artificially increasing the GEMCC and therefore

partly getting rid of its dependency has been investigated in [19]. It is suggested that the use of a negative capacitance, together with a resistor and an inductor, i.e. a resonant negative capacitance, highly improves shunt damping performance, a fact that has been shown analytically and experimentally.

Moreover, if a negative capacitance is inserted into an *RL*-shunt, the two arising poles, characteristic of the absorption effect of the *RL*-shunt, spread away from each other, making this application efficient in a broader frequency range. Another advantage is that the needed optimal inductance value is much smaller compared to the value of a pure *RL*-shunt. It can be therefore enough to use a physical coil and eliminate the non-trivial design of a gyrator circuit.

In contrast to other techniques, the shunt damping using a negative capacitance transmits external energy in form of actuation forces to the host structure, still without the need of sensor information. It is therefore defined as semi-active.

For an optimal vibration reduction, the appropriate values for the shunt resistance R_{sh}, shunt inductance L_{sh} and the negative capacitance C_{sh} must be chosen. With a similar approach used in mechanical vibration absorbers, a tuning method for an optimal *RLC*-shunt has been analytically derived first in [13] and further developed in [14]. The latter uses a slightly modified GEMCC that takes into account the open circuit eigenfrequency as reference and is applied exclusively to this tuning method, as shown in Eq. (2.16):

$$K_{31}^2 = \frac{\omega_{\mathrm{open}}^2 - \omega_{\mathrm{short}}^2}{\omega_{\mathrm{open}}^2} \tag{2.16}$$

By tuning the absorption frequency of the shunt circuit close to the resonance frequency of the mechanical structure, i.e. by varying the value of L_{sh}, the frequency response function will show two resonance peaks, as depicted in **Figure 2.10**.

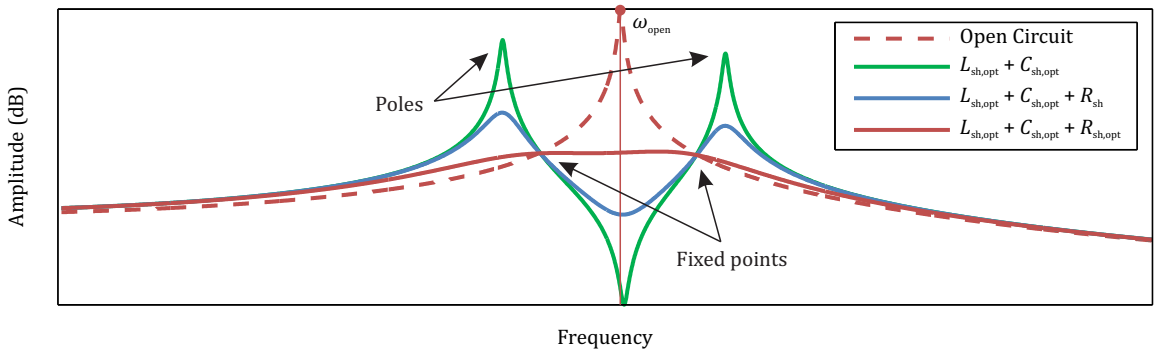

Figure 2.10. Mechanical response when tuning an optimal resonant negative capacitance

The optimal inductance can be calculated by Eq. (2.17):

$$L_{\mathrm{sh,opt}} = \frac{1 + \delta_{\mathrm{opt}}}{C_{\mathrm{p}}\omega_{\mathrm{open}}^2} \tag{2.17}$$

where δ_{opt} is defined in Eq. (2.18):

$$\delta_{\mathrm{opt}} = (2K_{31}^2 - 1)\beta \tag{2.18}$$

and β is introduced in this thesis as the safety margin to the stability boundary and can range between 0 and 1. When tuning the negative capacitance, it is advisable to keep a safe distance from the theoretical limit, especially in experimental analyses, to prevent instabilities due to uncertainties in the parameters.

By varying the damping resistance R_{sh}, two fixed points can be observed where the amplitude is independent from its value. The optimal damping is calculated by flattening out the amplitudes at the two fixed points to the same level, which leads to an optimal resistance value calculated in Eq. (2.19):

$$R_{\mathrm{sh,opt}} = K_{31}\sqrt{\frac{2L_{\mathrm{sh,opt}}}{C_{\mathrm{p}}}} \tag{2.19}$$

The value of the negative capacitance has to be correctly chosen in order to achieve optimal vibration attenuation and guarantee stability of the system and is calculated by Eq. (2.20):

$$C_{\mathrm{sh,opt}} = \frac{C_{\mathrm{p}}}{\delta_{\mathrm{opt}}} \tag{2.20}$$

2.3.3 Negative impedance converter

State-of-the-art techniques in semiconducting materials show that passive components with negative capacitance values do exist under certain conditions, but can only reach the lower nF range, as discussed in [100]. Since values needed for mechanical structures lie beyond this range, the only possible way to obtain such a component is to use a synthetic impedance.

The circuit shown in **Figure 2.11** has been first published in [101] and later in [102]. Its usage covers several applications in electronics, such as the Howland current source [103] and the Wien-Bridge oscillator [104]. When designed to meet certain requirements, the same circuit layout can be used to create a general class of circuits known as negative impedance converter (as from now called simply “NIC”). It creates an input impedance that is comparable to an ideal negative capacitance with a series resistance. The NIC is a relatively simple yet tricky circuit based on an operational amplifier (as from now called simply “op-amp”) that performs a sign change of a passive element, in this case, a capacitor.

To derive the input impedance of the NIC in the Laplace domain, basic circuit analysis [105] has been used. The input voltage of the NIC V_{in}, the voltages at the inverting V_{n}, the non-inverting V_{p} and the output V_{out} terminals of the op-amp have been defined relative to ground.

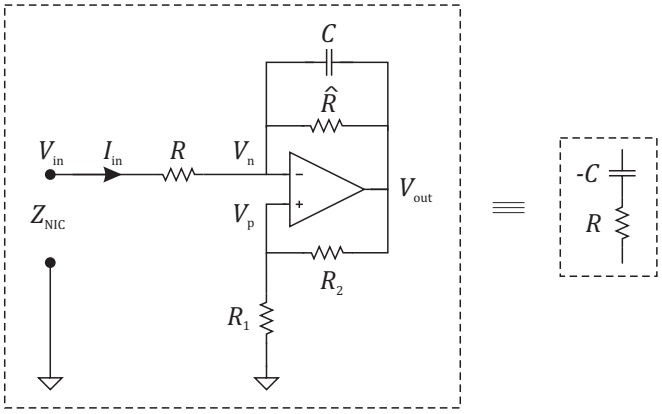

Figure 2.11. Negative impedance converter

The voltage divider for the inverting branch is represented in Eq. (2.21):

$$\frac{V_{\text{in}} - V_{\text{n}}}{V_{\text{n}} - V_{\text{out}}} = R\left(sC + \frac{1}{\hat{R}}\right) = \alpha_1 \tag{2.21}$$

The voltage divider for the non-inverting branch is represented in Eq. (2.22):

$$\frac{V_{\text{p}}}{V_{\text{out}}} = \frac{R_1}{R_2 + R_1} = \alpha_2 \tag{2.22}$$

The output voltage V_{out} of the op-amp depends on its open-loop gain A_{d} and on the voltage difference between the non-inverting and inverting terminals, as expressed in Eq. (2.23):

$$V_{\text{out}} = A_{\text{d}}(V_{\text{p}} - V_{\text{n}}) \tag{2.23}$$

In an ideal op-amp, the inverting and the non-inverting terminals draw no current and the open-loop gain A_{d} is infinite. In a real op-amp, however, the open-loop gain and phase vary with many conditions, such as output load and polarity. A precise measurement of this function can be very costly but some approximate plots can be found in datasheets. In order to simplify the analysis, a first order transfer function can be used to model the behavior of the op-amp in the lower frequency range [106], as described in Eq. (2.24):

$$A_{\text{d}} = \frac{A_{\text{ol}}}{s/\omega_{\text{co}} + 1} \tag{2.24}$$

where A_{ol} is the open-loop voltage gain and ω_{co} is the cutoff frequency, which are internal characteristics of the op-amp and can be found in any datasheet.

Rearranging the equations, the ratio between the output voltage of the op-amp and the input voltage of the NIC is shown in Eq. (2.25):

$$\frac{V_{\text{out}}}{V_{\text{in}}} = \frac{-A_{\text{d}}}{1 + \alpha_1 + A_{\text{d}}(\alpha_1 - \alpha_1\alpha_2 - \alpha_2)} \tag{2.25}$$

Finally, the input impedance of the NIC is represented in Eq. (2.26):

$$Z_{\mathrm{NIC}}(s) = \frac{V_{\mathrm{in}}}{I_{\mathrm{in}}} = \frac{R(\alpha_1 + 1)}{\alpha_1 \left(1 - \frac{V_{\mathrm{out}}}{V_{\mathrm{in}}}\right)} \tag{2.26}$$

Considering the case of an ideal op-amp, as thoroughly investigated in [24], the equation is simplified and shown in Eq. (2.27):

$$Z_{\mathrm{NIC}}(s) = -\frac{R_1}{R_2} \frac{1}{sC + 1/\hat{R}} + R \tag{2.27}$$

2.3.4 Stability analysis

As investigated in [13] and in [14], when the absolute value of the negative capacitance tends to the inherent capacitance of the piezoceramic, the determinant of the stiffness matrix of the electromechanical system tends to zero. In this case, the resonance frequency can be drastically changed and the system becomes very sensitive and eventually unstable. The stability boundary condition [14] defines the range of safe δ values that can be chosen and is shown in Eq. (2.28):

$$\delta > \delta_{\mathrm{crit}} = (K_{31}^2 - 1)\beta \tag{2.28}$$

In this sense, the actual resonance frequency cannot be reduced to zero and the critical resonance frequency attainable by the system can be calculated by substituting Eq. (2.28) in Eq. (2.14) leading to Eq. (2.29):

$$\omega_{crit} = \omega_{short} \sqrt{1 + \frac{\beta(K_{31}^2 - 1)}{\beta + (1 - \beta)/K_{31}^2}} \tag{2.29}$$

As previously mentioned, a negative capacitance can significantly improve the performance of an *RL*-shunt. Nevertheless, if not tuned correctly, it can destabilize the system. Even though the maximum attenuation using an *RLC*-shunt depends very little on the GEMCC, in contrast with the *RL*-shunt, a small value of GEMCC leads to an optimum negative capacitance value that lies very closely to the stability boundary, as evidenced by Eq. (2.18) and Eq. (2.28).

Besides the stability of an ideal negative capacitance connected to an electromechanical system, the stability of the NIC circuit itself must be taken into account. Since the op-amp is used with both positive and negative feedback, the circuit is potentially unstable and precaution must be taken. Furthermore, when connected to capacitive loads such as piezoelectric transducers, the op-amp may behave in undesirable ways and the circuit must be designed following certain rules, as described in [107] and in [108].

First, a suitable op-amp and the right component values must be chosen, not only to obtain the desired negative capacitance, but also to assure stability in a defined frequency band under normal operation conditions. Furthermore, if components are not designed properly, the circuit can be unstable under certain special conditions, e.g. when using a probe to measure the

voltage in the circuit. In this case, the finite impedance of the probe is taken into account in the feedback loop of the op-amp and can potentially destabilize the circuit.

Second, the physical construction of the circuit often requires more components than it is shown in **Figure 2.11**, which can influence the performance and therefore the stability of the circuit. The external power supply must be regulated [109], protected against voltage peaks through transient voltage suppressors and bypassed by appropriate capacitors [110]. It is also advisable to protect the input and output terminals of the op-amp with fast recovery diodes. If not already included in the op-amp, a circuit for external compensation [111] and current limiting might also be necessary. An example of a real circuit implementation is described in Appendix A. After following all design guidelines, if the circuit still does not perform as predicted or has stability problems, a systematic analysis might be necessary, as described in [112].

Furthermore, for a given piezoceramic displacement, the generated voltage with an *RLC*-shunt is much higher than with an *RL*-shunt. The op-amp must hence be able to withstand potentially high voltages and currents, otherwise saturation and non-linear effects will destabilize the circuit.

Several studies have been carried out using the NIC with shunt damping, but robust circuit design guidelines are yet to be explored. The work developed in [24] uses a closed-loop transfer function analysis to show that the circuit parameters must be chosen in a certain way to obtain stability for the complete electromechanical system. It is important to keep in mind that the mechanical structure, together with the piezoceramic and the shunt circuit, contribute with poles and zeros to form a single control loop. The overall performance and stability depend on each of them, so an understanding of the complete system is crucial when designing a smart structure with shunt damping. In this sense, an analysis of a global transfer function can indicate whether the final response is stable or not. One possible criterion is the phase margin, which can be obtained from the Bode plot of a transfer function. It is defined as the difference between the phase, measured in degrees, and +180°, at a frequency where the gain is equal to 0 dB. A negative phase margin ensures a proper non-oscillatory behavior of the transfer function, whereas a positive phase margin indicates instability issues. In control systems, the phase margin is typically designed to achieve between -30° and -60° for the best performance. Even though precise conditions for the tuning of parameters in the electromechanical transfer function have been derived, an empirical fine tuning is still needed in some cases.

3 Numerical modeling

This chapter presents the details of the numerical model of a laminate composite structure and also a piezoceramic plate. The analytical representation of the shunt circuit is also described, together with an experimental validation. Moreover, the electromechanical equation of motion of the coupled system is derived. Finally, the simultaneous optimization approach of both structure and shunt circuit is introduced and the software interface is explained.

3.1 Composite structures

Laminate composite structures are modeled with the finite element method using the software ANSYS Composite PrepPost. It is based on the classical laminate theory and facilitates the mechanical analysis using numerous variables.

The construction of a laminate structure model follows the basic guidelines of its real manufacturing. Initially, the material of a single ply must be defined. Prepregs of common materials such as carbon or glass fiber usually present orthotropic behavior. Appendix B shows the complete matrices of elastic material properties that will be used throughout this study. These values come from manufacturer data and experimental analyses and have been well established for linear vibration problems. Afterwards, the base surface of the structure must be drawn, on top of which the plies will be laid. The plies with a specified thickness and fiber orientation are then stacked on top of each other.

Once the resultant geometry and stacking sequence is obtained, the structure is meshed. The geometry can be modeled with a two-dimensional 8-node shell mesh, namely *"shell281"*, which is suitable for analyzing thin to moderately-thick shell structures. In some cases, the use of a three-dimensional 20-node solid mesh, namely *"solid186"* might be necessary. If the three-dimensional mesh is used and each ply is individually meshed, the contact between two plies is modeled with the pair *"conta174"* and *"targe170"*.

After the meshing process, the solver internally calculates the equivalent material properties of the laminate, generally in the form of an anisotropic matrix, and solves the partial differential equation governing the linear vibration movement.

The post-processing capabilities of the software are also relevant, especially the ply-wise strain and stress analysis and the embedded Puck failure criterion calculation. If the material constants are known, the reserve factor can be easily obtained and the weak areas of the laminate can be therefore analyzed.

3.2 Piezoelectric ceramics

Piezoceramic transducers are included in the finite element model as solid elements, usually in the form of rectangular plates, in which one dimension is much smaller than the others. The most common type of transducers uses the d_{31}-effect, so the local coordinate system is oriented in such a way that the polarization direction is along the 3-axis. Both top and bottom

surfaces of a single plate are individually equipotential, i.e. both electrodes are defined over the complete surface.

In ANSYS, the linear constitutive equation of a piezoelectric material is embedded in a 20-node solid element, namely *"solid226"*. An APDL code has been written to include the piezoceramic material characteristics in the model, such as the compliance, strain and permittivity matrices. In Appendix C, material descriptions of two types of piezoceramics provided by the manufacturer are presented.

In the finite element model of a piezoceramic, the mechanical degree of freedom is the displacement, the electrical is the voltage and the electrical exciting force is the electric charge. When the transducer is bonded to a structure, the contact between both meshes is modeled using the pair *"conta174"* and *"targe170"*, which is suitable to connect two deformable surfaces.

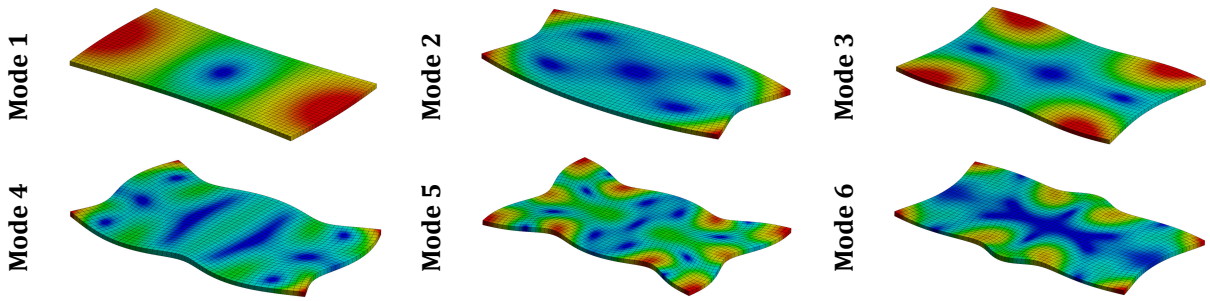

Figure 3.1. Mode shapes of a piezoceramic plate

In order to validate the numerical model of a piezoceramic, a comparison with experimental results has been made. A mechanically free plate of dimensions 50 x 30 x 1 mm made from the material PIC255 has been simulated using a finite element model. The calculated "static" capacitance is equal to 23,2 nF, against a measured value of 24,6 nF, which represents a -5,7 % error and shows a good agreement in the free condition. A numerical modal analysis has also been carried out. **Figure 3.1** shows the mode shapes of the first six eigenfrequencies with a significant GEMCC, i.e. $K_{31}^2 > 0$. It can be noticed that all deformations are in-plane.

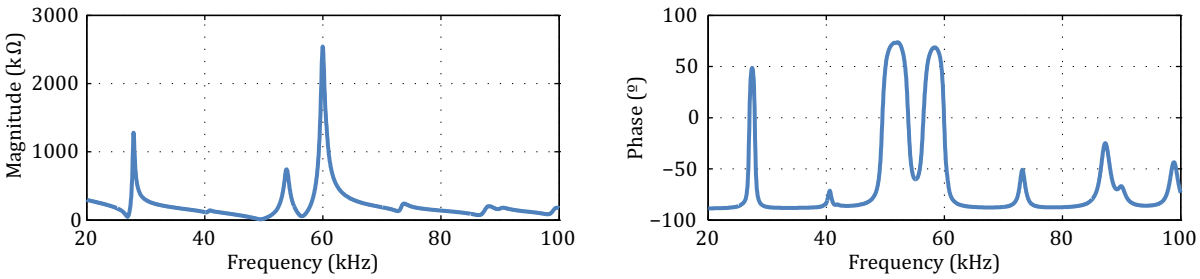

Figure 3.2. Impedance measurement of a piezoceramic transducer

For the experimental analysis, the same piezoceramic plate has been used. The electrical impedance over a frequency range was measured. By using this method, since the input excitation is in the electrical form, only the eigenfrequencies with a significant K_{31}^2 appear. **Figure 3.2** shows the impedance measurement results in the range 20-100 kHz, in the form of magnitude and phase.

Table 3.1 shows the first six short circuit eigenfrequencies of the piezoceramic plate obtained by the numerical analysis, as well as the values obtained by the impedance measurement. It can be noticed that the relative error is small and the simulation is hence assumed to be reliable. The simulated values for K_{31}^2 are also shown.

Table 3.1. Piezoceramic plate eigenfrequencies

Mode	K_{31}^2 (%)	Simulation (kHz)	Measurement (kHz)	Error (%)
1	5,035	27,615	27,450	0,60
2	0,339	41,016	40,610	1,00
3	7,232	51,532	51,520	0,02
4	3,553	58,790	58,420	0,63
5	0,977	73,731	73,180	0,75
6	1,553	87,810	87,240	0,65

3.3 Shunt circuit

The shunt circuit is modeled in the form of an electrical impedance. Its analytical representation in the Laplace domain is done using a script written in MATLAB®. In the case of a series *RLC*-shunt, where ideal components and their constitutive equations are considered, the shunt impedance is given by Eq. (3.1):

$$Z_{\text{shunt}}(s) = R_{\text{sh}} + sL_{\text{sh}} + \frac{1}{sC_{\text{sh}}} \tag{3.1}$$

On the other hand, when introducing a real circuit implementation, e.g. the NIC, the capacitive part should be replaced by Eq. (2.27). In order to validate the latter, a comparison with an impedance measurement has been made. **Table 3.2** shows the component values that have been used to calculate the impedance of the NIC and that have been set up in a real circuit implementation for the measurement. Two values of the series resistor have been chosen for comparison, a low 100 Ω and a higher 4 kΩ.

Figure 3.3 shows the comparison between the analytical representation of the impedance of the NIC circuit alone, given by Eq. (2.27), and its measurement. Moreover, the impedance of an ideal negative capacitance has been plotted, which is calculated by Eq. (3.2):

$$Z_{\text{ideal}} = -\frac{1}{Cs} \tag{3.2}$$

Table 3.2. NIC component values for impedance measurement

Component	Value	Unit
R	100 or 4000	Ω
R_1	920	Ω
R_2	1000	Ω
$\hat{R}$	10	MΩ
C	36	nF

It can be noticed that, for a low R value, the analytical impedance predicts well the measured curve. However, it has to be mentioned that the NIC circuit only behaves as an ideal negative capacitance in a limited frequency band, in this case below 1 kHz approximately, where the phase is around +90°. At higher frequencies, the NIC does not represent an ideal negative capacitance and the use of Eq. (2.27) is therefore necessary.

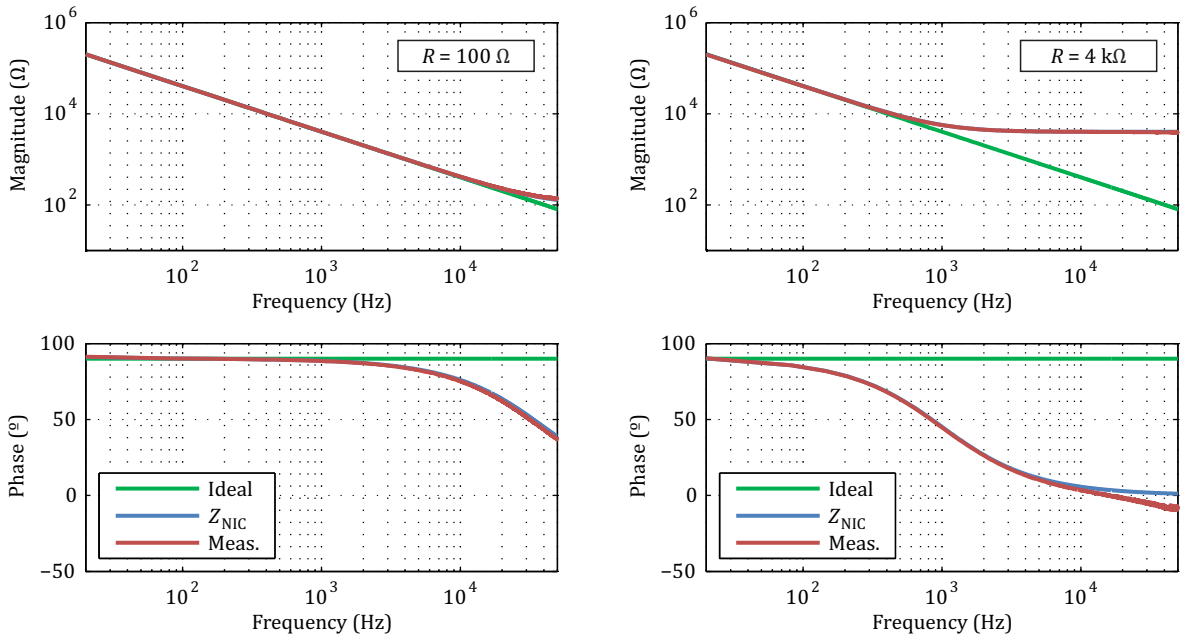

Figure 3.3. NIC impedance: Measurement *vs.* calculation for two different R values

For a higher R value, the frequency band where the NIC circuit behaves as an ideal negative capacitance is reduced, in this case below 100 Hz. Furthermore, at higher frequencies, the analytical equation is not able to predict the measured impedance. This is due to the non-ideal characteristic of the op-amp, which adds extra poles and zeros to the transfer function. A further analysis is outside the scope of this thesis.

3.4 Coupled system

Dynamic analyses using finite element simulations usually require a high computational effort, depending on the complexity of the structure and frequency range. In order to avoid these costly simulations and simplify post-processing calculations, a single degree of freedom model has been developed to represent a mechanical structure with piezoceramic transducers, so that, in the end, an arbitrary shunt circuit can be included.

Considering the vibration of a structure with multiple degrees of freedom, the equation of motion is represented by Eq. (3.3):

$$M\ddot{q} + C\dot{q} + Kq = F \tag{3.3}$$

where q is the mechanical displacement vector, M is the mass matrix, C is the damping coefficient matrix, K is the stiffness matrix and F is the excitation force vector.

A solution to the homogeneous form of Eq. (3.3) can be found in terms of eigenvalues and eigenvectors that satisfy Eq. (3.4):

$$(K - \lambda_i M)\Phi_i = 0 \tag{3.4}$$

where λ_i represent the eigenvalues and Φ_i, the eigenvectors for every mode i. The eigenvalues stand for the natural frequencies of the structure and the eigenvectors represent the deflected mode shape of a vibration mode.

Each mode is characterized by a modal mass and an effective mass, which is associated with different directions of vibration. Therefore, each mode can be interpreted as a single degree of freedom system oriented along a specific direction, where only the effective mass is the vibrating mass [113]. In order to calculate the effective mass, the generalized mass associated with each eigenvector has to be calculated using Eq. (3.5):

$$m_{\mathrm{gen},i} = \Phi_i^{\mathrm{T}} M \Phi_i \tag{3.5}$$

Afterwards, the modal participation factor $\Gamma_{k,i}$ for each mode i and for each direction k (k = 1 to 6) is calculated in Eq. (3.6):

$$\Gamma_{k,i} = \frac{\Phi_{k,i}^{\mathrm{T}} M_k}{m_{\mathrm{gen},i}} \tag{3.6}$$

The effective modal mass $m_{\mathrm{eff},k,i}$ of a given mode i and for a given direction k is defined as the square of the modal participation factor multiplied by the associated generalized mass, as written in Eq. (3.7):

$$m_{\mathrm{eff},k,i} = \Gamma_{k,i}^2 m_{\mathrm{gen},i} \tag{3.7}$$

Considering a structure with piezoelectric transducers, it is possible to investigate the single degree of freedom system by considering the preferred direction of the piezoelectric effect. In this case, the effective modal mass represents the equivalent vibrating mass of the structure, together with the transducers, along a specific direction.

Based on the single degree of freedom equation of motion that has been analytically derived in [13], it is possible to generalize the circuit that is shunted to the transducer through an electrical impedance, as can be seen in **Figure 3.4**.

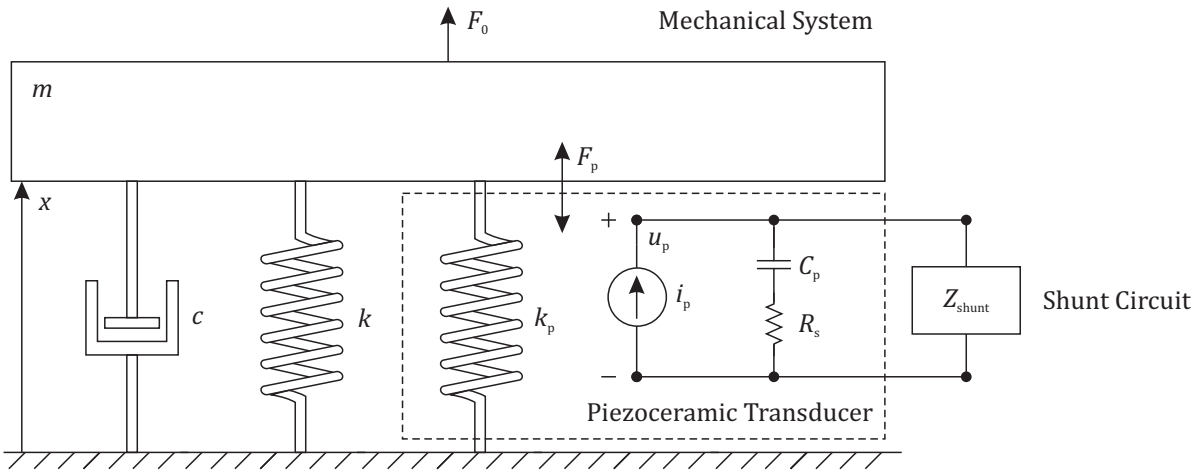

Figure 3.4. Single degree of freedom shunted electromechanical system

Consider the vibration motion of a mass m, which is the effective modal mass calculated in Eq. (3.7), connected to a spring of stiffness k, a damper of damping coefficient c and a piezoelectric element, which also has a mechanical stiffness k_p. The mechanical displacement x of the mass caused by a force F_0 can be written in the form of Eq. (3.8):

$$m\ddot{x} + c\dot{x} + kx + F_\mathrm{p} = F_0 \tag{3.8}$$

where the damping coefficient c can be obtained from the modal damping ratio ζ using Eq. (3.9):

$$c = 2\zeta\sqrt{km} \tag{3.9}$$

Due to the complexity of damping models in structural vibration, especially for laminate composite structures [114], the modal damping ratio ζ is usually obtained experimentally. If the amplitude of a measured frequency response function is available, the half-power bandwidth method can be used [115], as shown in Eq. (3.10):

$$\zeta = \frac{\omega_2 - \omega_1}{2\omega_\mathrm{n}} \tag{3.10}$$

where ω_n is the investigated eigenfrequency and ω_2 and ω_1 are the two neighboring frequencies that correspond to a 3 dB amplitude reduction, the so-called half-power frequencies.

In Eq. (3.8), F_p is the force generated by the piezoelectric element, which can be derived from the electromechanical constitutive equations of a linear piezoelectric material and is calculated in Eq. (3.11):

$$F_{\mathrm{p}} = k_{\mathrm{p}} x - k_{\mathrm{p}} d_{\mathrm{p}} u_{\mathrm{p}} \tag{3.11}$$

Here, u_{p} is the voltage generated by the piezoelectric element and d_{p} is the charge density per unit stress of the electromechanical system, as defined by [13], which can be obtained using Eq. (3.12):

$$d_{\mathrm{p}} = \frac{1}{k_{\mathrm{p}}} \sqrt{K_{31}^2 C_{\mathrm{p}} (k + k_{\mathrm{p}})} \tag{3.12}$$

The global stiffness of the system can be indirectly obtained using the vibrating mass m and the eigenfrequency of the structure when the electrodes of the piezoceramics are short-circuited ω_{short}, as defined in Eq. (3.13):

$$k + k_{\mathrm{p}} = m\omega_{\mathrm{short}}^2 \tag{3.13}$$

As mentioned before, the piezoceramic transducer can be electrically modeled as a current source i_{p} connected in parallel to a series *RC*-circuit of values R_{s} and C_{p}. The electric current generated by the transducer can be calculated using Eq. (3.14):

$$i_{\mathrm{p}} = -k_{\mathrm{p}} d_{\mathrm{p}} \dot{x} \tag{3.14}$$

Considering the external shunt circuit as a series *RLC*-circuit, where *C* is substituted by a NIC, Eq. (3.1) is modified and the shunt impedance in the Laplace domain $Z_{\mathrm{shunt}}(s)$ is represented by Eq. (3.15):

$$Z_{\mathrm{shunt}}(s) = R_{\mathrm{sh}} + sL_{\mathrm{sh}} + Z_{\mathrm{NIC}}(s) \tag{3.15}$$

Since the external impedance is connected in parallel to the internal *RC*-circuit of the piezoceramics, the equivalent impedance $Z_{\mathrm{eq}}(s)$ seen by the current source is given by Eq. (3.16):

$$\frac{1}{Z_{\mathrm{eq}}(s)} = \frac{1}{Z_{\mathrm{shunt}}(s)} + \frac{1}{R_{\mathrm{s}} + 1/sC_{\mathrm{p}}} \tag{3.16}$$

When combining Eq. (3.14) and Eq. (3.16), it is possible to obtain the final voltage U_{p} generated by the piezoceramic transducer in Eq. (3.17):

$$U_{\mathrm{p}}(s) = Z_{\mathrm{eq}}(s) I_{\mathrm{p}}(s) = -Z_{\mathrm{eq}}(s) k_{\mathrm{p}} d_{\mathrm{p}} X s \tag{3.17}$$

Considering the displacement X of the mass m and the voltage U_{p} as variables in the Laplace domain, substituting Eq. (3.11) into Eq. (3.8) and using Eq. (3.17), the dynamic behavior of the system is finally given by the electromechanical equation of motion represented in Eq. (3.18):

$$\begin{bmatrix} m & 0 \\ 0 & 0 \end{bmatrix} \begin{bmatrix} X \\ U_{\mathrm{p}} \end{bmatrix} s^2 + \begin{bmatrix} c & 0 \\ Z_{\mathrm{eq}} k_{\mathrm{p}} d_{\mathrm{p}} & 0 \end{bmatrix} \begin{bmatrix} X \\ U_{\mathrm{p}} \end{bmatrix} s + \begin{bmatrix} k + k_{\mathrm{p}} & -k_{\mathrm{p}} d_{\mathrm{p}} \\ 0 & 1 \end{bmatrix} \begin{bmatrix} X \\ U_{\mathrm{p}} \end{bmatrix} = \begin{bmatrix} F_0 \\ 0 \end{bmatrix} \tag{3.18}$$

In order to validate the analytical equation of motion, a dynamic forced response analysis has also been carried out using the numerical finite element method (FEM). A test structure with piezoceramics has been used in two configurations: When the electrodes are either open (O.C., $Z_{\text{shunt}} \to \infty$) or short-circuited (S.C., $Z_{\text{shunt}} = 0$). Since the numerical model has more than 100.000 nodes, each frequency step is solved within some minutes, whereas in the analytical model, the whole frequency range is solved within some seconds. The comparison results can be seen in **Figure 3.5**, where it is shown that, in the frequency range around the considered mode, the analytical equation of motion is able to correctly predict both frequency and amplitude of vibration.

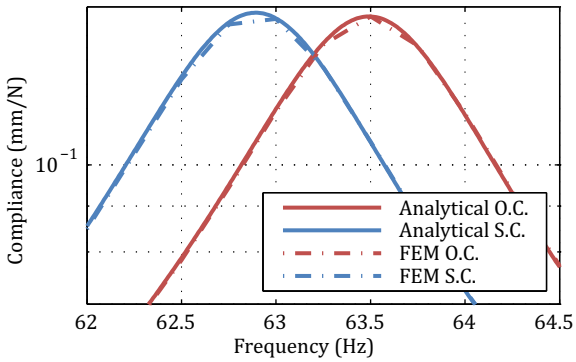

Figure 3.5. Vibration amplitude simulation: Analytical equation of motion *vs.* finite element

Once the voltage U_{p} generated by the transducer is available, in some analyses it might be useful to calculate the voltages across each component of the *RLC*-shunt. Using the principle of a voltage divider, the voltage across the inductor can be calculated using Eq. (3.19):

$$V_{L_{\text{sh}}} = U_{\text{p}} \frac{sL_{\text{sh}}}{Z_{\text{shunt}}} \tag{3.19}$$

and the voltage across the NIC can be calculated using Eq. (3.20):

$$V_{\text{in}} = U_{\text{p}} \frac{Z_{\text{NIC}}}{Z_{\text{shunt}}} \tag{3.20}$$

In this last case, if Eq. (3.20) is substituted into Eq. (2.25), the output voltage of the op-amp V_{out} can also be calculated. As already evidenced by [116], the performance of semi-active techniques is limited by the maximum output voltage the op-amp can withstand. This is hence a very important parameter when designing the shunt circuit. It is necessary to assure that no saturation occurs so that stability can be guaranteed.

3.5 Optimization approach

The effort to model laminate composite structures with complex geometries in analytical form is too high, so the use of finite element simulations is desired. Nevertheless, structural dynamic analyses of large finite element models are usually computationally expensive. To reduce the complexity of the mechanical structure, a simple model reduction method is used within the scope of this thesis. Only a single degree of freedom system is taken into account and the higher modes are truncated. The most important structural and piezoelectric parameters needed for the equation of motion Eq. (3.18) are reduced from the finite element model. This method presents good approximation and low computational cost.

On the other hand, the implementation of electrical circuits is not always possible in commercial finite element softwares. So in order to be able to simultaneously optimize a composite structure with piezoceramics and connected to a shunt circuit, an interface between the numerical and analytical simulations must be established.

A method that can be easily implemented, presents a good convergence and has not yet been applied in the context of shunt damping is the nested approach. Here, the structural optimization is used as the main process, whereas the shunt circuit optimization is used as the sub-process, as shown in **Figure 3.6**. For every structure Str_i calculated in the main optimization process, one optimization loop is performed to find the best shunt circuit $Sh_{i,n}$ that minimizes a chosen mechanical response, e.g. acceleration or velocity. The optimal combination of structure Str_{opt} and shunt circuit Sh_{opt} that satisfies the objective function is found in the main optimization process. This has been implemented using the ANSYS Workbench Platform, an automated workflow for multi-physics simulations that highly simplifies the process. The details of both the structural and shunt circuit optimizations are described next.

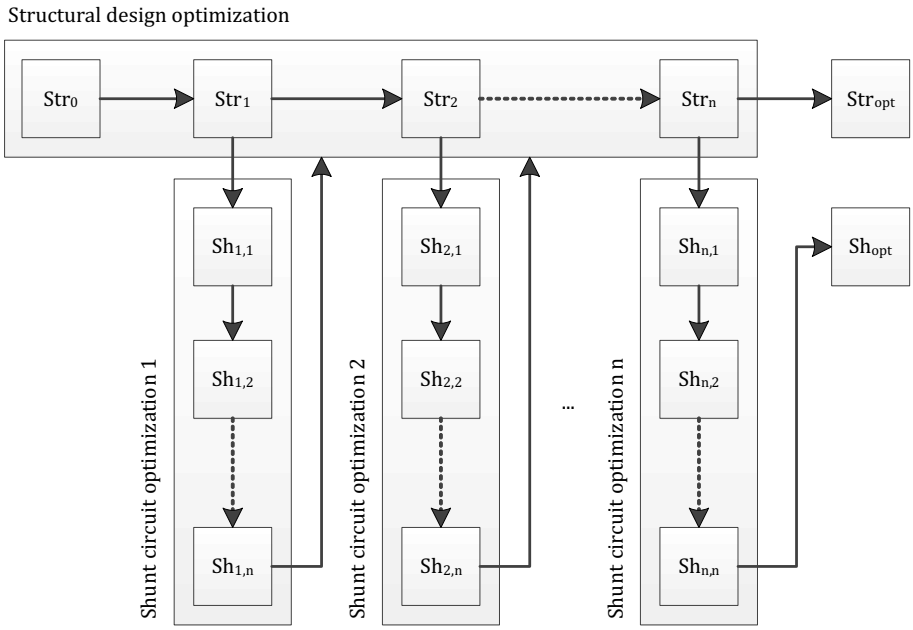

Figure 3.6. Nested approach for simultaneous optimization of structure and shunt circuit

3.5.1 Structural optimization

The optimization of the mechanical structure, together with the piezoceramic transducer, is also carried out using the ANSYS Workbench Platform.

In the design phase of the structure, it is possible to define geometric constraints, relations and parameters that play an important role for its mechanical properties and can be varied during the optimization. When a piezoceramic transducer is included, its dimensions and position are the most relevant input parameters in the design.

Additionally, in the case of laminate composites, other input parameters might be included, such as fiber material, ply type and thickness, number of plies and stacking sequence. For both discrete and continuous variables, high efforts are often required to define the intervals of interest before the optimization. In this sense, the engineering of a composite structure is an iterative process. This involves the evaluation of results and, in the case of an insufficient design or material failure, the geometry or laminate has to be modified and the evaluation is repeated. For this reason, when optimizing a composite part, a compromise must be found between several input and output variables, since a mathematical global optimum might be difficult to attain.

In the case of a structural optimization, several analyses can be carried out, although the most common concerning vibration problems are static, modal and harmonic analyses. The main output results that can be obtained include static stiffness, stress and strain levels in both structure and piezoceramic, eigenfrequencies, GEMCC, voltage and capacitance of the piezoceramic, composite failure reserve factor, among others.

After defining input and output variables, the finite element model is used to create a design of experiments, where a certain number of design points inside pre-defined boundary values are calculated. In the nested approach, the design points correspond to each structure Str_i and its associated optimal shunt circuit $Sh_{i,n}$. In order to achieve a more uniform space distribution of design points inside the boundaries, the optimal space-filling method [117] has been used, which maximizes the distance between points. With this method, the appropriate boundary values and the correct number of design points have to be chosen, otherwise the prediction of the response in the extremes can be of lower quality.

One of the oldest and most robust techniques for parametric optimization is the response surface method. Once the design points are calculated, a response surface is created by interpolating the results. Several techniques for function fitting exist, such as non-parametric regression [118] and neural networks [119]. The non-parametric regression does not consider any predetermined function and the surface is derived according to the data. A neural network algorithm is used to minimize the distance between the interpolation and the design points. In order to be reliable, this method requires a high number of design points. Both techniques have been successfully tested within this work.

In order to measure the quality of the interpolation, the goodness of fit can be used to describe how well the response surface predicts the observed design points. Using the coefficient of determination criterion, a value of 1 indicates that the interpolation line perfectly fits the data. The response surface also allows the analysis of the local sensitivity, i.e. the impact of input parameters on output parameters. The larger the value, the more significant is the role of the parameter.

The final step in the main optimization process is the definition of the objective function. Several objectives can be chosen, for both input and output parameters, such as minimization, maximization or target seek. The selection procedure of the best candidate is carried out using the multi-objective genetic algorithm [120], which is robust enough to consider tradeoffs between conflicting objectives and is able to find reasonable global optima in a population of points.

3.5.2 Shunt circuit optimization

The optimization of the *RLC*-shunt circuit is carried out using a script written in MATLAB®. For each given structure, the script performs one optimization loop to find the best circuit configuration that minimizes a chosen mechanical response. The script also reads the structural parameters from the design points needed for the shunt, namely the effective modal mass, piezoceramic capacitance, open and short circuit eigenfrequencies.

In order to start the optimization loop as close to the optimum as possible, the initial values for R_{sh} and L_{sh} are calculated using Eq. (2.19) and Eq. (2.17), respectively. C_{sh} is initially considered ideal and its value is calculated using Eq. (2.20). With this ideal value, it is possible to obtain the values of all five components in the NIC circuit using some design guidelines [24].

Experimental results showed that the capacitor C in the NIC circuit should be chosen as close as possible to the value of the capacitance of the piezoceramics C_{p}. Furthermore, $\hat{R}$ should be chosen as high as possible, usually in the kΩ or MΩ range. A stable NIC circuit that behaves as a negative capacitance should satisfy two further conditions, which are shown in Eq. (3.21) and Eq. (3.22):

$$\frac{R_1}{R_2} = \mu_1 \frac{C}{|C_{\mathrm{sh}}|} \text{ and } R = \mu_2 \frac{\hat{R}C/|C_{\mathrm{sh}}|}{1 + (\omega_r C_{\mathrm{p}} \hat{R} C/C_{\mathrm{sh}})^2} \tag{3.21}$$

$$\mu_1 < 1 \text{ and } \mu_2 > 1 \tag{3.22}$$

where C_{sh} is the negative capacitance that the NIC circuit should stand for and ω_r is the tuning frequency of the NIC circuit, at which its impedance has the phase equal to +90°. This value is usually chosen to be the short circuit eigenfrequency of a mechanical structure. The R_2 value can be arbitrarily fixed and is not subjected to any particular restrictions.

Using these assumptions, the number of input variables can be reduced, more specifically L_{sh} for the inductive part, and μ_1, μ_2 and $\hat{R}$ for the NIC. During the optimization loop, the impedance of the shunt circuit is integrated in the equation of motion of the coupled system, as described in Chapter 3.4. The objective function to be minimized is the maximum absolute value of the mechanical response, i.e. displacement, velocity or acceleration, over a determined frequency range. The optimization is implemented through the function *fmincon* using the interior point algorithm. This method solves a sequence of approximate minimization problems in a region constrained by boundary conditions and for this specific problem presents a fast local convergence. At the end of the optimization loop, Eq. (3.18) is solved and the phase margin of the resultant transfer function is calculated, so that the stability of the complete electromechanical system can be always guaranteed.

4 Piezoceramics integration

In this chapter, the physical integration of piezoceramic transducers into fiber-reinforced plastics is discussed. In order to evaluate the effectiveness of embedded piezoceramics, it is important to assess the characteristics of the coupled system before analyzing complex-shaped structures. To facilitate all analyses, several test coupons have been designed, manufactured and tested. **Table 4.1** sums up the numerical and experimental analyses that have been carried out and the main results that have been obtained for two different sets of coupons, using two types of boundary conditions. A special attention is given to the GEMCC, as it is the driving parameter in shunt damping applications.

Table 4.1. Analyses of coupons with integrated piezoceramics

	Glass fiber coupons		**Carbon fiber coupons**	
Boundary cond.	Free-Free	Clamped-Free	Free-Free	Clamped-Free
Simulations	Modal analysis	Forced response	Modal analysis	Modal analysis
Experiments	Impedance	Forced response	Impedance	Modal analysis
Results	K_{31}^2	Strain	Optimized K_{31}^2	Mode shape

4.1 Coupons design

In large structures with integrated d_{31}-piezoceramics, if the area of the transducer is small enough, a uniform plane stress state can be assumed, in which the largest strain in the piezoceramics occurs along axis 1. For that reason, the coupons have been designed in regard to their longitudinal extensional vibration.

They consist of a rectangular plate of dimensions 60 x 188 mm and variable thickness made of FRPs with unidirectional layers. The 0° fiber direction is longitudinally aligned. Several piezoceramic transducers are embedded in the coupons. They have dimensions of 50 x 30 mm with variable thickness and are made of the material PIC255. Copper wires connected to the transducers assure the electrical connection. In the case of a forced extensional test, 4 holes assure the mechanical connection on both sides. The transducers are centered in order to avoid border effects. The basic coupon layout is represented in **Figure 4.1**.

Two sets of coupons have been tested. The first set contains only glass fiber (GFRP) coupons and is used to analyze different integration patterns and test the manufacturing process. The second set contains carbon fiber (CFRP) coupons and is used to test the electrical isolation of the piezoceramic and validate the optimization procedure.

In the first set, four different integration patterns have been conceived. **Figure 4.2** shows the different cross-sections A-A that have been tested, where the orange color represents the piezoceramic transducer and the blue colors represent the glass fiber layers with two different orientations, +45° and -45°. In pattern 1, the layers around the transducer are discontinuous. Pattern 2 has both continuous and discontinuous layers that surround the piezoceramic, which represents a transition to pattern 3, where only continuous layers are present. In pattern 4, thinner transducers are used and continuous and discontinuous layers are alternated. An initial

study carried out in [121] has determined the right number of layers to be used in each pattern, so that all of them can have the same GEMCC with the same amount of piezoceramic material.

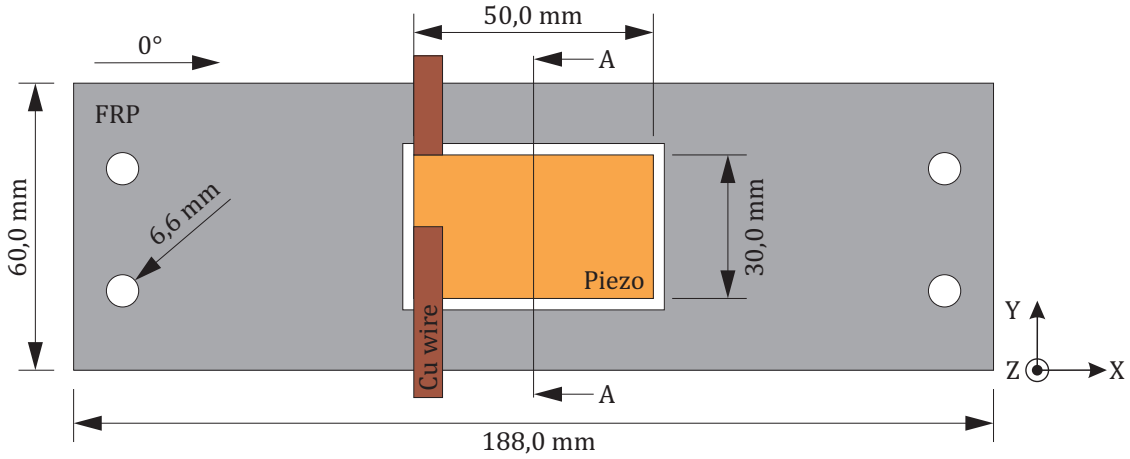

Figure 4.1. Coupon layout for piezoceramic integration evaluation

The transducers in patterns 1, 2 and 3 have a thickness of 1 mm each and in pattern 4, 0,2 mm. The polarization direction is the same for all piezoceramics and they are electrically connected in parallel. For all patterns, two different piezoceramic transducers have been tested: Monolithic piezoceramic plates and DuraAct patch transducers, both with the same amount of active material and using the d_{31}-effect.

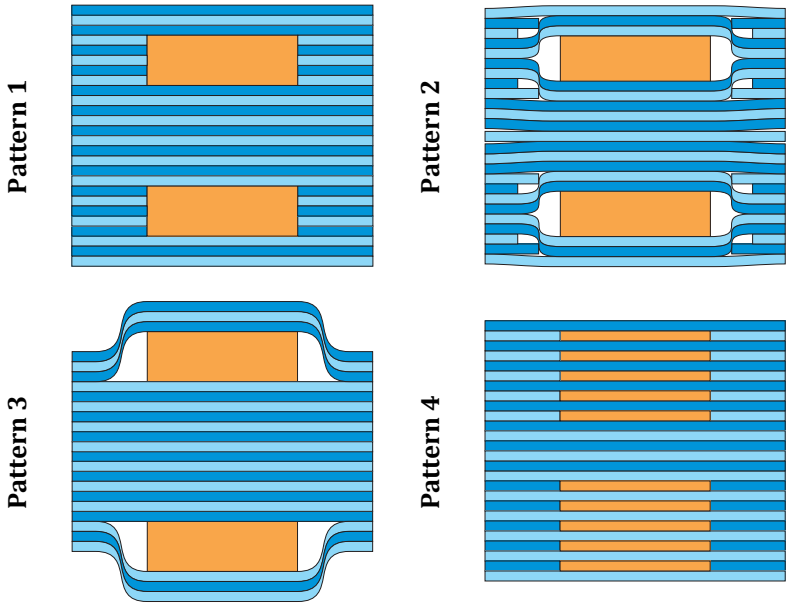

Figure 4.2. Integration patterns of glass fiber coupons

In the second set, two integration patterns have been investigated and are depicted in **Figure 4.3**. Both include three DuraAct patch transducers of 0,5 mm thickness (0,2 mm of active material). In pattern 5, the transducers are surrounded by continuous glass fiber layers, in order to guarantee electrical isolation, whereas the other layers are made of carbon fiber and are either continuous or discontinuous. In this pattern, the orientation of each layer is determined by a numerical optimization. The integration pattern number 6 consists of woven layers that are thicker than the transducers and can be either continuous (90°) or discontinuous (0°).

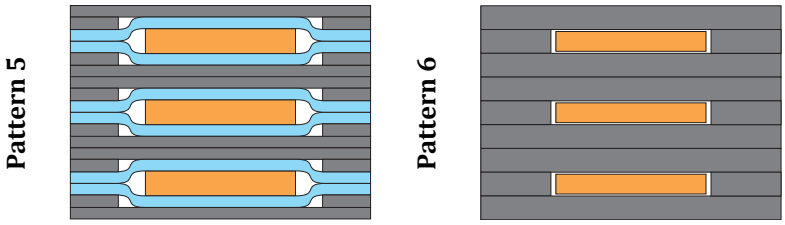

Figure 4.3. Integration patterns of carbon fiber coupons

4.2 Numerical analyses

Finite element simulations have been carried out with both glass and carbon fiber coupons. The GEMCC of the glass fiber coupon of pattern number 1 has been calculated using a modal analysis, whereas the strain distribution has been obtained using a forced response. The stacking sequence in the carbon fiber coupon of pattern number 5 has been optimized in order to maximize the GEMCC.

4.2.1 Glass fiber coupons

Among the glass fiber coupons in the first set, only patterns 1 and 2 have been analyzed using a finite element model, with the aim to verify the capability of the model to correctly predict the GEMCC, the strain distribution and the static strength. Patterns 3 and 4 have not been simulated and only measured data are analyzed, as discussed later.

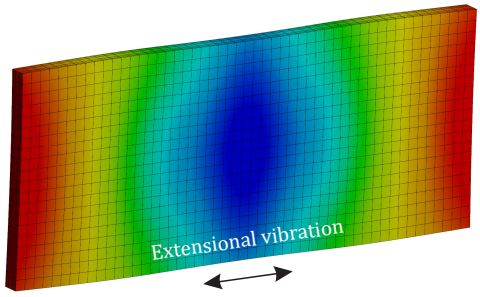

Figure 4.4. First extensional vibration mode of a glass fiber coupon

In a first analysis using pattern 1, the used material properties correspond to the hot pressing process, which are presented in Appendix B. Here, the coupon is mechanically free and two modal analyses have been carried out, one when the electrodes of the piezoceramics are open and another when the electrodes are short-circuited. Using Eq. (2.11), it is possible to calculate the GEMCC. As previously mentioned, the mode shape of interest is the longitudinal extensional vibration, as depicted in **Figure 4.4**. The simulated short circuit eigenfrequency in the free condition is equal to 8,212 kHz and the square of the GEMCC is equal to 1,905 %.

In a second analysis, the same coupon is mechanically clamped on one side and a tip mass of 0,622 kg is attached to the other. In the case of a mechanical test, this scenario better represents a mass-spring system. A force in the longitudinal direction is applied to the tip mass and a harmonic analysis is carried out. In this case, the open circuit eigenfrequency is equal to 1,273 kHz. The used damping ratio is equal to 1,2 % and comes from the experimental results presented later. The maximum elongation of the coupon at this frequency is equal to 5,6 µm/m/N at the tip.

It has been observed that the strain on the surface of the coupon follows a clear distribution, as shown in **Figure 4.5**. On the area SG1, where the piezoceramic is located, the calculated longitudinal strain is 3,6 µm/m/N. On the area SG2, where no transducer is integrated, the strain level is 7,7 µm/m/N. This value is two times higher and shows that the piezoceramic reduces the strain in the laminate on the area where it is integrated. It can be therefore concluded that the total dynamic load applied to the coupon is distributed between the piezoceramic and the composite material. The piezoceramic has in this case a double role: It works as a load carrying element and serves as a protection to the composite material. **Figure 4.5** also shows the calculated longitudinal normal stress of the piezoceramics, on average 0,28 MPa per applied unit force.

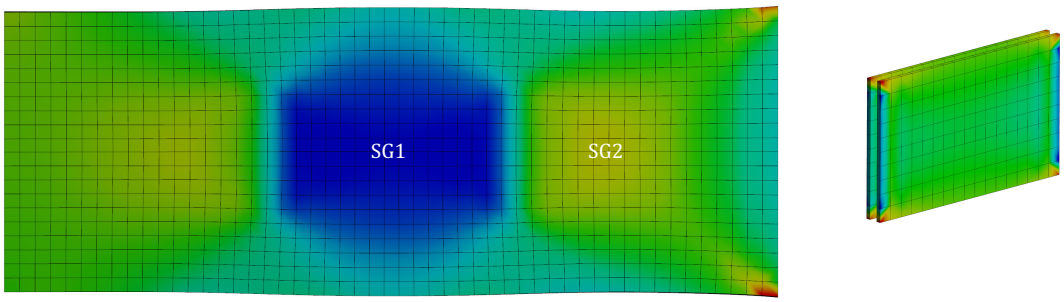

Figure 4.5. Strain on the glass fiber coupon (left) and stress in the piezoceramics (right)

At last, a numerical analysis with the coupons of patterns 1 and 2 has been carried out to compare their static strengths, when the electrodes of the piezoceramics are open. This is achieved by applying a constant tip elongation of 1 mm/m on both coupons and comparing the calculated Puck reserve factor. In this case, even though they have the same static stiffness and GEMCC, pattern 1 presents a reserve factor almost two times higher than pattern 2. This is due to the presence of a ply drop-off in pattern 2, a resin-rich area that induces stress concentration and thus reduces the static strength of the laminate.

4.2.2 Carbon fiber coupons

For the carbon fiber coupons, finite element models have also been created. The used material properties correspond to the vacuum bag process and the coupon is mechanically free. In pattern 5, the goal was to optimize the stacking sequence and improve the GEMCC. The orientations of all 18 layers have been defined as variable input parameters and the objective function was set to maximize the GEMCC. The optimization procedure presented in Chapter 3.5.1 has been applied. **Figure 4.6** shows the goodness of fit, which represents the quality of the response surface using the non-parametric regression. It can be seen that the response surface is able to predict the finite element model in a reliable interval for several outputs, such as the short circuit eigenfrequency, the failure reserve factor and the GEMCC. **Figure 4.6** also shows the local sensitivity of the GEMCC to the orientation of all layers of the coupon, layer 1 being at the bottom and 18 at the top. It can be noticed that layers 12 and 13 influence the GEMCC the most, since they are continuous layers and contribute with a high stiffness in the cross-section.

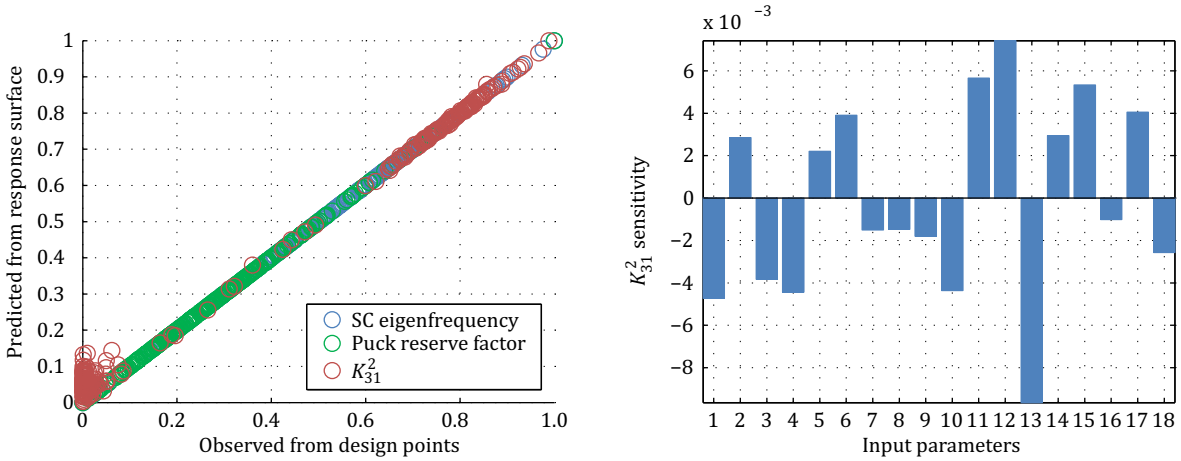

Figure 4.6. Carbon fiber coupon: Goodness of fit (left) and sensitivity (right) plots

Figure 4.7 shows a local representation of the response surface for the square of the GEMCC. It can be noticed that, for the two most sensitive parameters, i.e. the orientation of layers 12 and 13, there is a point that maximizes the response, even though the difference between the extremes are not so high. In this sense, the optimization approach is valid and a compromise must be found among all input and output variables.

The exclusive maximization of the GEMCC results in the following stacking sequence: [75/-15/55/70/90/-55/70/40/5/-75/-25/75/90/15/65/-75/-10/80], in degrees, starting from layer 1 to 18. With this configuration, the simulated short circuit eigenfrequency is equal to 8,798 kHz and the square of the GEMCC is equal to 3,586 %. The numerical results of pattern 6 indicate that this coupon has an eigenfrequency of 16,973 kHz and the square of the GEMCC is equal to 1,281 %.

A second analysis has also been carried out, where the coupon of pattern 5 is mechanically clamped on one side and a tip mass is attached to the other. The results are used to perform a model update, as discussed later in the experimental analyses.

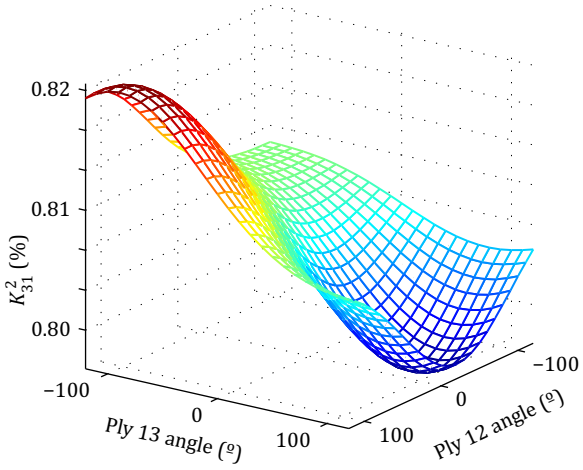

Figure 4.7. Carbon fiber coupon: Response surface of the coupling coefficient

4.3 Manufacturing

In order to assess the practical feasibility of integrating piezoceramic transducers inside laminate composites, several test coupons have been manufactured. For the first set, 3 pieces for each pattern of the glass fiber coupons have been manufactured, using both monolithic plates and DuraAct patch transducers, which results in 24 coupons. For the second set, 2 coupons of each pattern made of carbon fiber have been manufactured, using both types of transducers.

In the case of the monolithic piezoceramics, the electrical connections of the transducers were assured by use of a conductive adhesive copper foil (1181 Tape, 3M) that was applied on both electrodes and were long enough to provide an external connection to the coupon. In the case of the DuraAct patch transducers, an enameled copper wire (Ø 0,40 mm, BLOCK) was soldered to the terminals. In order to assure a better electrical isolation, the terminals were covered by a polyimide tape (1205 Tape, 3M) and locally protected by an acrylic coating spray (HPA200H, Electrolube).

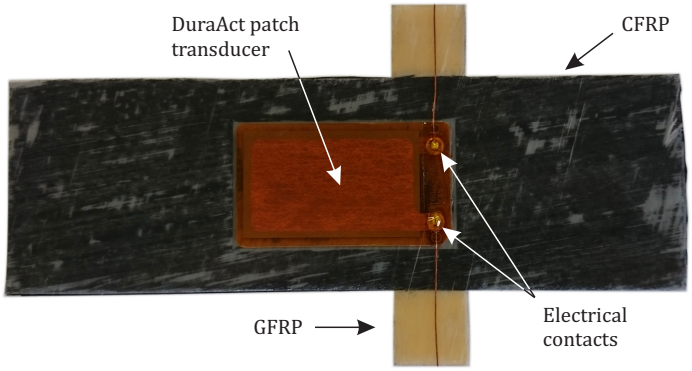

Figure 4.8. Stacking of FRP plies and DuraAct patch transducers

The coupons were manufactured by hand lamination and no considerable extra effort was needed in comparison to a normal lamination without piezoceramics, except for the number of steps. **Figure 4.8** shows the stacking of several FRP layers and the DuraAct patch transducers during the hand lamination.

So that the piezoceramics can still be functional after the manufacturing, it is important to assure that depolarization does not occur. For that, half of the Curie temperature should not be exceeded, so the coupons have been cured at a temperature of 80°C.

Two different manufacturing processes have been tested. Hot pressing was used for the glass fiber coupons of pattern 1, 2 and 4. Vacuum bag was used for glass fiber coupons of pattern 3 and also for the carbon fiber coupons.

Since there are no manufacturing standards for integrated piezoceramics, several new techniques have been experimented. Moreover, due to the high number of coupons produced, manufacturing problems were expected to occur and, to a certain extent, have been mastered and reduced. Nevertheless, experience showed that integrating transducers in laminate composites still represents a technological challenge.

In some coupons with the copper foil, its external portion was torn due to high pressure and electric contact was lost. This was solved by a vertical interconnect access (VIA) using a conductive rivet, the same technique used for multi-layer printed circuit electronic boards, as shown in **Figure 4.9**. Even though this solution recovered electric contact, it is not desired to have a mechanical failure in the composite material. Other coupons with the copper foil did not have electric contact because either the conductive adhesive was substituted by epoxy resin during curing, or there was a short circuit between two copper foils inside the laminate.

In some coupons with the monolithic plates, the most challenging problems were related to broken piezoceramics. Initially, it was thought that the thermal shrinking of the fibers after curing was generating stress levels inside the piezoceramics that would be able to damage them. By analyzing the capacitance values of the unharmed coupons, it is possible to conclude that the piezoceramics are indeed compressed. Moreover, a thermal simulation was carried out, since the thermal interaction among piezoceramics, carbon and glass fiber is not straightforward, as evidenced by the coefficients of thermal expansion presented in **Table 4.2**. Nevertheless, the simulation revealed that the stress levels are not high enough to break the piezoceramics.

Table 4.2. Comparison of different coefficients of thermal expansion

Direction	Coefficients of thermal expansion ($\times 10^{-6}$ K^{-1})			
	Steel	PZT	UD CFRP (55 %)	UD GFRP (55 %)
X	12,0	8,00	-0,50	5,50
Y	12,0	8,00	30,0	25,0
Z	12,0	-6,00	30,0	25,0

A more reasonable assumption is that the damaged piezoceramics are associated with a high pressure in the process and an uneven surface due to the electrical connections. **Figure 4.9** shows an X-ray photograph of broken piezoceramics inside one carbon fiber coupon with

monolithic piezoceramic plates. It can be noticed that all cracks have propagated in the area of application of the copper foil, due to an increased thickness of the cross-section. Moreover, one of the three piezoceramics seems to be displaced, probably due to resin flow during curing, which also indicates that the damage occurred when the resin was still liquid and is not related to thermal stresses during solidification.

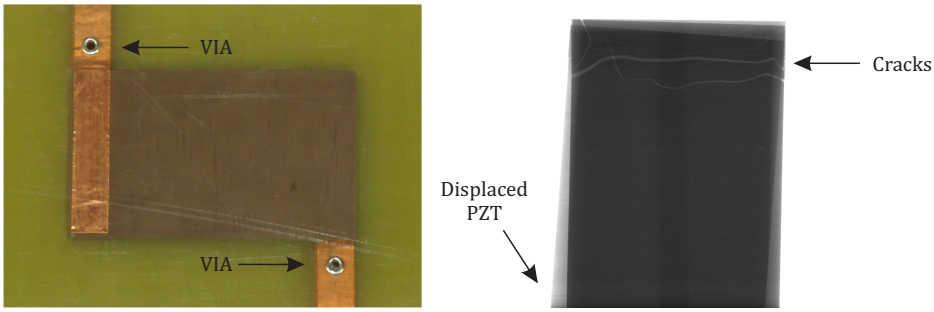

Figure 4.9. Vertical interconnect access (left) and X-ray of damaged piezoceramics (right)

4.4 Experimental results

Several tests have been carried out with the coupons in order to assess the manufacturing quality and the relevance of the integration pattern to the GEMCC. Initially, the coupons have been electrically measured, so as to assure that all transducers were functional and to calculate the GEMCC. Mechanical tests have also been carried out to update the numerical model and to verify the strain distribution on the surface of the coupons.

4.4.1 Electrical test

In order to check whether all coupons have been successfully manufactured, a simple electrical test was carried out. The "static" capacitance and resistance of the coupons were measured by an LCR-meter, at a frequency of 200 Hz, which is far below the first eigenfrequency. **Table 4.3** shows the average results for all coupons that were not damaged. Patterns 1, 2 and 3 are grouped together since no substantial difference has been observed. The capacitance and resistance values were also compared to the same quantities obtained for the piezoceramics in the free condition, measured before the lamination, and the deviation Δ has been calculated.

It is important to see that, in all coupons, the capacitance has dropped after curing. Taking benefit from the electrical and mechanical impedance analogy, this means that the mechanical stiffness has increased and that the piezoceramics have a residual compression stress, which is beneficial for ceramic material. Moreover, the DuraAct transducers suffer less change in comparison to the monolithic plates because they are already in a pre-stressed state. According to information from the manufacturer, the DuraAct patch transducers have an average pre-stress of approximately 45 MPa. Considering a linear behavior between stress levels and capacitance value, this would mean that piezoceramics manufactured in the coupons suffer an estimated additional pre-stress of 20-40 MPa. In relation to the carbon fiber coupons, the

reduction of the resistance indicates that the structural damping also decreased, in contrast to the glass fiber coupons.

Table 4.3. Measured capacitance and resistance from manufactured coupons

Pattern	$\bar{C}$ (nF)	$\bar{R}$ (Ω)	ΔC (%)	ΔR (%)
1-3 PZT Plate	36,9	310	-25	+38
1-3 DuraAct	38,7	285	-21	+11
4 PZT Plate	890	13,5	-25	+11
4 DuraAct	732	16,9	-14	+2,0
5 DuraAct	220	50,3	-15	-3,0
6 DuraAct	227	49,6	-12	-4,0

4.4.2 Impedance measurement

To investigate the influence of different integration patterns on the GEMCC, the impedance of the manufactured coupons has been measured. Each coupon is mechanically free and the electrodes are connected to an Impedance Analyzer, as shown in **Figure 4.10**. The device generates a sinusoidal voltage with increasing frequency and internally calculates the electrical impedance of the coupons.

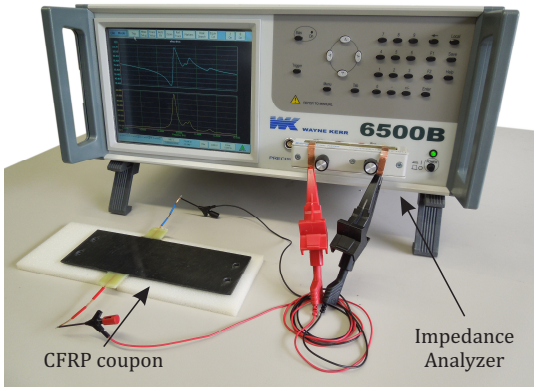

Figure 4.10. Experimental setup for the impedance analysis

Figure 4.11 shows the impedance measured from a coupon of pattern 1 and 6, in form of magnitude and phase. The first extensional vibration mode can be identified by the highest phase value, since it corresponds to the highest GEMCC.

In the nearby frequency range, it is possible to represent the impedance in the form of the Van Dyke equivalent circuit, as depicted in **Figure 2.6** (1), and fit the parameters of Eq. (2.8). **Figure 4.11** also shows the fitted impedance predicted by the equivalent circuit.

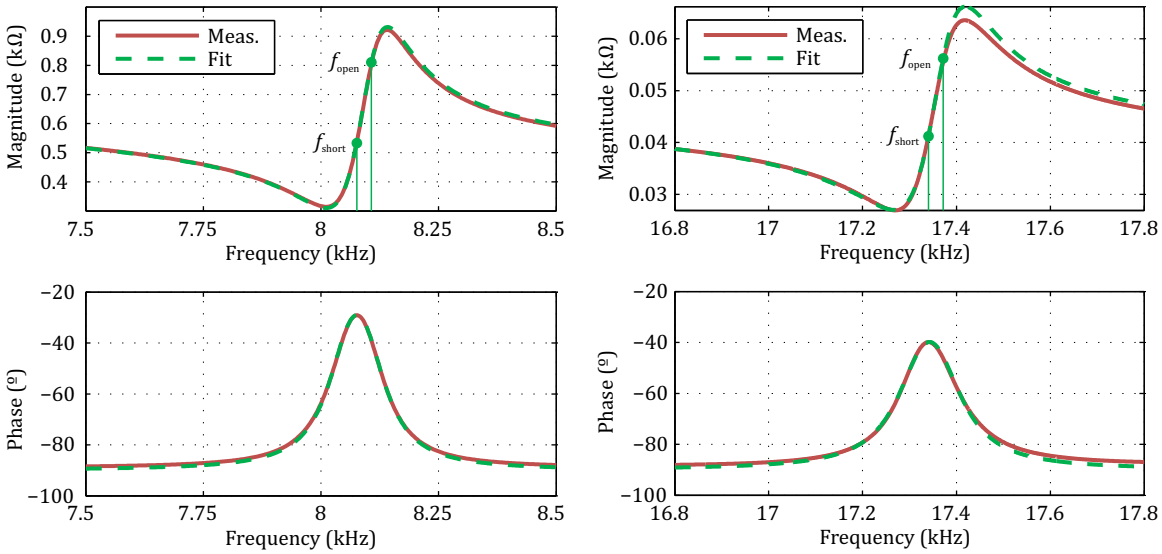

Figure 4.11. Impedance measurements from coupons of pattern 1 (left) and 6 (right)

In order to verify the quality of the theoretical prediction in comparison to the real measurement, the root mean square (RMS) error can be used to indicate how far on average the error is from 0. The RMS error between the measured and calculated discrete signals can be obtained according to Eq. (4.1):

$$\Delta_{\mathrm{RMS}} = \sqrt{\frac{1}{N}\sum_{i=1}^{N}\left|\frac{X_{i,\mathrm{calc}}}{X_{i,\mathrm{meas}}}\right|^2} \tag{4.1}$$

In the case of the carbon fiber coupon, the fit has not perfectly matched the measured impedance. One possible explanation could be a non-linear hysteresis effect in the piezoelectric material [122] that is not included in the impedance equation. Nevertheless, the RMS error of the magnitude is equal to 0,92 %, which indicates a good fit of the parameters.

The measured short circuit eigenfrequency of pattern 1 is equal to 8,043 kHz, a -2 % difference from the simulated value, whereas pattern 6 has an eigenfrequency of 17,340 kHz, a +2 % difference, which indicates that the finite element is precise enough to predict the eigenfrequency the coupons.

From the impedance curve it is possible to calculate the GEMCC. **Figure 4.11** qualitatively shows the identified open and short circuit eigenfrequencies calculated using Eq. (2.12) and Eq. (2.13). **Table 4.4** shows the square of the GEMCC measured for all coupons. For most patterns, all three manufactured coupons could be tested, so an average value has been calculated. First fact to be noticed is that there is a 35 % difference between the highest and lowest value among patterns 1-5, which indicates that the integration pattern can influence the energy conversion efficiency. Pattern 1 has a slight advantage over 2, which can be explained by the fact that straight plies transmit loads in a more regular way than curved plies. Patterns 1 and 2 seem to have an advantage over 3, but this is more likely to be explained by the manufacturing

process, where the fiber volume achieved is lower. In the case of pattern 4, several ceramics can reduce the GEMCC, due to a higher stiffness or misalignment, but they have a higher capacitance, which is desirable in some applications. It can also be noticed that, for a given pattern, there is no clear indication whether a monolithic piezoceramic plate is better than a DuraAct transducer, although the integration pattern influences both in the same degree. It can be therefore said that the use of DuraAct transducers is preferable due to the robustness in manufacturing.

Table 4.4 also shows the previously simulated values for patterns 1, 5 and 6. It has to be mentioned that the error between simulation and measurement comes from the fact that the bonding between ceramics and laminate is not perfect. In the numerical analysis, the bonding between ceramics and laminate is considered rigid and ideal. In reality, the so-called shear lag effect accounts for the loss in strain transmitted from the host structure to the transducer and vice versa as a result of the finite stiffness of the bonding layer. Both the transducer thickness and border effects have an influence. Furthermore, since epoxy resin has a viscoelastic behavior and it assures the contact between transducer and fibers, an efficient energy conversion is not assured, so the GEMCC is reduced. In the case of pattern 5, the measured value is much lower than predicted by simulation, since the parameters fit of the Van Dyke model was not perfect. Nevertheless, the simulation of pattern 5 shows that a much better GEMCC can be achieved if the stacking sequence of the laminate is optimized, even with less piezoceramic material, compared to the glass fiber coupons.

Finally, pattern 6 exhibits a 41 % reduction in the GEMCC compared to the average of all other DuraAct coupons. This is a strong evidence that the woven fibers are not the best option for integrating piezoceramic transducers. The woven plies do not have one definite direction in which the Young's modulus is higher and therefore the piezoelectric effect cannot be maximized in one preferred orientation.

Table 4.4. Measured GEMCC of coupons in the mechanically free condition

	Measured $\overline{K_{31}^2}$ (%)		Simulated K_{31}^2 (%)
Pattern	**PZT Plate**	**DuraAct**	**PZT Plate**
1	1,492	1,559	1,905
2	1,487	1,453	—
3	1,213	1,148	—
4	1,273	1,310	—
5	—	1,300	3,586
6	—	0,797	1,281

4.4.3 Modal analysis

A further analysis consisted in analyzing the carbon fiber coupon of pattern 5 in the clamped-free condition experimentally. An impact hammer and an accelerometer, together with an FFT analyzer, have been used to identify the first seven eigenfrequencies of the coupon, including the GEMCC in the new condition. **Figure 4.12** shows the main mode shapes. A special attention is given to mode number 7, the longitudinal extensional vibration. Since the optimal orientation of layers results in an asymmetrical laminate, and therefore highly anisotropic, the

extension movement is associated with a torsion. This has helped to increase the GEMCC because the transducer is extended in both in-plane directions.

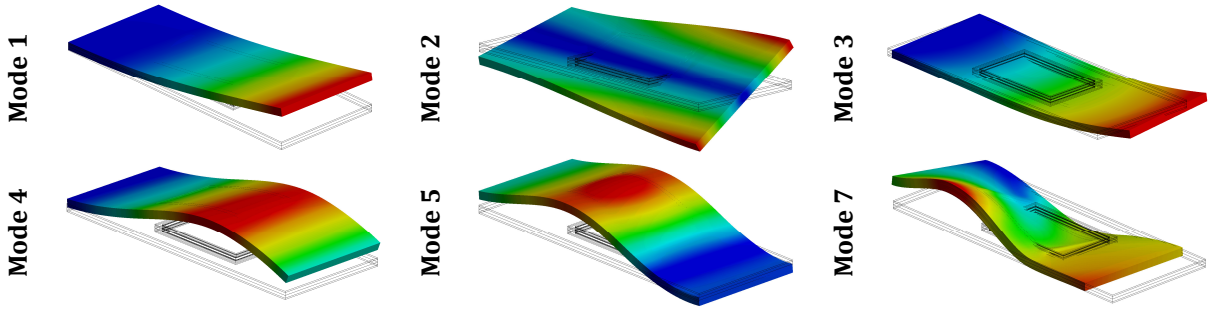

Figure 4.12. Mode shapes of the carbon fiber coupon of pattern 5

In order to verify that the numerical model of a piezoceramic transducer integrated in a laminate composite is able to correctly predict the main phenomena previously discussed, the results of this test were used to update the model. Three parameters have the most relevant influence on the elastic behavior of the coupon: The laminate material properties, the stiffness of the clamp and the contact of the piezoceramics and the composite. In order to better represent the latter, an elastic bonding was introduced in the contact between all surfaces of the piezoceramics and the composite through a stiffness coefficient factor (SCF).

To update the numerical model, a fitting has been performed similarly to the optimization procedure from Chapter 3.5.1. The input parameters were 1) the material properties, 2) a six degree of freedom stiffness at the clamp and 3) the stiffness coefficient factor. The objective function was to fit 1) the measured eigenfrequencies and 2) the GEMCC of mode 7. **Table 4.5** shows the translational and rotational stiffnesses of the clamp that have been found by the numerical fit. The stiffness coefficient factor is also represented.

Table 4.5. Updated clamp stiffness and stiffness coefficient factor of piezoceramics

Description	Value	Unit
X-stiff.	$4{,}250 \times 10^{5}$	N/mm
Y-stiff.	$7{,}396 \times 10^{3}$	N/mm
Z-stiff.	$8{,}250 \times 10^{2}$	N/mm
RX-stiff.	$2{,}500 \times 10^{3}$	N·mm/°
RY-stiff.	$2{,}100 \times 10^{4}$	N·mm/°
RZ-stiff.	$2{,}432 \times 10^{6}$	N·mm/°
SCF	$3{,}160 \times 10^{-4}$	—

Table 4.6 shows the eigenfrequencies of the updated model of the carbon fiber coupon of pattern 5 in the clamped-free condition. Interestingly, the measured GEMCC in the new test setup is much lower than the same measured value in the mechanically free condition.

Moreover, despite the updated SCF value, the error between simulation and measurement of the GEMCC is high and questions the effectiveness of this correction method.

Table 4.6. Carbon fiber coupon of pattern 5: Experiment *vs.* simulation results

Mode	Simulation (Hz)	Measurement (Hz)	Error (%)
1	15,212	15,000	1,41
2	76,456	79,750	-4,13
3	177,01	177,75	-0,42
4	184,95	191,75	-3,55
5	628,47	624,50	0,64
6	832,54	808,00	3,04
7	1097,4	1097,0	0,04
K_{31}^2	0,806 %	0,348 %	56,8

4.4.4 Forced response

The final test consisted in using a glass fiber coupon of pattern 1 to check the strain distribution on the surface, as has been done in the numerical analysis. Two strain gauges have been fixed on the coupon, on area SG1 and SG2. The coupon is clamped on one side and an electromagnetic shaker, together with a force sensor, is connected to the other side, to excite the tip mass in the longitudinal direction. Data processing is made by a real-time FFT analyzer. The experimental setup can be seen in **Figure 4.13**.

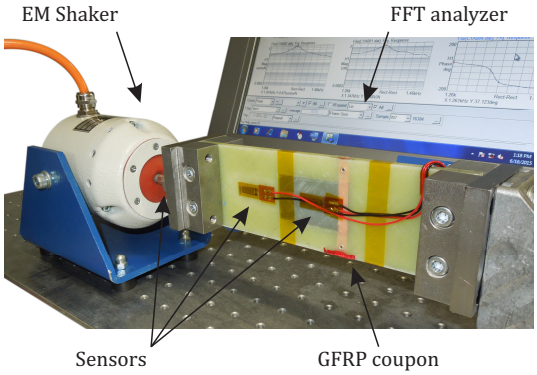

Figure 4.13. Experimental setup for the forced response

The measured open circuit eigenfrequency is equal to 1,347 kHz, an error of +5,8 % in comparison to the numerical result. **Figure 4.14** shows the longitudinal strain measured over a frequency range. Even though the absolute values diverge from the simulation, probably due to the test setup, the different strain levels in the area where the piezoceramic is located and outside is confirmed. In this case, the piezoceramic has reduced in more than 3 times the strain on the surface of the coupon. This can potentially have a positive effect on the durability of the

composite material. Nevertheless, if not integrated correctly, instead of holding fibers together, the piezoceramics can induce crack propagation and facilitate delamination.

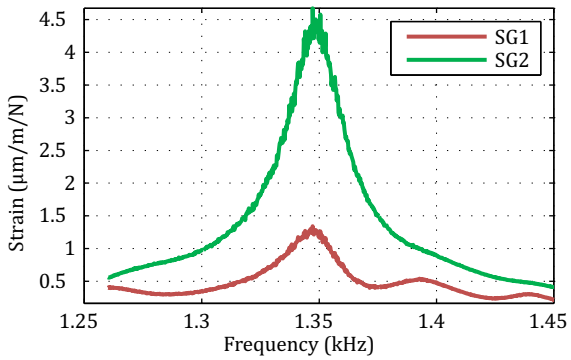

Figure 4.14. Measured dynamic strain on the glass fiber coupon of pattern 1

4.5 Conclusions

In this chapter, the integration of piezoceramic transducers inside laminate composite materials has been proposed and an analysis procedure has been investigated. Within the scope of shunt damping, the importance of the GEMCC was emphasized. So as to evaluate the effectiveness of integrated piezoceramics before dealing with complex structures, different coupons of carbon and glass fiber have been designed in regard to their longitudinal vibration.

The numerical analyses have shown that, by changing the orientations of layers and therefore the mechanical behavior of the laminate structure, it is possible to maximize the GEMCC. Nevertheless, a new correction factor for the contact between piezoceramic and laminate might be necessary, due to the viscoelastic behavior of the resin, since the SCF value was not enough, as evidenced by the experimental model update. The experimental analyses have also confirmed the numerical results, which show that the piezoceramic has a protection role, since it works as a load carrying element and therefore highly reduces the strain of the composite material. The measurement of the GEMCC has shown that slight differences among the integration patterns do exist and that patterns 1 and 2 show better results. Simulation results have also shown that pattern 1 exhibit a better static strength than pattern 2, since the latter presents a ply drop-off, which induces stress concentration. Nevertheless, the choice of the pattern has to be associated with the manufacturing process and a compromise must be found. A high pressure will assure a high fiber volume and therefore a better GEMCC, but this represents a major challenge when dealing with brittle ceramics. In this sense, it is advisable to use DuraAct patch transducers or an equivalent piezoelectric module that is able to pre-stress the ceramic material and adequately prepare it for the lamination process. The knowledge developed in this chapter is exploited in the next chapter, where the integration of piezoceramics in a more complex structure is brought to the next level.

5 Simultaneous design of a smart structure

As shown in Chapter 4, the physical integration of piezoceramics into fiber-reinforced plastics is not only possible, but can even improve the GEMCC if designed correctly. This technique can be hence combined with piezoelectric shunt damping in order to reduce structural vibrations. While the first part of this study dealt with the physical integration, this chapter takes the integration to the next level: The integration in the design process. As has been shown by numerical and experimental analyses, the piezoceramic works as a load carrying element. Therefore, it must be taken into account during the design of the structure itself, otherwise an optimal design cannot be guaranteed.

This chapter initially presents the derivation of the technical requirements for a smart structure, which are based on a realistic component, the control arm from an automotive suspension. As a starting point, a passive CFRP structure is developed from a scale model of the control arm, so that it can be further optimized and eventually meet the requirements. The first technique to be presented is the classical serial approach, in which the structure is first optimized, then the piezoceramic transducers and finally the *RLC*-shunt circuit, independently from each other. This enables the construction of a first prototype to experimentally validate the numerical model and later improve the concept, in the case of an insufficient design.

After analyzing the prototype and adjusting the numerical model, the physical integration of piezoceramics is performed. This allows not only the protection of the transducers, but also the complete redesign of the smart structure. The simultaneous design approach is then presented, in which the passive structure, the transducers and the *RLC*-shunt circuit are analyzed together in one iteration loop, so that the resultant smart structure can meet all the technical requirements at the same time.

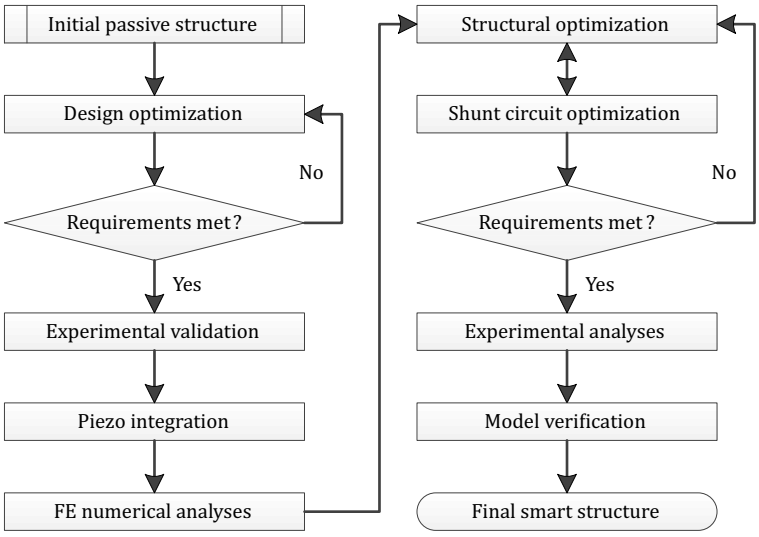

Figure 5.1. Smart structure optimization flowchart

The flowchart of the optimization process of a smart structure is presented in **Figure 5.1**, from the first concept until the final smart structure. Initially, a composite structure is chosen in

order to represent a real structure, the control arm. Then, its static and dynamic behaviors are analyzed and optimized to meet as many requirements as possible. In order to validate the resultant structure, experimental analyses are then carried out. Afterwards, piezoceramic transducers are inserted in the design and the measured electromechanical data are used to update the numerical model, which at this stage can be used for further optimizations. After that, a simultaneous optimization of structural parameters, transducer characteristics and *RLC*-shunt circuit is performed, so that the requirements for the smart structure can be met. Finally, experimental analyses of the optimized smart structure are carried out to show whether the requirements are met and high vibration attenuation is achieved.

5.1 Definition of technical requirements

The development of an engineering product for a given application usually demands the previous determination of a design space and definition of all technical requirements that the system must fulfill. In the case of load carrying structures, not only the static characteristics are specified, but also the dynamic behavior is part of the main criteria, since high vibration amplitudes may prevent normal operation and eventually lead to failure.

During the concept phase, technical requirements are usually defined based on knowledge of previous projects or on numerical analysis. Early-stage experimental identification of prototypes can be very costly and time consuming. In this way, physical tests are often carried out in later development phases, in order to update numerical predictions and, if necessary, make technical requirements more accurate.

In the case of replacing metal structures by lightweight composite solutions, the pre-existing metal part can be evaluated and used as a reference for the definition of technical requirements. In this study, the initial investigations are inspired from the steel control arm shown in **Figure 5.2**, which is part of the right-hand side of the front suspension of the Fiat 500.

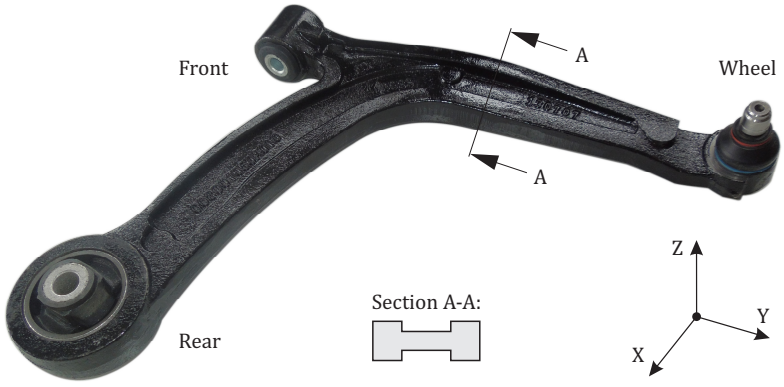

Figure 5.2. The control arm of a Fiat 500

To reduce the large number of variables to be analyzed, some assumptions are made for the control arm and taken into account to create a scale model, or a simplified structure.

No rotational degrees of freedom or lateral efforts in the Y direction will be considered, since dynamic efforts inputted into the wheel occur mostly in the XZ plane. For example, when passing over a small obstacle, the wheel first suffers an impact contrary to the direction of travel (X direction) and then rolls over the obstacle (Z direction). In some special cases, however, efforts in the Y direction can be high, depending on the suspension architecture, tire characteristics, road roughness and frequency range.

Furthermore, since the elastic characteristics of the rubber mounts cannot be easily assessed in a linear model, the control arm is assumed to be rigidly connected at the front and at the rear. In reality, the rubber mounts play a major role in the overall dynamic behavior of the control arm. At low frequencies, the motion of the control arm can be supported by the mounts and therefore the dynamic strain inside the part is softened. In terms of shunt damping techniques, this would mean that a piezoceramic transducer could not be placed in the part, but should be included in the mounts. An exhaustive description of possible design solutions is outside the scope of this thesis.

Additionally, it is assumed that a mass corresponding to the wheel is connected to the control arm. This better represents the condition in the vehicle and lowers the eigenfrequencies to more realistic values.

Finally, the knowledge of the load case the control arm is subjected to is of crucial importance. Without the correct assessment of loads, the technical requirements might be insufficient and several design iterations might be needed. In the case of dynamic loads, the spectrum of input efforts at the wheel should be evaluated in advance in order to correctly identify the eigenfrequencies that contribute to the dynamic response. Nevertheless, in order to keep the generality of the problem, a unit force will be assumed in the entire frequency range.

Instead of dealing with the complex geometry of the control arm, numerical simulations of a simplified structure facilitate the analyses and enable the definition of some technical requirements. The simplified structure consists of a metal beam with an I-profile and constant cross-section, as depicted in **Figure 5.3**, where the dimensions of the cross-section A-A and the length of the front side of the control arm have been taken into account. The beam is ideally clamped on one side and a tip mass representing the wheel is attached to the other.

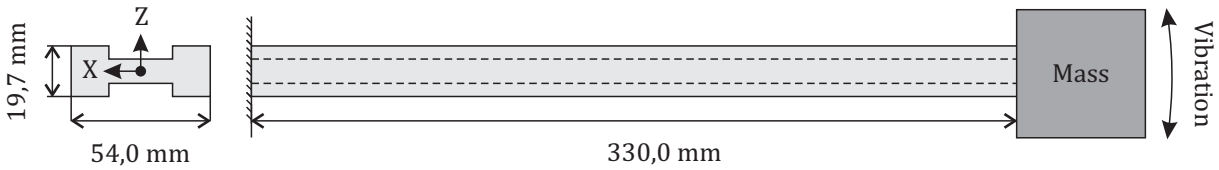

Figure 5.3. Simplified metal beam representing the control arm (scale model)

First, a numerical static analysis was carried out to calculate the stiffness of the simplified metal beam when it is subjected to vertical and longitudinal efforts. In the first case, a static force is applied at the end of the beam in the Z direction, and in the second, in the X direction. The resultant stiffnesses are equal to 0,35 and 3,98 kN/mm, respectively.

Then, a modal analysis allowed the identification of two important mode shapes: The first bending mode in the Z direction and the first bending mode in the X direction. In order to have a realistic behavior of the scale model, the value of the tip mass has been scaled down to 1,57 kg, so the obtained eigenfrequencies were approximately 60 Hz and 203 Hz, respectively. These resulting resonance frequencies are set in a relation to a real control arm in a midsize vehicle and the values are inside a frequency range that is highly relevant to vibration issues in the front suspension, as investigated in [123] and [124]. In this sense, the attenuation of these modes has a positive effect on noise levels and driving comfort, since they might coincide with potential vibration modes of other vehicle components, such as the subframe, suspension, tire or roof panel.

The numerical results of the simplified metal beam are summarized in **Table 5.1**. Since the shunt technique will be applied to a single degree of freedom system, from now on, focus will be given to the Z direction and the technical requirements will be studied in more details.

Table 5.1. Numerical analyses results of the simplified metal beam

Characteristics	Z direction	X direction
Structural mass (kg)	2,11	
Tip mass (kg)	1,57	
Static stiffness (kN/mm)	0,35	3,98
Eigenfrequency (Hz)	59,6	203

Once the characteristics of the simplified metal beam are calculated, it is desirable to have a composite structure not only with the same passive performance, but also suitable for the application of piezoceramics and shunt damping. In this sense, the initial passive structure should have at least the same static stiffness. Furthermore, since a lightweight material will substitute the metal, a commonly acceptable criterion [125] is that the structural weight saving should be of approximately 50 %. Finally, a relevant design guideline for a composite part is the strength behavior through a failure criterion, e.g. the Puck reserve factor, since it will guarantee that the new structure support the same loads as the metal part. In the case of this study, the maximum allowable static load has been scaled down from previously known project requirements [126] and is equal to 0,686 kN in the Z direction.

In regard to the smart functions of the structure, a set of technical requirements must also be defined. Since a new smart structure is being created from scratch, the requirements are based on information from available literature and previous own works.

As already mentioned, the GEMCC is the driving parameter in shunt damping applications, so its maximization and a minimum requirement are needed. As evidenced by the previous chapter, when integrating piezoceramics in composite materials, the measured GEMCC is lower than predicted by simulations. Additionally, experience has shown that, in order to attain a minimum effectiveness with shunt damping techniques, the value of the square of the GEMCC should be greater than 0,1 %, which is a realistic value to be obtained in practical terms.

Another important criterion is the stress level generated inside the piezoceramic material when the structure is subjected to the maximum allowable load. As brought out by the previous chapter, the ceramic behaves as a load carrying element and its mechanical strength must be respected. Most failures with piezoceramics occur because of excessive mechanical stress, since the ceramic material is brittle and cannot withstand high tensile or shear forces. Fatigue also represents a degradation of the piezoelectric material properties due to cyclic loads [127] but will not be addressed here. As described in [1], most existing works investigate the effect of static compressive loads on piezoceramics, but limited work has been done considering tensile loads. In this work, it is therefore assumed that compressive stresses are far below the material capabilities and only the tensile load threshold is a requirement and should not be exceeded. According to [89], tensile loads of non-preloaded piezoceramics are limited to 25 MPa, which is a conservative value that will also allow a higher durability. However, data published in [128] indicate that the measured tensile strength of the piezoceramic material PIC151 is around 45 MPa, which corresponds to a normal free strain of 0,757 mm/m in the short circuit condition.

From the point of view of the shunt circuit, several requirements can be defined, such as the voltages and currents in the circuit, the power dissipation or even the physical dimensions of the components. However, when designing a shunt circuit with a NIC, one of the most important parameter is the maximum voltage (or current) at the output terminal of the op-amp. At this terminal, the value can be several times higher than it appears across the piezoceramic element. When the output voltage (or current) of the op-amp is higher than the absolute maximum supply ratings, saturation can occur, leading to instabilities, overheating or even permanent damage to the component. It is hence very important to design a smart structure and calculate this value in advance, so that the shunt circuit can work properly for the given load case. The NIC and the power supply implemented in this work have a maximum supply voltage of ±150 V.

Table 5.2 shows the main technical requirements that have been described above. These values serve as the development basis of the initial passive structure and afterwards also of the smart structure. As described later, these requirements have to be met during the simultaneous optimization and do not mean to exclude other aspects, but only exemplify the typical complexity of the demands in the design of a smart structure.

Table 5.2. Technical requirements for the smart lightweight structure

Sub-system	Description	Value	Unit
Composite structure	Mass	< 1,06	kg
	Vertical stiffness	> 0,35	kN/mm
	Puck reserve factor	> 1,00	—
Piezoceramics	K_{31}^2	> 0,10	%
	Normal stress	< 45,0	MPa
Shunt circuit	Op-amp output voltage	< ±150	V

5.2 Initial passive structure

As previously described, the simplified metal beam served to establish some of the technical requirements that the smart solution has to meet later in the design process.

Furthermore, the simplified metal beam can also be used to create an initial passive structure that can be optimized and eventually meet the requirements. The idea is to develop an initial lightweight concept that can be used as a starting point for the simultaneous optimization carried out later. In the context of techniques such as piezoceramics integration and shunt damping, this method allows an easier understanding of physical phenomena at the sub-component level and, once the techniques are well comprehended, the possibility of applying them on complex-shaped structures can be evaluated.

The initial passive structure has been inspired from the simplified metal beam. It also consists of a cantilever beam with I-shaped cross-section of similar dimensions, but has thin wall and hollow profile. This represents an additional mass saving, since material is removed from low strain regions. The chosen material is CFRP, due to its high specific modulus and strength. Unidirectional fiber was preferred rather than woven, so as to better orient the strain when placing the piezoceramic transducers. The tip mass and the length of the beam remain unchanged. **Figure 5.4** shows the finite element model of the initial cantilever CFRP I-beam used for the numerical simulations.

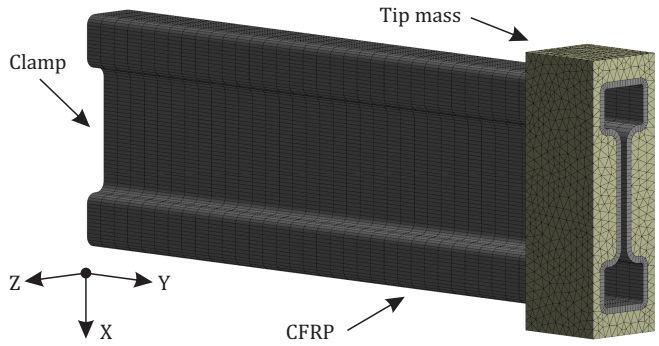

Figure 5.4. Finite element model of the initial cantilever CFRP I-beam

Prior to the actual optimization, the choice of a laminate stacking sequence must be made. At this stage, a simple approach is used: It is assumed that a 90° layer on the external surface can increase the strain and potentially enhance the GEMCC in the case of applied piezoceramics, a 0° layer on the internal surface increases the stiffness of the part, whereas ±45° layers in between make a smooth transition. For more complicated geometries, other techniques could also be applied, for example using the study carried out in [129], where the concept of stacking sequence table is introduced and an evolutionary algorithm optimizes the laminate.

In order to be as close as possible to the requirements, an optimization of the sole composite beam has been carried out. The input parameters have been defined as 1) the beam cross-section dimensions and 2) the number of plies for each of the three pre-defined orientations. The objectives of the optimization problem were 1) to minimize the mass of the beam, 2) to fit the vertical static stiffness (Z direction) to the minimum permissible value and 3) to maximize the Puck reserve factor when the beam is subjected to the maximum allowable vertical load. The optimized composite structure can be seen in **Figure 5.5**.

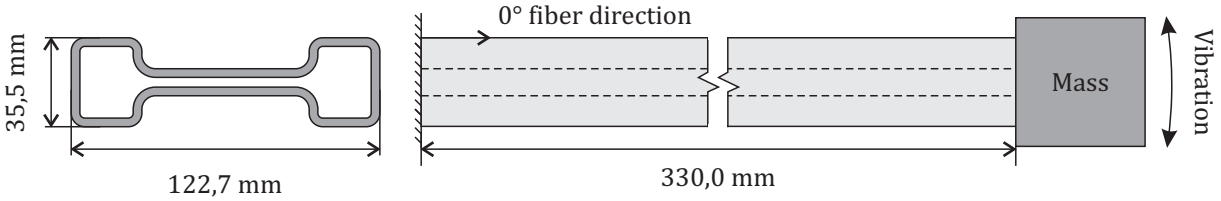

Figure 5.5. Optimized configuration of the cantilever CFRP I-beam

Having an initial passive structure prior to the simultaneous optimization has several advantages. Since it has already met part of the requirements, if correctly designed, major adjustments can be avoided when passing to the smart solution. Moreover, this composite structure serves as the base to physically integrate piezoceramics transducers. Even though a new numerical model might be necessary, the need for a new geometry can be eliminated, thanks to the knowledge of a previous similar system. Additionally, before launching a simultaneous optimization, it is very important to experimentally validate the numerical model of the composite structure. In this case, not only the mechanical response can be examined, but also the capability of the model to correctly predict the GEMCC and eventually the shunt circuit characteristics. Finally, as it is of common practice in a product development process, the evaluation of an early-stage prototype helps to identify problems and to improve the concept.

The main characteristics of the passive composite structure can be seen in **Table 5.3**. The optimal laminate stacking sequence is [0/0/0/±45/±45/±45/90/90/90/90/90/90], in degrees, from the inside to the outside. These 15 plies result in a wall thickness of 3,6 mm. Even though the composite beam has larger cross-section dimensions, due to the hollow profile and material design, it is important to notice that all requirements have been met with this concept and a mass saving of 73 % has been achieved compared to the metal beam, with the same static stiffness.

Table 5.3. Characteristics of the optimized cantilever CFRP I-beam

Characteristics	Optimal CFRP I-beam
Structural mass (kg)	0,58
Tip mass (kg)	1,57
Static stiffness (kN/mm)	0,35
Eigenfrequency (Hz)	63,1
Puck reserve factor	2,27

5.3 Traditional design approach

One of the mostly used methods of smart structure optimization consists in finding an optimal transducer configuration and controller circuit that minimizes the mechanical response of a pre-determined structure. This means that the structural parameters are optimized first and then optimal transducer and controller are designed for the resulting structure. Nevertheless, due to the interaction between structure, transducer and controller, the parameters obtained with this traditional method may not be optimal for the complete system.

In order to have a basis for comparison, this approach has been applied to the cantilever CFRP I-beam designed previously. Four rectangular piezoceramic transducers have been bonded to the outer surface of the structure, where the distance to the neutral axis is the maximum. A numerical analysis has been carried out regarding their position, size and boundary conditions. In this case, the composite structure remains invariable.

Considering the first bending mode in the Z direction, the optimal position of the transducers is as close as possible to the clamp, which is the location of maximum strain. Two boundary conditions for the piezoceramics were considered: Whether they should be clamped or free to rotate at the coordinate Y = 0. The top and bottom transducers have the same polarization orientation and they are electrically connected in parallel so that they are in phase when the beam is bending and only one shunt circuit can be used. **Figure 5.6** shows the electrical connection of the transducers, together with the two possible mechanical boundary conditions.

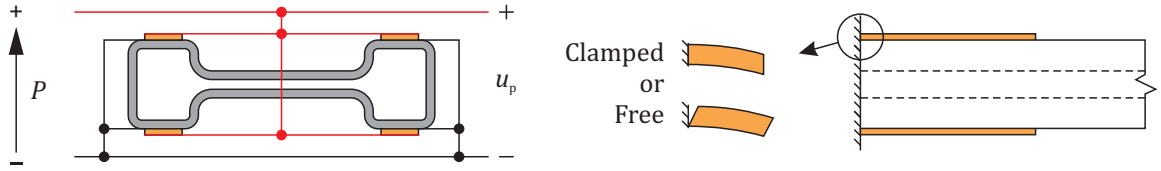

Figure 5.6. Bonded piezoceramics: Electrical connection and boundary conditions

A sensitivity analysis showed that the thickness of the piezoceramic influences the GEMCC more than its width or length, so it has been defined as the input variable. The width has been fixed at 15 mm, limited by the geometry of the beam, and the length has been fixed at 70 mm, the maximum available value for plate transducers. **Figure 5.7** shows how the GEMCC varies when the thickness of the piezoceramics is changed. Most importantly, it can be seen that there is only one optimal thickness value that maximizes the GEMCC. Moreover, for most thickness values, the GEMCC shows better values when the piezoceramic is clamped. It can also be noticed that the clamped condition shifts the optimal thickness to higher values. Nevertheless, since the technical construction of a clamp might not be ideal, in some cases it may not be worth increasing piezoceramic mass and having only a small gain in GEMCC.

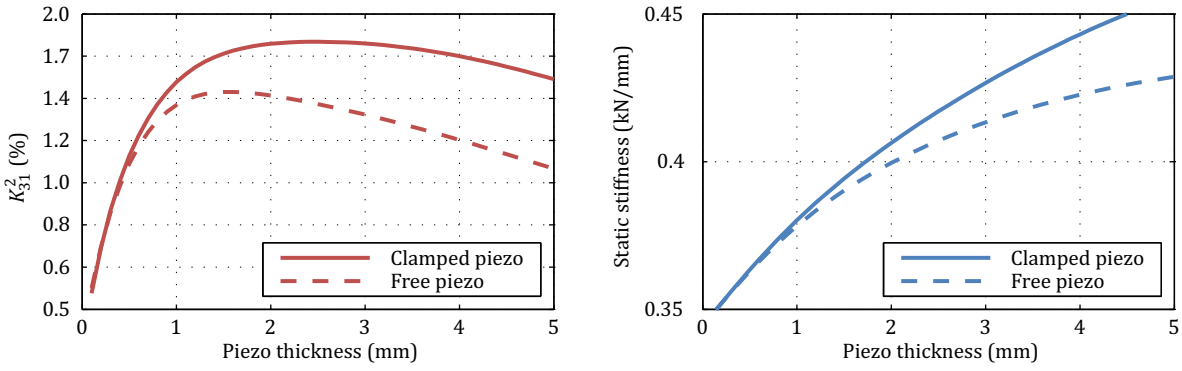

Figure 5.7. Transducers thickness optimization and influence on static stiffness

It has to be noticed, however, that, in any condition, the resultant static stiffness of the overall structure is higher than the original passive structure, and is even higher when the piezoceramics are clamped, compared to when they are free. The best calculated K_{31}^2 is equal to 1,757 %, for which the piezoceramics have a thickness of 2,5 mm. In this case, the resultant static stiffness is equal to 0,42 kN/mm and the calculated open circuit eigenfrequency is equal to 69,42 Hz. In terms of optimal conditions, this overdimensioned configuration is not desirable, since the static stiffness is far beyond the minimum requirements, and other parameters such as the mass may not be optimal.

In this serial approach, the last step consists in connecting the *RLC*-shunt circuit to the previously optimized transducers. At this point, only the shunt circuit is optimized, according to the method described in Chapter 3.5.2, whereas the composite structure and the piezoceramics configuration remain invariable. The objective function is to minimize a mechanical response. The numerical results, together with an experimental validation, are presented next.

5.4 Experimental validation

Since the initial passive structure is the base for the simultaneous optimization, the evaluation of its real properties is extremely valuable. This allows verifying whether the finite element model is capable of correctly predicting the static and dynamic properties of the structure, or if a model update is necessary.

First of all, the CFRP I-beam was manufactured and an experimental dynamic analysis was performed using an electromagnetic shaker. The acceleration per unit force, i.e. inertance, was measured at the tip mass of the cantilever beam through a force sensor and an accelerometer. The data has been processed using a real-time FFT analyzer. The strain in the Y direction was measured using a resistive strain gauge at a location near the clamp, where the Z coordinate of the structure has a maximum. This represents the location where the piezoceramic transducers are bonded in the case of the traditional design approach. Only the first eigenfrequency has been investigated, which corresponds to the bending in the Z direction.

After the first analyses of the passive structure, the experimental results were used to update the finite element model, in order to have a more precise representation. Since the support of the cantilever beam does not represent an ideal clamp, a steel support has been included in the model. This has decreased the expected eigenfrequency of the passive structure from 63,1 Hz to 53,6 Hz. Moreover, the modal damping ratio has been calculated from the measurement using Eq. (3.10) and is equal to 0,50 %. A comparison between the experimental and numerical results, before and after the model update, can be seen in **Figure 5.8**.

Despite the accurate prediction of the inertance by the numerical model, the simulated strain has an RMS error of -24 % in comparison to the measurement result. This can be explained by the fact that the results are very sensitive to the position of the sensor in the Y direction and also that a shell mesh was used to represent the beam, instead of a solid mesh, in which the strain distribution across the laminate thickness would not be constant.

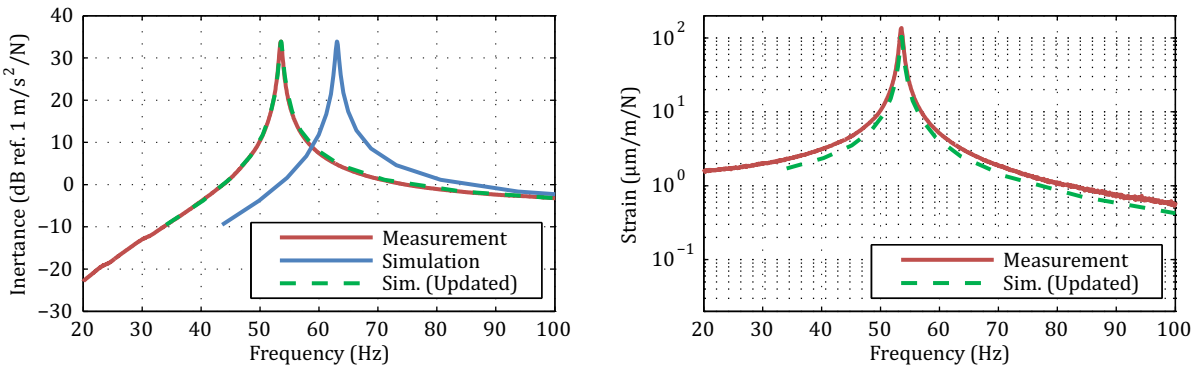

Figure 5.8. Dynamic response of the passive structure: Measurement *vs.* simulation

In order to validate the traditional design approach, piezoceramic transducers of optimal dimensions have been bonded to the manufactured CFRP I-beam and further experimental analyses have been carried out. This allows the correct assessment not only of mechanical, but also electrical parameters that are calculated by the analytical equation of motion.

Initially, the "dynamic" capacitance of the piezoceramics was measured by an LCR-meter, at a frequency of 120 Hz, which is above the first eigenfrequency. The obtained value was 36,5 nF. When calculated using the finite element model, the obtained capacitance was equal to 28,4 nF, which represents an error of -22 %. If the simulated capacitance value of the transducers is not correct, the optimization of the shunt circuit leads to an insufficient tuning that will possibly not meet the requirements. Since this is a very important parameter in the design process, an update of the finite element model is necessary. The driving parameter for the capacitance is the permittivity of the piezoceramic material. This value depends on the mechanical boundary conditions and is only known at two ideal conditions given by the manufacturer, i.e. free and clamped. As in a real structure the transducers are neither clamped nor free, the permittivity has to be adjusted to match the measured capacitance.

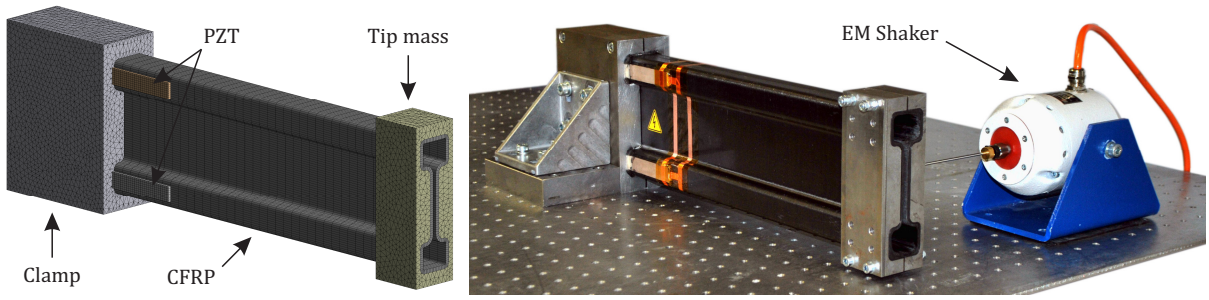

Figure 5.9. Updated model and experimental setup of the cantilever CFRP I-beam

Once the transducers were applied to the structure, the inertance was also measured at the tip mass, but this time when the electrodes of the piezoceramics were open. The measured eigenfrequency in this condition is equal to 62,5 Hz and the modal damping ratio is equal to 0,93 %, slightly higher than the passive structure. The dynamic voltage generated by the

transducers per unit force was also measured. The experimental results were also used to update the finite element model and, as described in Chapter 4.4.3, a stiffness coefficient factor in the contact between the piezoceramics and the beam has been introduced. This can be explained by the fact that the glue used to bond the transducers is relatively soft (X60, HBM, E = 13 GPa). The stiffness coefficient factor (SCF) was found by fitting the calculated GEMCC to the value found in the experimental analysis (K_{31}^2 = 1,408 %). **Figure 5.9** shows the updated finite element model together with the experimental setup used for the mechanical tests.

Figure 5.10 shows the measured inertance and dynamic voltage per unit force for the first eigenfrequency of the beam. The simulated results, before and after the model update, are also shown. It is noticeable that the model describes with a very good precision the dynamic response of the first eigenfrequency and can therefore be used to predict the behavior when the shunt circuit is also connected. In this case, the resultant static stiffness is equal to 0,33 kN/mm, which is smaller than the simulated result and also does not meet the minimum requirement.

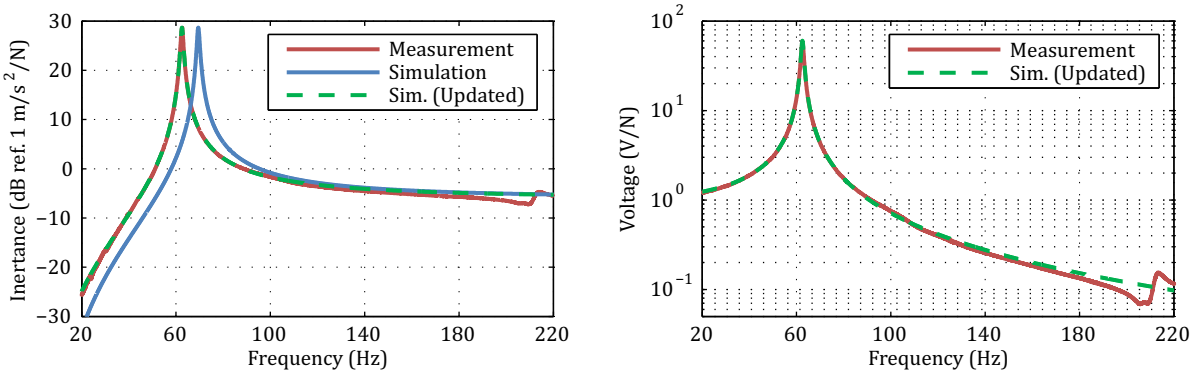

Figure 5.10. Dynamic response of the structure designed using the traditional approach

Using the analytical equation of motion and the method described in Chapter 3.5.2, it is possible to calculate the optimal *RLC*-shunt circuit that minimizes the inertance. The component values can be found in Appendix D. The circuit has been implemented and the experimental results can be seen in **Figure 5.11**. It can be noticed that the measured inertance of the mechanical structure when the optimal shunt circuit is connected is very well predicted by the analytical calculation. The RMS error in this case is only 3,0 %.

In order to verify how well the shunt circuit is described by the analytical equation, the calculated voltage across the inductor has been compared to the measurement. This specific voltage has been chosen due to the ease in measuring a real component, whereas measuring the voltage across a synthetic component, such as the NIC, may cause instability due to the finite impedance of the measurement probe. In **Figure 5.11**, it can be seen that the analytical calculation of the voltage magnitude across the inductor predicts fairly well the measurement results. The RMS error in this case is 8,9 %. Finally, using Eq. (2.25), the maximum voltage at the output terminal of the op-amp has been calculated and is equal to 213 V per unit force applied to the structure, which is far beyond the maximum requirement.

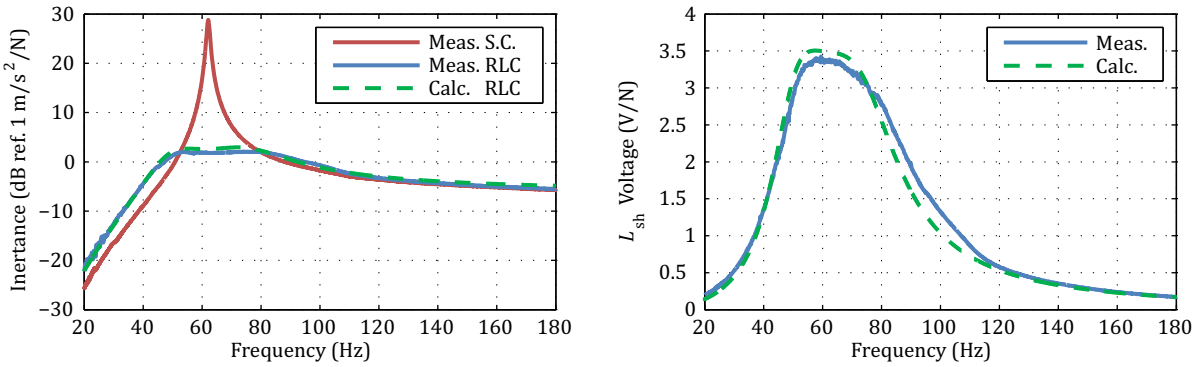

Figure 5.11. Optimal *RLC*-shunt experimental results

A final experimental finding with the *RLC*-shunt circuit is related to the stability of the electromechanical system, as previously discussed in Chapter 2.3.4. It has been observed that, if the output voltage of the op-amp is higher than the supply voltage, saturation occurs. Even if the negative capacitance value is far away from the stability boundary, this saturation leads to a non-linear effect that destabilizes the complete system. **Figure 5.12** shows the time signal of the voltage across the inductor, together with the voltage at the output terminal of the op-amp, at 85 Hz, when the optimal *RLC*-shunt circuit is used. If a very low force excites the structure, it can be noticed that, when the supply voltage of the op-amp is decreased from ±20 V to ±15 V, a non-linear overshoot appears in the measured voltage across the inductor. This effect is confirmed by a time simulation that shows the saturation of the op-amp. After a few seconds in this condition, the system goes unstable and the structure oscillates uncontrollably until the circuit is turned off.

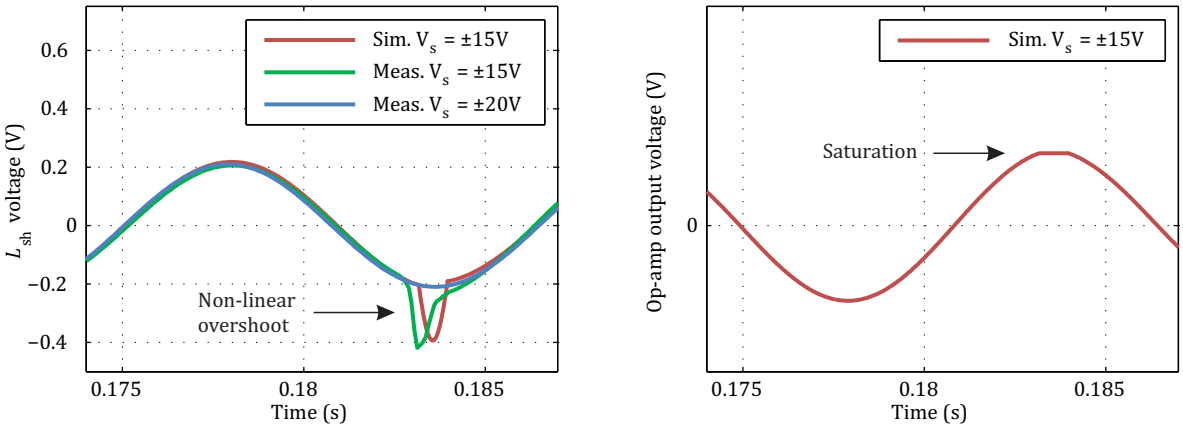

Figure 5.12. Saturation effect on an optimal *RLC*-shunt circuit at 85 Hz

5.5 Simultaneous design approach

It has been shown that the traditional approach alone is not capable of designing a smart structure that meets all the requirements at the same time. If the optimal piezoceramic design is

found for a pre-determined structure, the resultant stiffness is simply too high. Moreover, the experimental validation showed that small variations are to be expected in the measurements in comparison to the numerical simulations. The model update is therefore a useful method to adjust the most sensitive parameters, so that the model can better represent real conditions. In this sense, the traditional approach, together with an initial experimental validation, is a useful tool to validate a first prototype in the design process of a smart structure. Even though the requirements were not met, this allows a better understanding of physical phenomena that can be taken into account later in the design process.

The novel design approach proposed in this thesis consists in taking into account structural parameters, together with the configuration of piezoceramics and shunt circuit, in one optimization loop only. The ultimate goal is to find a compromise between the input parameters so that all requirements can be simultaneously met, despite possibly conflicting objectives.

Furthermore, in contrast to the traditional approach, the new method allows the integration of piezoceramic transducers. In the case of dealing with composite structures, two different levels of integration are specified here: The "physical" integration of piezoceramics, in which the transducers are placed between the plies of the laminate, as studied in Chapter 4, and the "design process" integration, in which the transducers take part in the design process of the smart structure. In the latter case, as will be shown later, the piezoceramics are not considered as add-on solutions placed externally to the structure, but rather as structural elements with an active role in carrying mechanical loads additionally to the smart functions.

Once a representative and trustworthy model of the passive composite structure is obtained, it can be further refined with embedded piezoceramics. The finite element model of the cantilever CFRP I-beam has been remade to take into account the physical integration of piezoceramics, as can be seen in **Figure 5.13**.

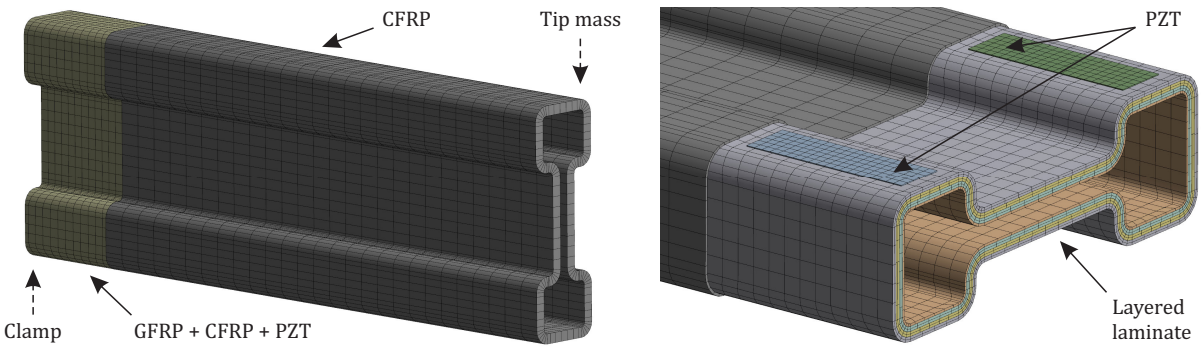

Figure 5.13. Cantilever CFRP I-beam with integrated piezoceramics

The model consists of a hollow beam with I-shaped cross-section, clamped on one side and with a tip mass attached to the other. The laminate material consists of unidirectional fibers. Near the clamped part of the beam, several piezoceramic plate transducers are embedded inside the thin wall of the laminate, where the distance to the neutral axis is the maximum, in all four regions. The position of the piezoceramics is fixed, since for the first bending mode, the highest strain occurs in this region. In order to guarantee a better electrical isolation, the piezoceramics

are surrounded by continuous glass fiber layers, whereas all other layers are made of carbon fiber, to assure a better specific strength of the structure. The design pattern has been inspired from previous analyses on the coupon level, as described in Chapter 4. The cross-section of the laminate where the piezoceramics are located can be seen in **Figure 5.14**. The part of the beam where no piezoceramics are present is made exclusively of carbon fiber layers.

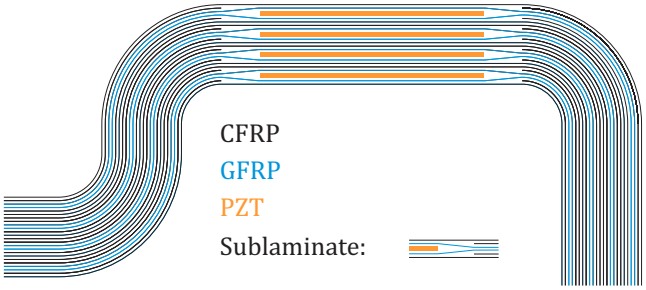

Figure 5.14. Cross-section of the I-beam with integrated piezoceramics

Before the optimization takes place, it is very important to assess the impact of the mesh quality on the simulation responses using the finite element model. Since now piezoceramic transducers are included between the laminate plies, a solid mesh has been preferred, so as to better represent the strain distribution across the wall thickness. Moreover, the mesh type has been chosen to be quadrilateral and the mesh size has been evaluated through a convergence analysis. **Figure 5.15** shows the behavior of the simulated K_{31}^2 for different mesh sizes of the laminate material. A compromise between accuracy and model size has been found using a mesh size of 6 mm, which corresponds to a K_{31}^2 equal to 1,7 % and represents an error of less than 6 % in comparison to the convergence value of 1,8 %.

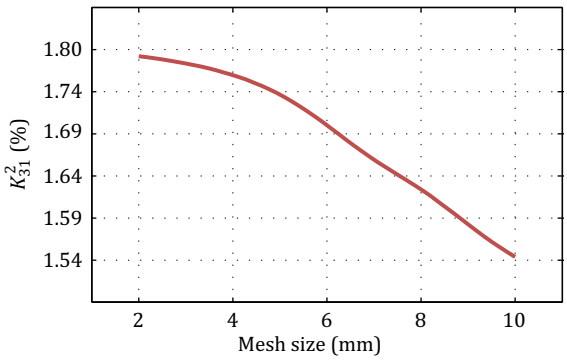

Figure 5.15. Mesh size convergence analysis

To continue with the design of the smart structure, several design variables have been chosen for the composite structure, the piezoceramics and the shunt circuit. This allows the

simultaneous variation of all input parameters, so that all requirements can be met as precisely as possible, in one optimization loop only.

For the composite structure, some design rules have been defined. The tip mass and the length of the beam remain unchanged compared to the previous design. Since the integration pattern of the piezoceramics requires a minimum number of layers, a unitary sublaminate has been defined for the beam. Near the clamp, it consists of four piezoceramic plate transducers, four carbon fiber plies and two glass fiber plies, whereas in the rest of the beam, it consists of six carbon fiber plies. In the optimization process, this reduces the number of variables to be studied, since several unitary sublaminates can be stacked up to form the desired geometry.

The input variables for the beam have been defined as 1) the cross-section dimensions, 2) the number of sublaminates, which also defines the number of piezoceramic transducers, and 3) the fiber orientation of each one of the six plies inside the sublaminate. For the piezoceramic transducers, the length and width have been fixed at 50 mm and 15 mm, respectively, whereas the variable has been defined as 4) the thickness, since it is the most influential parameter. For the *RLC*-shunt circuit, the defined input parameters are 5) the values of all components.

After these definitions, the simultaneous optimization process is carried out according to the approach presented in Chapter 3.5. The objectives of the optimization problem were 1) to minimize the mass of the beam, 2) to fit the static stiffness, 3) to maximize the Puck reserve factor, 4) to maximize K_{31}^2, 5) to minimize the stress inside the piezoceramics, when the beam is subjected to the maximum allowable load, and 6) to minimize the maximum voltage at the output terminal of the op-amp in the NIC, when an optimal *RLC*-shunt is connected to the beam.

Since mixing continuous and discrete variables can be computationally expensive during the optimization, the choice of the number of sublaminates is very important. When only one sublaminate is used, the minimum required static stiffness cannot be met. When using two sublaminates, the output voltage in the op-amp is very high, since not enough transducers are used. When using three sublaminates, the value of K_{31}^2 is not sufficient. Therefore, the best compromise has been found when using four sublaminates and a more detailed optimization has been carried out with this configuration.

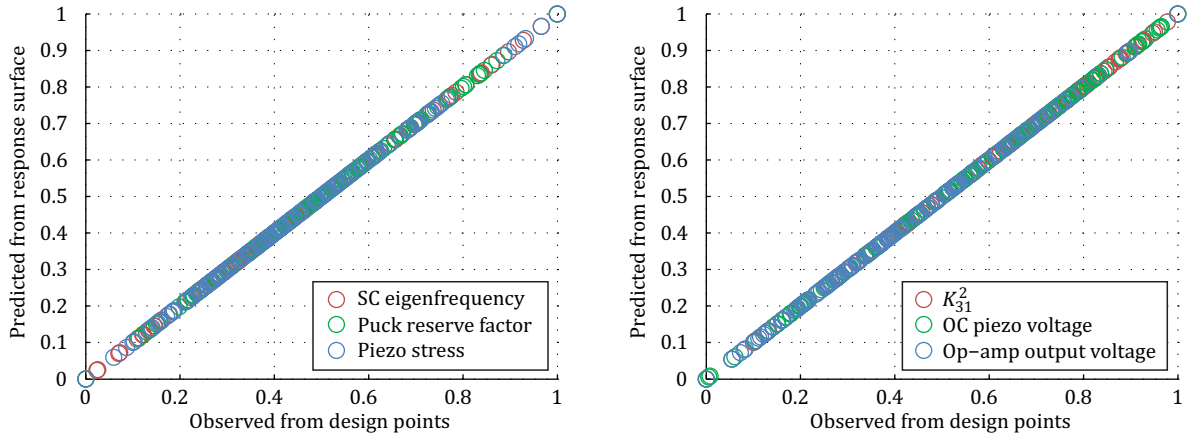

Figure 5.16. Goodness of fit for the most important output parameters

To guarantee the stability of the optimization, it is important to previously examine the goodness of fit for the most important output parameters. This represents the quality of the response surface used for the calculation. **Figure 5.16** shows the goodness of fit for some of the simulated output parameters using the non-parametric regression. It can be seen that the response surface is able to predict the finite element model in a reliable interval for several simulated outputs.

In order to evaluate the potential of the current design before the actual optimization, the most relevant response surfaces have been investigated. **Figure 5.17** shows the response surfaces obtained with the design of experiments using variables from all three sub-systems simultaneously, the composite structure, the piezoceramics and the shunt circuit. It is important to notice that, inside the considered interval, the cross-dependency among the three different sub-systems is evident, so the simultaneous optimization is justified. Moreover, from the depicted case, it can be seen that the best design solution for the I-beam tends to larger height values, since this reduces the voltage in the shunt circuit and simultaneously reduces the stress levels in the piezoceramics. This shows that the geometric dimensions of the beam not only define its mechanical properties, but also has an essential role in the final behavior of the shunt circuit and the transducers. The choice of the stacking sequence is also shown to be very important, since this can considerably increase the stress in the transducers. It is also noticeable that the span in the output voltage is small compared to the span in the mechanical stress, 7 % against 40 % approximately. This indicates that the sensitivity around this local response point is higher for the stress and any changes in the input variables will have a greater impact on its value, rather than on the output voltage.

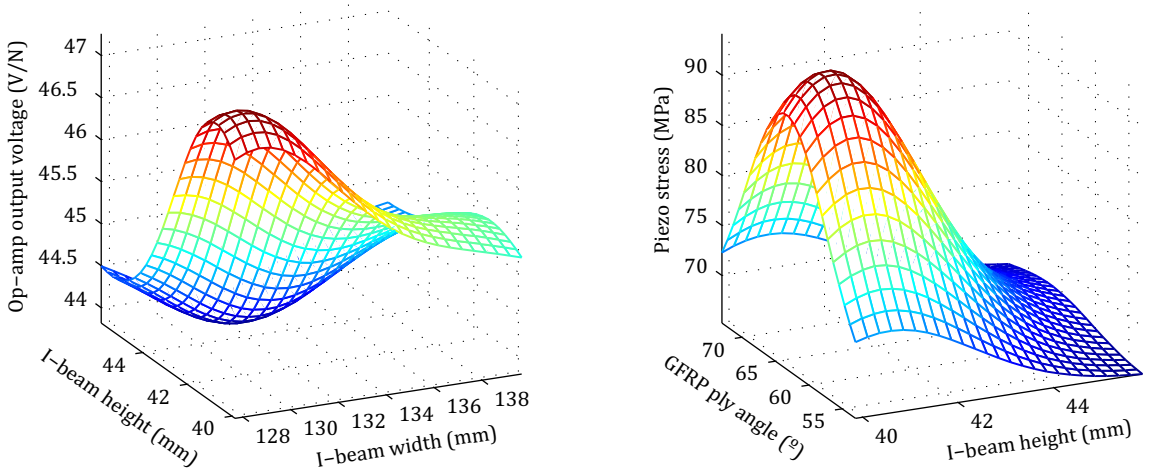

Figure 5.17. Response surfaces with geometry and ply variables

Among all possible solutions in the design space, the effort to identify the optimal set of parameters is not negligible. Despite the fact that optimization algorithms can be robust enough to consider tradeoffs, the analysis of input variables is of crucial importance to identify possible conflicting demands. This allows a re-evaluation of the requirements in the case of an unrealistic design space. As can be seen in the local response surfaces plotted in **Figure 5.18** and **Figure 5.19**,

conflicts are present in the design of the smart structure. When considering the thickness of the piezoceramic transducer, the optimal value that maximizes the K_{31}^2 is the same that minimizes the Puck reserve factor and maximizes the output voltage in the shunt circuit. This leads to the conclusion that, in the traditional approach, designing the transducers regardless of the structure and the shunt circuit could lead to a solution that is not globally optimal.

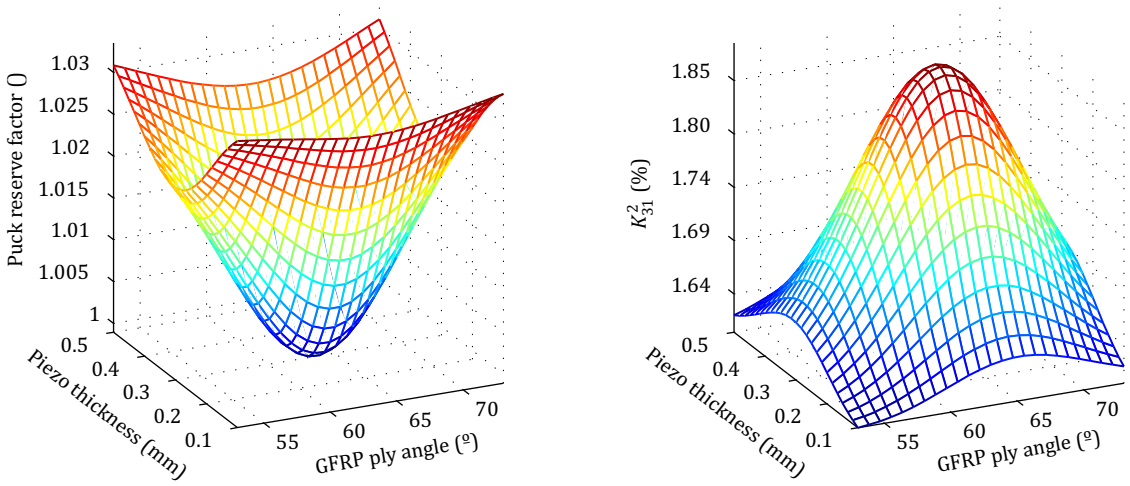

Figure 5.18. Response surfaces with piezoceramic and ply variables

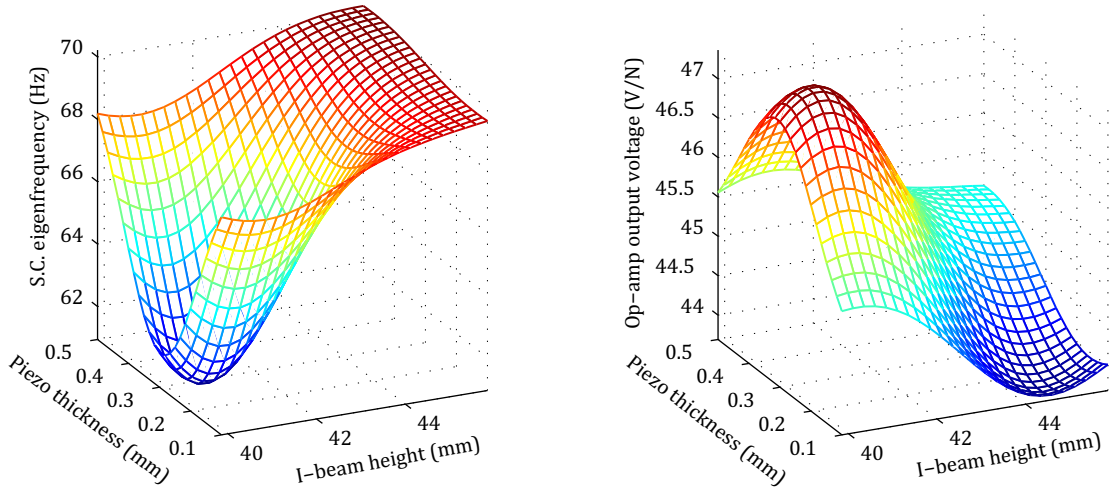

Figure 5.19. Response surfaces with piezoceramic and geometry variables

The final optimized smart structure can be seen in **Figure 5.20**. It can be noticed that, when the composite structure is optimized together with the piezoceramic transducers, a slightly different geometry is obtained in comparison to the initial passive structure. The detailed geometric characteristics can be found in Appendix D. The optimized stacking sequence is [-40/70/65/60/90/50], in degrees, and is considered for the six layers of the sublaminate,

starting from the inside to the outside. The sublaminate is repeated four times in the cross-section, so the 24 plies result in a wall thickness of 5,6 mm. In total, 16 piezoceramic transducers are embedded in the composite structure, each of them with an optimal thickness of 0,27 mm.

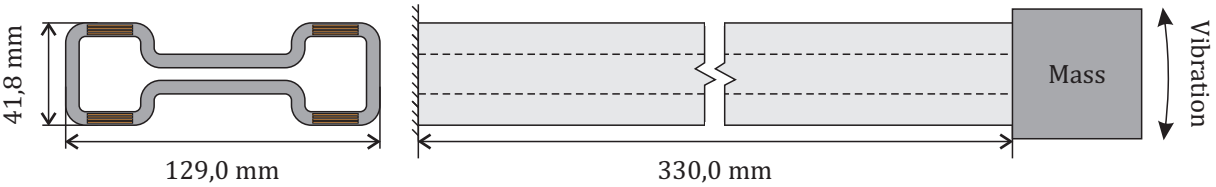

Figure 5.20. Simultaneously optimized CFRP I-beam with integrated piezoceramics

With this configuration, the calculated static stiffness is equal to 0,38 kN/mm, the Puck reserve factor is equal to 1,05 and the K_{31}^2 is equal to 1,914 %, which are all above the minimum requirements. More importantly, if the static stiffness of the beam is calculated without the piezoceramic transducers, it is equal to 0,33 kN/mm. It can be therefore inferred that, when optimizing the composite beam together with the piezoceramics, the beam itself is compelled to have a lower stiffness than the requirement, i.e. to be weakened. From the global design point of view, however, this should not be seen as a structural issue, because when the optimal piezoceramics are also taken into account, the calculated stiffness attains the desired value. In this case, the piezoceramic material is responsible for 15 % of the total static stiffness.

The total mass of the beam has been calculated at 0,936 kg, which is higher than the initial passive structure but still meets the requirement. This value may not represent the absolute minimum in the optimization problem, but is the global optimum that satisfies all requirements of the smart structure. As evidenced by the traditional approach, the beam with the smallest mass may not satisfy the conditions of a shunt circuit when piezoceramics are included afterwards in the design process. However, in the simultaneous approach, it is preferable to obtain a heavier structure, rather than not to meet the requirements for the electronics. From a product development point of view, this still represents a potential overall mass saving, since the carbon fiber in the structure is replacing the need for power electronics in the circuit, which would mean heavy boards and metals.

When the smart structure is subjected to the maximum allowable load, i.e. 0,696 kN, the normal stress in the Y direction inside the piezoceramics has been calculated at 93 MPa, which is far above the maximum requirement. Nevertheless, the numerical model only considers the piezoceramic plate without taking into consideration any manufacturing process. As evidenced by Chapter 4.4.1, one of the advantages of using DuraAct patch transducers is that the piezoceramics come in a pre-stressed state. Moreover, the physical integration in the FRP increases even more the pre-stress, which results in a total value of up to 65-85 MPa in the ceramic material. This results in a stress of 8-28 MPa in operation condition, which satisfies the minimum requirement.

5.6 Analytical results

If the optimally calculated *RLC*-shunt circuit is connected to the smart structure, the mechanical response is minimized, as can be seen in **Figure 5.21**. The detailed component values of the optimal *RLC*-shunt can be found in Appendix D. The short circuit eigenfrequency is equal to 62,9 Hz and the modal damping ratio taken into account is equal to 1 %. It can be noticed that, using a safety margin of 1,00, the mechanical response suffers the highest attenuation, -27 dB. In this case, the voltage at the output terminal of the op-amp in the NIC has the maximum value. It has a peak value of 44,9 V/N at 47,5 Hz, which interestingly does not correspond to the original eigenfrequency of the structure. This value is in agreement with the maximum technical requirements, as long as the force inputted into the structure does not exceed 3,34 N at that frequency. At this stage, it is important to emphasize the importance of knowing the load case previously to the design process. The real output voltage is the product of the transfer function output voltage per unit force and the input force spectrum. Without the real force spectrum, the frequency distribution of the output voltage might be inaccurate and the maximum requirements might not be met.

Moreover, if a safety margin of 0,90 is used, the vibration attenuation using the optimal *RLC*-shunt is slightly worse, -23 dB, but the maximum output voltage is smaller, 36 V/N. This shows that choosing the negative capacitance away from the stability limit generates lower voltages in the circuit and the vibration attenuation is still considerably high. Depending on the input force spectrum, introducing the safety margin during the design can be a beneficial tool in order to meet the requirements with less effort.

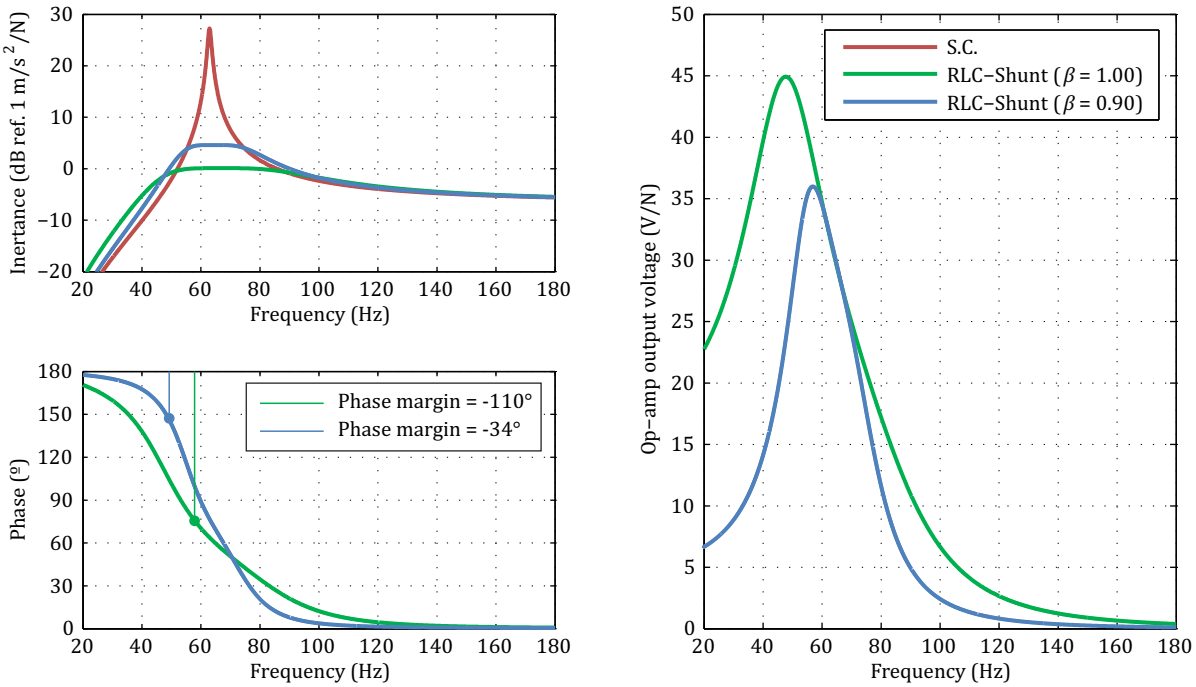

Figure 5.21. Optimally calculated *RLC*-shunt circuit connected to the smart structure

The frequency response function also enables an analysis of the stability of the complete electromechanical system. If a safety margin of 1,00 is used, the phase margin can be obtained from the phase response and is equal to -110°, which indicates that the system is stable. Considering a safety margin of 0,90, the phase margin is equal to -34°, which is a more robust value in terms of stability in control systems. In this sense, a lower β value offers mostly positive aspects, since this improves stability and reduces the voltage in the electronics, even though the vibration attenuation is not at its maximum capacity.

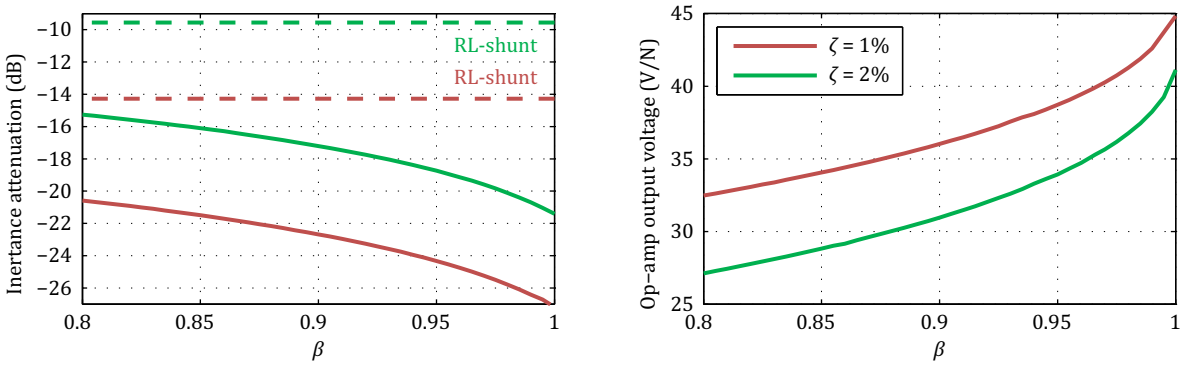

Figure 5.22. Vibration attenuation and op-amp output voltage as a function of safety margin

The plots in **Figure 5.22** show how the vibration attenuation level of the inertance and the output voltage of the op-amp vary as a function of the safety margin β, considering two different modal damping ratios. It is interesting to see that, when using small values of β, the output voltage is reduced, which results in a less significant vibration reduction. Nevertheless, even though small values of β limit the potential of the *RLC*-shunt to reduce vibrations, the *RLC*-shunt always performs better than a simple *RL*-shunt, which depends only on the GEMCC. This custom characteristic of the negative capacitance circuit is a further advantage in comparison to other shunt techniques. In order to meet all requirements of the smart structure, the designer is free to choose the best compromise between mechanical and electrical behavior.

When the tuning of the sole negative capacitance circuit is analyzed, regardless of the optimal resistance or inductance values in the shunt, the safety margin also plays a role in the stability of the circuit, as can be seen in **Figure 5.23**. If the ratio δ, as defined in Eq. (2.15), is allowed to vary from 0 until δ_{crit}, as defined in Eq. (2.28), the eigenfrequency of the smart structure is reduced from its original state, i.e. the short circuit eigenfrequency at 62,9 Hz , until a lower value, in this case around 5 Hz, which proves the negative stiffness behavior of the circuit. This strategy can be useful to attenuate vibrations, so that the eigenfrequency of the smart structure can be shifted to a frequency range where the excitation is low. It can also be seen that a safety margin of 0,98 corresponds to an eigenfrequency of 45 Hz, therefore allowing an optimal vibration attenuation when the resistor and inductor are connected to this “softer” structural configuration.

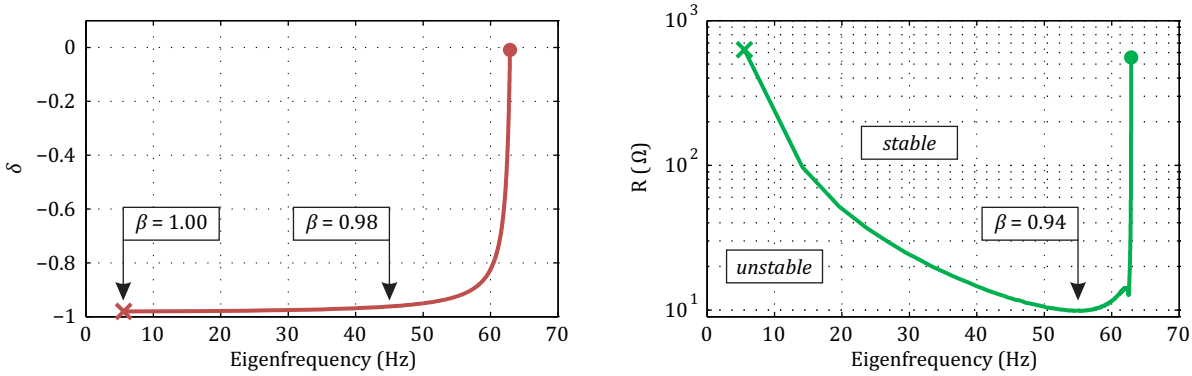

Figure 5.23. Eigenfrequency and stability region when tuning with a NIC circuit

At the same time, if the safety margin β is increased and therefore the eigenfrequency decreased, the value of the series resistance R in the NIC circuit has to be adjusted, otherwise the resultant shunt circuit can be unstable. This adjustment is explained by the fact that, in the frequency band below the eigenfrequency, the NIC circuit exhibits a negative resistance behavior [88], which has to be compensated, otherwise vibration levels are amplified thus leading to instabilities. The unstable und stable regions are plotted in **Figure 5.23**. In reality, this series resistance is a combination of the inherent resistance of the piezoceramics, possible cables or lossy components and the R resistor in the NIC circuit itself. Therefore, if a piezoceramic with low inherent resistance is used, an external component can increase the global resistance until the optimal value. This situation is desirable, since a low safety margin can be used and therefore avoid instability problems. For example, if β = 0,94, R is as low as 10 Ω. However, if a piezoceramic with high inherent resistance is used, the optimal resistance may not be reachable, depending on the β value, and therefore vibration attenuation will not be optimal, even though the circuit is stable. If an optimal shunt is desired, a value of β close to 1 has to be chosen, which means being closer to the stability limit.

5.7 Manufacturing and experimental analyses

In order to test the smart structure developed using the simultaneous optimization approach, the laminate composite with integrated piezoceramic transducers has been manufactured. An aluminum mold with the external shape of the I-beam has been used together with the pressure bag process. The prepregs have been laid onto the surface and DuraAct patch transducers have been included according to what had been presented in the simulation. The stacking followed the same pattern number 5 as for the carbon fiber coupon. **Figure 5.24** shows the prepreg layers and the embedded patch transducers during the lamination process.

After the manufacturing, the smart beam has been setup in a cantilever configuration, according to what is shown in **Figure 5.24**. An electromagnetic shaker has been attached to the tip mass, together with a force sensor and an accelerometer, and data has been processed using a real-time FFT analyzer.

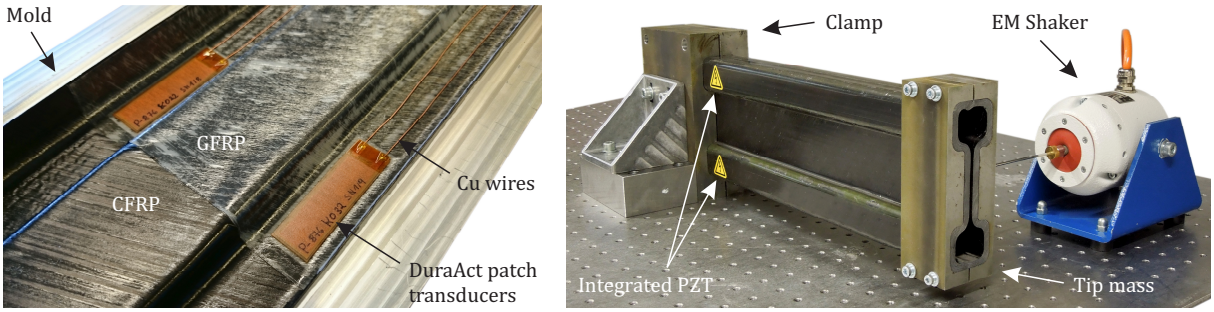

Figure 5.24. Manufacturing and experimental setup of the smart structure

Initially, the "static" capacitance and resistance of the smart structure have been measured by an LCR-meter, which resulted in 561 nF and 71 Ω, respectively. Compared to the simulated value, the measured capacitance presents an error of -0,8 %. Compared to the values obtained with the DuraAct patch transducers in the free condition before the manufacturing, the measured values deviate from -5 % and +195 %, for the capacitance and resistance, respectively. According to what had been discussed in Chapter 4.4.1, it is possible to say that the transducers suffered an estimated additional pre-stress of 8 MPa. The resistance value is much higher than expected mainly because of the pre-stressed mechanical boundary condition of each patch transducer, which increased the dielectric loss factor of the piezoceramic material [130].

The vibration response for the first eigenfrequency of the smart structure can be seen in **Figure 5.25**. The measured short circuit eigenfrequency is equal to 59 Hz. This value is 6 % smaller than predicted by simulation, which is a very good agreement taking into account the complexity of the system. The modal damping ratio has been calculated from the measurement and is equal to 0,72 %.

In spite of the high modeling effort, the measured K_{31}^2 was only equal to 0,247 %, which is still above the minimum requirement. Possible reasons for this are the alignment of the transducers during manufacturing, the pressure used in the process and therefore the low fiber volume, the viscoelastic behavior of the epoxy resin, the increased loss factor of the piezoceramic material and also the assembly of the composite part to the metal clamp. Even though the stiffness coefficient factor was shown to be little effective in predicting the correct GEMCC in the case of the coupons, it has been used to update the finite element model. In the case of this smart structure, the updated value of K_{31}^2 is then equal to 0,593 %, which represents an error of 58,3 % against the measurement, the exact same difference as for the coupons. Moreover, it has to be noticed that the measured K_{31}^2 of the surface-bonded piezoceramics in the traditional design approach was almost six times higher than the measured value of the integrated piezoceramics. This can be explained by the fact that, in the case of integrated transducers, the piezoceramic material is closer to the neutral axis and is therefore subjected to smaller strain levels. Furthermore, although it improves computational speed, the use of a unique sublaminate in the cross-section might reduce the strain in the inner transducers to increase the strain in the outer ones. If the sublaminates had been optimized independently from each other, the strain distribution across the wall thickness could have been maximized at all locations of the transducers.

Figure 5.25 also shows the optimal damping using the *RLC*-shunt circuit. Two different safety margin values have been used, 0,90 and 0,95. It can be noticed that two different levels of

vibration attenuation have been achieved, -18,7 dB and -20,7 dB, respectively. The error in comparison to what had been shown in **Figure 5.22** comes from the low GEMCC and the high inherent resistance of the piezoceramics. As previously mentioned, since the optimal resistance in the shunt cannot be reached, the vibration attenuation cannot achieve its maximum value and is underused.

Additionally, a different strategy of adaptation has been demonstrated using this smart structure. Using solely the negative capacitance, the eigenfrequency of the structure can be reduced. According to Eq. (2.29), if $\beta = 1$, the eigenfrequency can be as low as 3 Hz, but this cannot be achieved in practical terms. The experimental results have shown that the adjustment range can go from the short circuit value, 59 Hz, until 56 Hz, which corresponds to a safety margin of 0,970. Beyond this point, the system becomes unstable and the only way to go further is by increasing R_{sh} and therefore introducing damping, as shown in **Figure 5.25**.

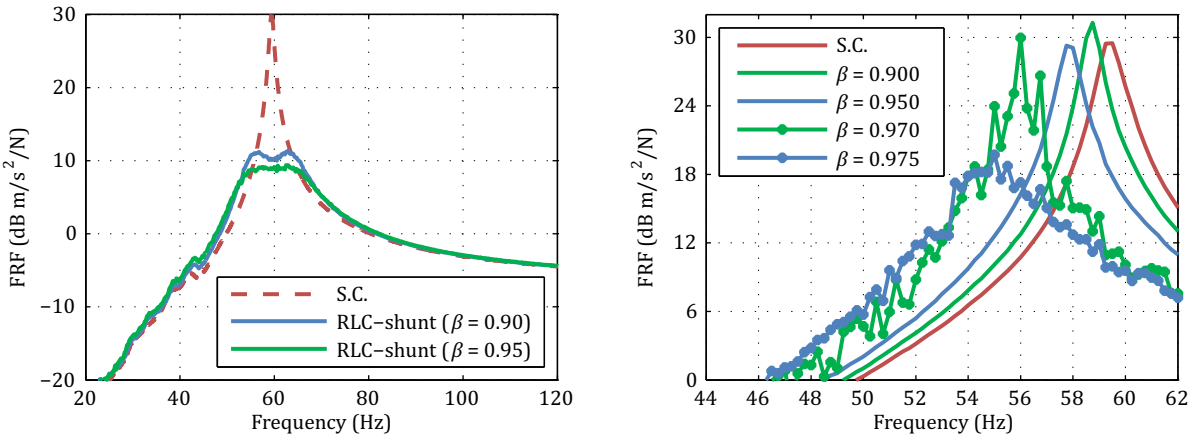

Figure 5.25. Smart structure test results: Optimal damping and eigenfrequency tuning

5.8 Conclusions

Based on an existing component, the control arm, a set of technical requirements has been initially defined. In this sense, a substitute lightweight solution must be capable of carrying the same static loads, additionally to providing smart functionalities in the dynamic range. This chapter contributed with a novel technique to design smart lightweight structures. It is suggested that, when considering the base passive structure, the piezoceramic transducers and the *RLC*-shunt circuit simultaneously in one optimization loop only, a better compromise among the output variables can be found and the resultant smart structure can more easily meet the technical requirements. Moreover, the simultaneous approach profited from the physical integration of piezoceramics, in which the load carrying role of the transducers is demonstrated. When optimizing the structure with the piezoceramics, the structure itself is compelled to have a lower stiffness than the requirement, but when the optimal piezoceramics are considered, the total stiffness attains the desired value.

It is important to notice that, even though the traditional serial approach could not find a global optimum for the smart structure, it is an important tool to validate a first prototype in the

design process and to have a better understanding of the requirements. Additionally, experimental results have shown that, in spite of the high effort, the most important technical requirement was very low, namely the GEMCC, but still above the minimum requirement. This is mainly due to the piezoceramics being closer to the neutral axis, to the sublaminate definition and also to the manufacturing process. Nevertheless, the optimal damping using the *RLC*-shunt circuit could be validated. To sum up, **Figure 5.26** presents the workflow of a smart structure design, in which the development of the lightweight smart structure is shown, according to what has been discussed. In the next chapter, a novel method for shunt damping tuning is presented using the smart structure developed here.

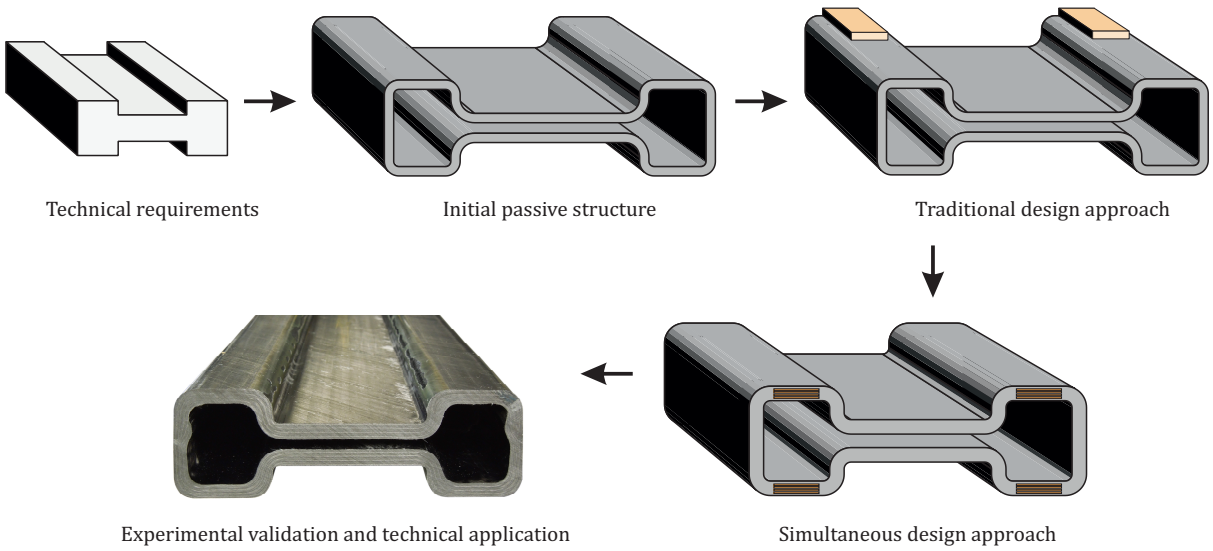

Figure 5.26. Workflow of a smart structure design

6 Optimal shunt parameters: An experimental approach

In this chapter, a new tuning method for shunt damping with a series resistance, inductance and negative capacitance is proposed. This method is based on the measured electromechanical impedance of a piezoelectric system, as first suggested by [131] in the context of shunt damping. The system is represented through an equivalent electrical circuit that takes into account the characteristics of the piezoelectric transducer and the host structure. This allows the tuning of the shunt parameters so as to maximize the damping performance.

To validate this approach, a numerical optimization and an experimental analysis are carried out in order to compare the damping performance of the proposed method and the conventional analytical method that minimizes a mechanical frequency response function. This is investigated using the smart structure developed in the previous chapter, to which optimized shunts are applied for the first three eigenfrequencies.

Benefiting from the electrical representation of the structure, it is hence possible to connect the shunt circuit to the network and analyze all quantities in a purely electrical form. Then, the Norton equivalent impedance is obtained at the terminals that represent the mechanical mode of interest. During the tuning process, the optimal shunt parameters are found by minimizing the maximum absolute value of the Norton equivalent impedance over a defined frequency range through a numerical optimization. Taking benefit from the analogy between electrical impedance and mechanical admittance, the minimization of different mechanical responses is also proposed and the different optima are compared.

In view of real technical applications, since this method is based on one simple measurement, it can be applied to arbitrary structures without the need of complicated mechanical tests. Furthermore, this method allows the integration of a real negative capacitance circuit, i.e. a NIC, rather than an ideal component. It is thus possible to use the impedance of this circuit and optimize the individual component values. It will also be shown that the proposed method is easily applicable to multi-mode systems with high modal density, where the analytical methods are not sufficient when using only one piezoceramic and one shunt circuit. Finally, experimental analyses prove that the optimization of the mechanical response of the structure is indeed correlated with the optimization of the Norton equivalent impedance.

6.1 Equivalent electrical circuit

In order to correctly tune the parameters of the shunt circuit, the measured impedance of the smart structure must be correctly represented. So as to simplify further analyses of electrical circuits coupled to a resonant mechanical structure, it is possible to represent all mechanical quantities in an electrical form, as previously discussed in Chapter 2.2.4.

In regard to a piezoelectric ceramic mounted to a resonant structure, the equivalent electrical circuit shown in **Figure 2.6** (3) can be easily extended to represent several degrees of freedom. The modified electrical circuit consists of a series connection of a resistor, a capacitor and several parallel RLC branches. This circuit is depicted in **Figure 6.1**.

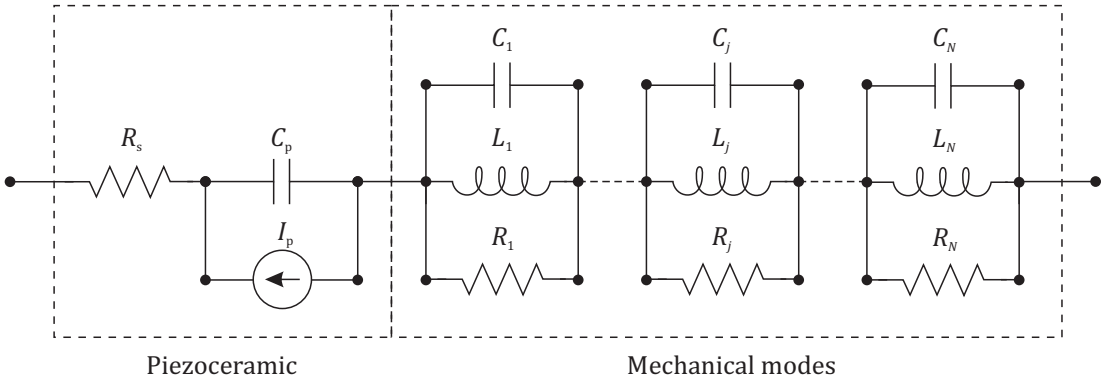

Figure 6.1. Equivalent electrical circuit of a piezoceramic and a resonant structure

The electrical impedance of the piezoceramic can be calculated by Eq. (6.1):

$$Z_{\text{piezo}} = \frac{1}{C_{\text{p}} s} + R_{\text{s}} \tag{6.1}$$

where R_{s} is the inherent resistance and C_{p} is the inherent capacitance of the piezoceramic.

The electrical impedance of the j^{th} mechanical mode can be calculated using Eq. (6.2):

$$Z_{\text{mech}-j} = \frac{s}{C_j s^2 + s/R_j + 1/L_j} \tag{6.2}$$

Finally, the electrical impedance of the complete electromechanical resonant structure can be obtained by Eq. (6.3):

$$Z_{\text{total}} = Z_{\text{piezo}} + \sum_{j=1}^{N} Z_{\text{mech}-j} \tag{6.3}$$

6.2 Electromechanical impedance measurement

In order to investigate the effectiveness of the proposed method, measurements are carried out using the smart structure developed in Chapter 5 with the simultaneous design approach. To obtain the equivalent electrical circuit, one simple measurement is carried out. The electrodes of the piezoceramics are connected to an Impedance Analyzer and a frequency sweep is done around the eigenfrequencies of interest. Since the mechanical validations will be carried out later using an electromagnetic shaker, it is desirable to leave it attached to the structure, in order to consider its complex dynamic behavior [132], although it might be neglected for some frequency ranges. **Figure 6.2** shows in solid lines the measured electromechanical impedance represented by magnitude and phase for the first three eigenfrequencies of the smart structure.

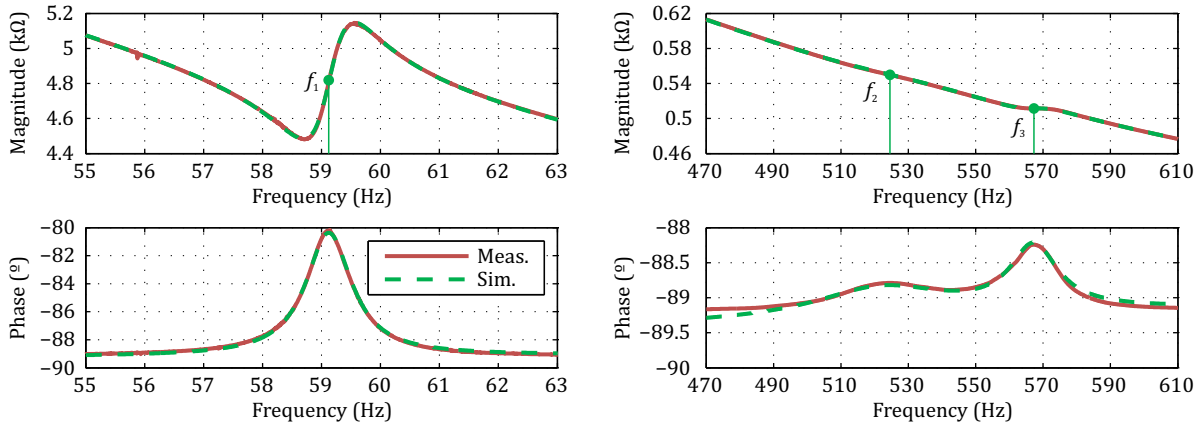

Figure 6.2. Measured and fitted impedance of the cantilever CFRP I-beam

Afterwards, the impedance calculated using Eq. (6.3) is fitted to the measurement by minimizing the RMS error between the two signals, for both magnitude and phase. The minimization is done using a derivative-free algorithm implemented through a MATLAB® script. As a starting point, the "static" capacitance of the piezoceramics C_p is used, together with L_j and C_j values that correspond to the measured resonance frequencies. **Figure 6.2** shows in dashed lines the result of the curve fitting. The fit error in the frequency range 55-63 Hz is 0,15 % and in 470-610 Hz is 0,10 %, which confirms the effectiveness of this representation.

Table 6.1 shows the obtained circuit coefficients after the curve fitting. As evidenced by [95], the inherent capacitance C_p and the series resistance R_s of the piezoceramics depend on the frequency of the excitation. Therefore, in order to correctly obtain these values, two separate fits have been carried out, one for the first frequency range and another for the second. It can be noticed from **Table 6.1** that the value of the inherent capacitance is slightly different between the first and the second frequency ranges. This effect is more visible for the series resistance, which is ten times smaller in the second frequency range compared to the first one.

Table 6.1. Fitted circuit coefficients of the cantilever CFRP I-beam

	1	**2**	**3**
Mechanical modes	R_1 = 737,3 Ω	R_2 = 4,212 Ω	R_3 = 8,069 Ω
	L_1 = 31,79 mH	L_2 = 121,6 µH	L_3 = 68,65 µH
	C_1 = 227,6 µF	C_2 = 764,1 µF	C_3 = 1,147 mF
PZT capacitance	C_p = 561,4 nF	C_p = 551,9 nF	
PZT resistance	R_s = 71,46 Ω	R_s = 6,865 Ω	

Table 6.2 shows the short circuit eigenfrequency obtained from the fitted impedance for the first three eigenfrequencies, together with the respective GEMCC, obtained by Eq. (2.11).

Table 6.2. Eigenfrequencies and GEMCC of the smart structure

Mode	Frequency (Hz)	K_{31}^2 (%)
1	59,09	0,247
2	521,2	0,072
3	567,1	0,048

6.3 Norton equivalent impedance

Once the equivalent electrical circuit of the smart structure has been determined, it is possible to include the shunt circuit in the analysis. Since the mechanical modes are represented in an electrical form, the obtained electrical network consists of a closed series connection of all sub-systems, i.e. the piezoceramic, the resonant branches and the shunt circuit.

If the shunt circuit is to be designed to dampen one single mode of the structure, the electrical representation of this mode serves as a reference to calculate the impedance of the closed electrical network. This is eventually analogous to the calculation of the mechanical admittance for the same mode when the shunt circuit is connected.

Considering that *j* is the mechanical mode of interest, it is possible to define a virtual current source across the terminals of its equivalent electrical impedance. This current source is analogous to a mechanical force that would excite the mode *j*. The next step consists in calculating the Norton equivalent impedance using the Norton's theorem. This can be easily obtained by analyzing the circuit in **Figure 6.3**.

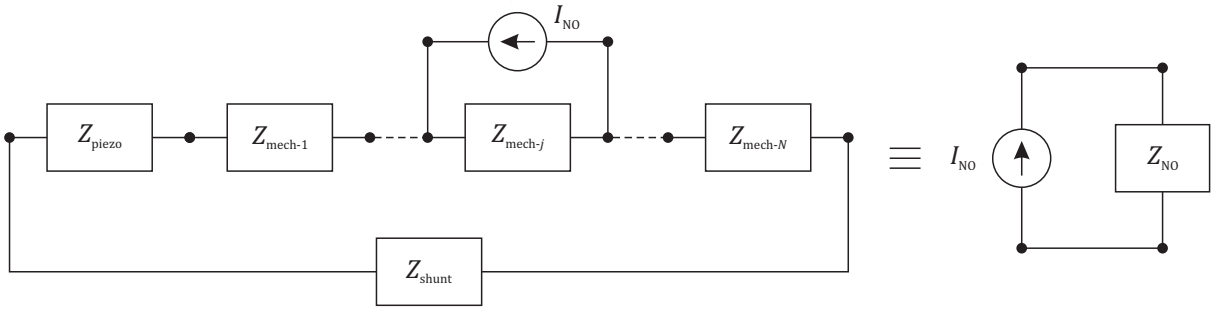

Figure 6.3. Norton equivalent impedance obtained for the j^{th} mechanical mode

The current source is in parallel with the electrical impedance that represents the mechanical mode of interest *j*. It is also in parallel with the series connection of the piezoceramics, the shunt circuit and all branches of the mechanical modes, except the one being analyzed. The mathematical description of the Norton equivalent impedance in the Laplace domain is shown in Eq. (6.4):

$$Z_{\mathrm{NO}} = \left(\frac{1}{Z_{\mathrm{total}} - Z_{\mathrm{mech}-j} + Z_{\mathrm{shunt}}} + \frac{1}{Z_{\mathrm{mech}-j}} \right)^{-1} \tag{6.4}$$

Within the scope of this method, only the shunt circuit is regarded as a design variable. The impedance of the *RLC*-shunt can be calculated using Eq. (2.27) together with Eq. (3.15), where the resistance R of the NIC can be merged into one single value of R_{sh}.

6.4 Numerical optimization approach

The proposed method for tuning the shunt parameters consists in numerically minimizing the maximum singular absolute value of the Norton equivalent impedance over a defined frequency range. This numerical optimization is carried out using a derivative-free algorithm, taking into account constraints for the input parameters according to design guidelines presented in Chapter 3.5.2. Using the analogy presented by Eq. (2.9), it can be concluded that minimizing the electrical impedance is equivalent to minimizing the mechanical admittance, i.e. for a unit force, the velocity. Moreover, it is known that the derivative or the integral of the velocity results in acceleration or displacement, respectively. It is therefore possible to tune the shunt parameters to minimize mechanical acceleration or displacement, by simply using the same mathematical operations for the Norton equivalent impedance in the Laplace domain, i.e. s for derivative and $1/s$ for integral. Eq. (6.5), (6.6) and (6.7) show the objective functions that are minimized and the mechanical analogous response.

$$\min(vel.) \equiv \min(|Z_{\mathrm{NO}}|) \tag{6.5}$$

$$\min(accel.) \equiv \min(|Z_{\mathrm{NO}} s|) \tag{6.6}$$

$$\min(disp.) \equiv \min(|Z_{\mathrm{NO}}/s|) \tag{6.7}$$

6.5 Simulation results

A numerical optimization has been performed targeting two separate frequency ranges. This is due to the fact that the measured impedance has very different magnitudes for each of them, as seen in **Figure 6.2**, and also that the series resistance of the piezoceramics are considerably different. The first range is 40-120 Hz, which contains the first eigenfrequency of the beam. The second range is 470-610 Hz, where both the second and the third eigenfrequencies have been simultaneously analyzed.

The first objective function was set to be the absolute value of the derivative of the Norton equivalent impedance, which means that the acceleration response is minimized, as described by Eq. (6.6). The obtained values can be seen in **Table 6.3**. To prove the validity of the proposed method, a second objective function was defined and the results compared with the conventional analytical tuning method, as presented in Chapter 2.3.2. This function was set to be the absolute value of the integral of the Norton equivalent impedance, which means that the displacement response is minimized. **Table 6.3** shows the optimal shunt parameters, for both the new numerical method and the conventional analytical method. For practical reasons, β has been chosen to be equal to 0,95. Since the analytical method is based on a mechanical measurement, it will only be validated experimentally, and its Norton equivalent impedance will not be depicted.

Table 6.3. Optimal *RLC*-shunt circuit parameters

Objective	**$\min(\lvert Z_{NO}s\rvert)$**		**$\min(\lvert Z_{NO}/s\rvert)$**			
Mode	**1**	**2 & 3**	**1**		**2 & 3**	
Method	**Numerical**	**Numerical**	**Numerical**	**Analytical**	**Numerical**	**Analytical**
L_{sh} (mH)	717,3	7,593	722,0	704,9	8,452	8,672
R_{sh} (Ω)	80,00	10,00	80,00	78,60	7,500	7,500
R_1 (Ω)	954,2	997,4	956,3	956,9	996,6	998,2
R_2 (kΩ)	1,000	1,000	1,000	1,000	1,000	1,000
$\widehat{R}$ (kΩ)	305,5	91,13	299,2	299,2	102,0	102,0
C (nF)	580,4	580,4	580,4	580,4	580,4	580,4

Figure 6.4 shows the absolute values of the derivative and integral of the Norton equivalent impedance when the piezoceramics are short-circuited, i.e. $Z_{\text{shunt}} = 0$, for both frequency ranges. It also shows the Norton equivalent impedance when the numerically optimized shunt parameters from **Table 6.3** are inserted into Z_{shunt}.

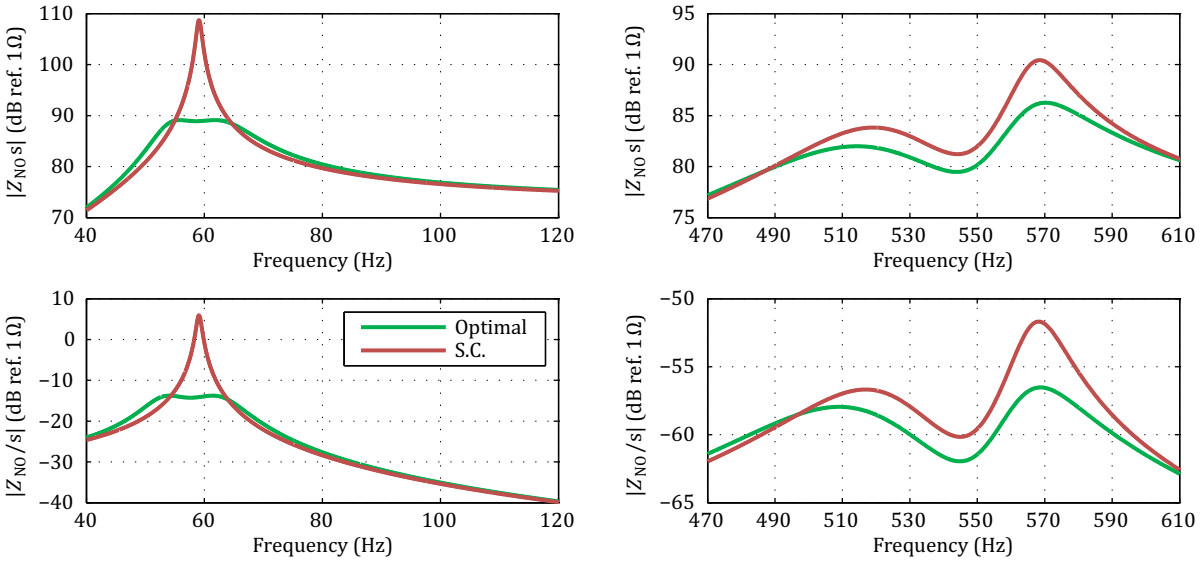

Figure 6.4. Simulation results of optimized Norton equivalent impedances

It can be noticed that, for the first eigenfrequency, the optimal shunt has the characteristic two peaks with the same amplitude and highly damped, as already evidenced by **Figure 2.10** with the analytical method. The reductions obtained here are -19,6 dB and -19,7 dB for derivative and integral, respectively.

However, when trying to optimize one single shunt circuit simultaneously for the second and third modes, which are close to each other, the shape of the Norton equivalent impedance is not straightforward. The two symmetric peaks with the same amplitude do not appear anymore.

Nevertheless, the reduction levels are still significant: -4,17 dB for the derivative and -4,18 dB for the integral.

6.6 Experimental validation

To validate the optimization of the Norton equivalent impedance and the actual effect in the mechanical response, experimental analyses have been carried out. An electromagnetic shaker has been attached to the tip mass of the cantilever beam, together with a force sensor and an accelerometer. An FFT analyzer makes the data processing in real time. The shunt circuit was implemented as described in Appendix A.

The first analyses consisted in evaluating the FRF of the acceleration per unit force. The mechanical response when the electrodes of the piezoceramics were short-circuited was compared to when the numerically optimized parameters were configured in the shunt. Even though the parameters of the analytical method are optimized for displacement, their effect on the acceleration response was also measured for matters of comparison.

Figure 6.5 shows the magnitude of the experimental FRF comparing the short circuit configuration (dashed lines) and the optimized shunts (solid lines). It can be noticed that the performance of the numerical optimization is slightly better than the conventional method. In the frequency range 20-120 Hz, there was a peak reduction of -20,7 dB using the proposed numerical optimization method, which outperformed the classical method in only -0,5 dB. It can be noticed that the new method indeed minimizes the response, since a "flat" peak with constant amplitude appears. Even though a small GEMCC is present, the optimized shunt is capable of significantly reducing the vibration level. In the frequency range around the second and third modes, the new method performed -1,72 dB better than the analytical method.

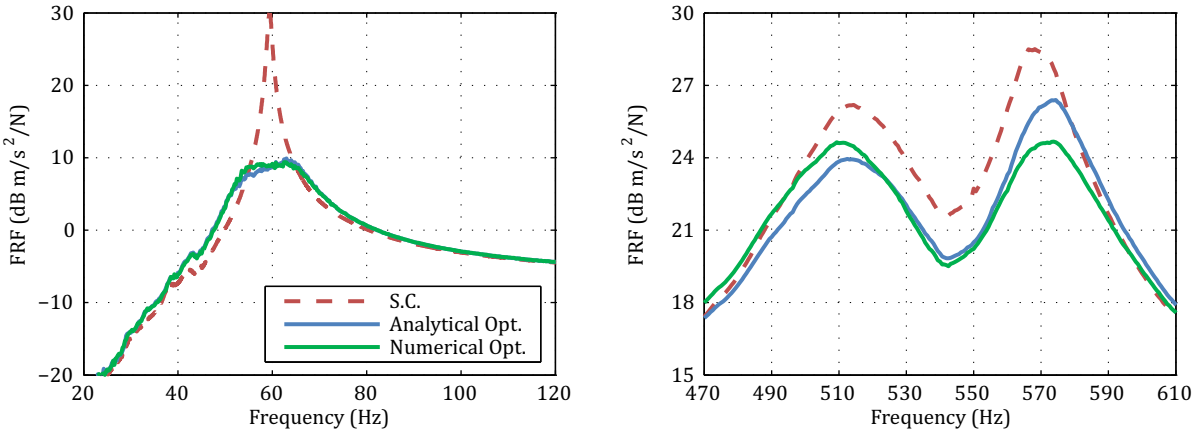

Figure 6.5. Experimental results for optimized FRF (acceleration per unit force)

The next analyses consisted in evaluating the FRF of the displacement per unit force. **Figure 6.6** shows the magnitude of the experimental FRFs. In the frequency range 20-120 Hz, the

numerical method performed equally to the classical method. In the frequency range around the second and third modes, the new method performed -0,5 dB better.

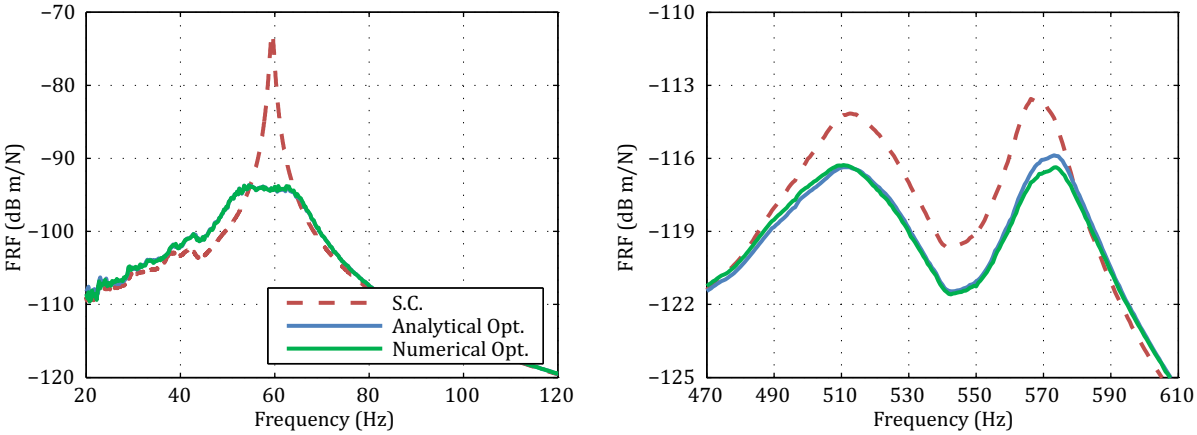

Figure 6.6. Experimental results for optimized FRF (displacement per unit force)

Table 6.4 shows the vibration reduction experimentally obtained from the acceleration and displacement per unit force, when different optimal shunts were connected to the smart structure. It is evident that the new tuning method performs better than the analytical method, even though the attenuation levels do not match those from the numerical analysis. This can be explained by the fact that the Norton equivalent impedance does not take into account all the modes simultaneously, which is evidenced by the different appearance of the calculated and the actual measured FRF.

In spite of the good performance of the new method, the optimization effort can be questioned. This can be mostly explained by the difficulty in fitting the measured impedance to the equivalent electrical circuit, and also by the high sensitivity of the shunt parameters when configuring the real circuit. During the experimental analyses, it has been noticed that a 1 % change in the design variables can dramatically change the optimal FRF.

Table 6.4. Vibration attenuation with optimal *RLC*-shunt

Mode	**1**		**2 & 3**	
Method	**Numerical**	**Analytical**	**Numerical**	**Analytical**
Accel. (dB)	-20,7	-20,2	-3,83	-2,11
Disp. (dB)	-20,9	-20,9	-2,80	-2,30

6.7 Conclusions

A novel tuning method for piezoelectric shunt damping with a resonant negative capacitance has been proposed. It is based on the measured electromechanical impedance of a smart structure, which is represented through an equivalent electrical circuit. The Norton

equivalent impedance obtained at the terminals that represent the mechanical mode of interest is numerically minimized over a defined frequency range. To validate the proposed approach, numerical and experimental analyses have been carried out using the cantilever CFRP I-beam with integrated piezoceramics developed previously and taking into account its first three eigenfrequencies. It has been shown that there is a relation between the Norton equivalent impedance and the mechanical behavior of the structure when it is connected to the shunt circuit. The numerically optimized shunt parameters have been implemented through a real circuit and mechanical FRFs have been successfully measured. However, experimental results indicate that the optimization effort can be too high in comparison to the attenuation obtained by the conventional method. Nevertheless, the conventional method has been shown to be unable of precisely tuning the shunt parameters when two modes close to each other are considered, in contrast to the proposed method. A further benefit of the numerical optimization proposed here is that, in contrast to conventional analytical methods, it takes into account the inherent structural damping present in real structures. Finally, the main advantage of dealing with electrical quantities is that all components in the NIC circuit are taken into account in the optimization. This is especially desirable because some components can have an unwanted effect on modes outside the frequency range of interest.

7 Application on a control arm

After introducing all the basic concepts of piezoceramic integration, structural optimization and shunt damping, this chapter is dedicated to applying this knowledge to a more realistic case study: The control arm. Initially, the mechanical design of this part is introduced and different numerical simulations are carried out using the laminate composite structure. The concept of transmissibility is introduced, which represents the dynamic amplification of wheel efforts that are transmitted through the part and inputted into the vehicle chassis. In order to improve the vibration behavior of the part, a fiber-reinforced piezoelectric module has been developed and simulated together with an *RLC*-shunt. The effectiveness of this technique is finally compared with a classical tuned mass damper.

7.1 Case study description

The selected case study is a CFRP control arm developed within the framework of the FP7 European Project ENLIGHT, which deals with highly innovative and sustainable lightweight technologies for the application in future electric vehicles intended to reach the market within the next 12 years. The initial lightweight design of the control arm has been inspired from the metal part found in the vehicle VW Golf V, which can be seen in **Figure 7.1**. This part is characterized by a complex three-dimensional geometry that is capable of dealing with high stresses, mainly due to high loads applied during vehicle acceleration or brake.

Figure 7.1. The control arm of a Volkswagen Golf V

The external geometry of the CFRP control arm has been previously designed in [133]. In the current study, this definition remains frozen. The connection points to the subframe, front and rear, and to the wheel are defined by the same geometric positions as for the metal part. The mass target for the lightweight control arm has been set to 2,2 kg, in contrast to the existing 4,0 kg of the metal control arm. At this stage, the laminate alone weighs 0,65 kg, without taking into account any metal inserts or rubber mounts.

The inner structure of the original laminate is composed of 22 layers of a woven carbon fiber fabric made from the material T300. A first prototype has been built to validate the manufacturing process and a ply thickness of 0,22 mm has been achieved, which results in a laminate thickness of 4,84 mm. Moreover, unidirectional fibers alternated between the woven fabrics have been placed in strategic areas in order to improve the static strength of the points connecting the load inputs. **Figure 7.2** shows the external geometry of the control arm, together with a cross-section view of the laminate. The original laminate stacking sequence is [30/15/0/-30/45/0/-15/15/30/45/-30] symmetric.

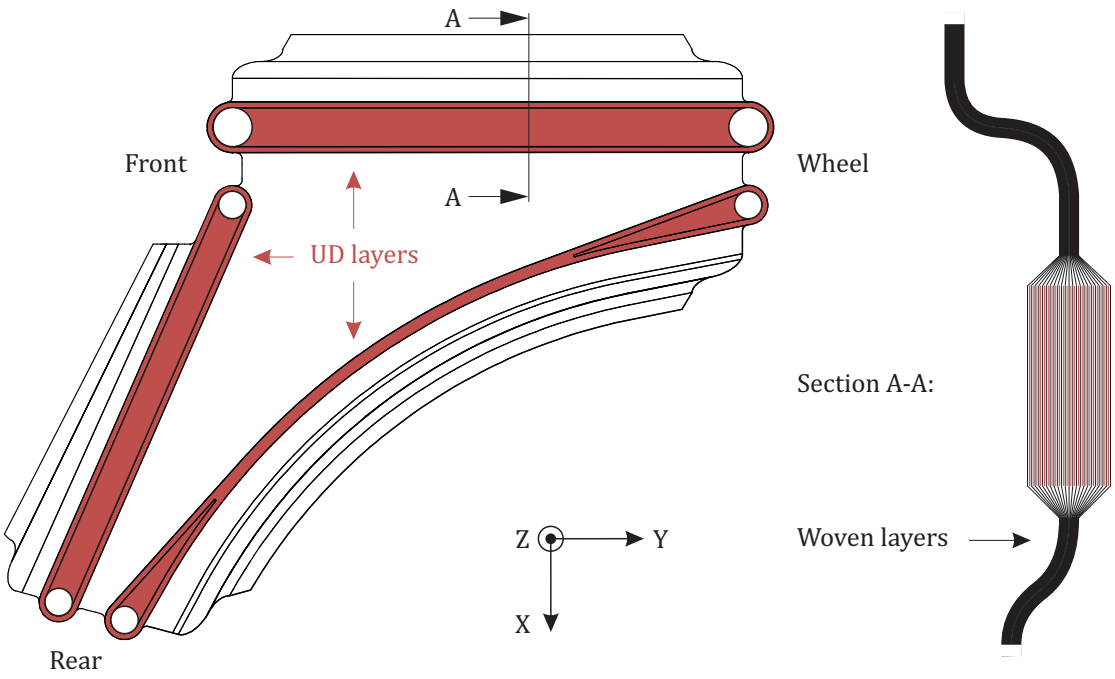

Figure 7.2. The CFRP control arm

7.2 Numerical investigations

The original CFRP control arm has been numerically investigated. In order to evaluate the vibration behavior of this part, static, modal and harmonic analyses have been performed. The strength properties of the control arm are not part of this study.

Early in the design process, the metal inserts and the characteristics of rubber mounts are not taken into account since preliminary data are inaccurate or unavailable. Later in the validation phase, it is important to consider realistic boundary conditions, in order to correctly simulate the strain distribution inside the laminate, which is highly relevant for vibration analyses and eventually for shunt damping techniques. In this study, however, ideal boundary conditions are used to demonstrate whether the techniques presented here have the potential of being used or not. In this sense, the front connection point of the control arm is fixed in all directions, the rear point is free to move in the X direction only, and the wheel point is free to move in the XY plane only. This configuration represents the different stiffnesses in different directions of the rubber mounts.

Initially, it is important to calculate the static stiffness of the wheel connection point of the control arm. This value is usually a very strict criterion in the vehicle requirements, since it is the input stage of all forces coming from the wheel. The longitudinal stiffness in the X direction corresponds to brake and acceleration efforts, whereas the lateral stiffness in the Y direction should carry the efforts when the vehicle drives in a curve. When applying a force in the X direction, the average displacement of the connection point is calculated and an equivalent longitudinal stiffness of 9,906 kN/mm is found. If the force is applied in the Y direction, the lateral stiffness is equal to 219,9 kN/mm. These values respect the minimum project requirements of 2 and 60 kN/mm, respectively.

Next, a harmonic analysis of the control arm has been carried out. The aim is to quantify the vibration transmission through the part, i.e. how much of the input forces at the wheel pass through the front and rear connection points into the subframe. The inputs are hence defined as translational forces at the wheel, whereas outputs are reaction forces at the front and rear points. These transfer functions are called transmissibility and allow the identification of transmission paths. For each direction of force input, it shows how much amplification or reduction there is in each direction in each point at the subframe. The transmissibility is an important factor in the definition of the orientation of rubber mounts, so as to correctly filter the highest force peaks.

In the case of dynamic analyses, the total mass of the system plays a major role. Therefore, a tip mass has been attached to the wheel point in the model. This fictitious mass represents a steering knuckle, a disc brake and a wheel of a midsize vehicle. **Table 7.1** describes the value of the mass, the principle moments of inertia relative to its center of gravity, and the center of gravity relative to the center of the wheel connection point.

Table 7.1. Definition of the tip mass representing the wheel

	X	Y	Z
***m* (kg)**	22,50		
***I* (kg·m²)**	0,697	0,409	0,409
***CG* (mm)**	112,7	1,922	95,46

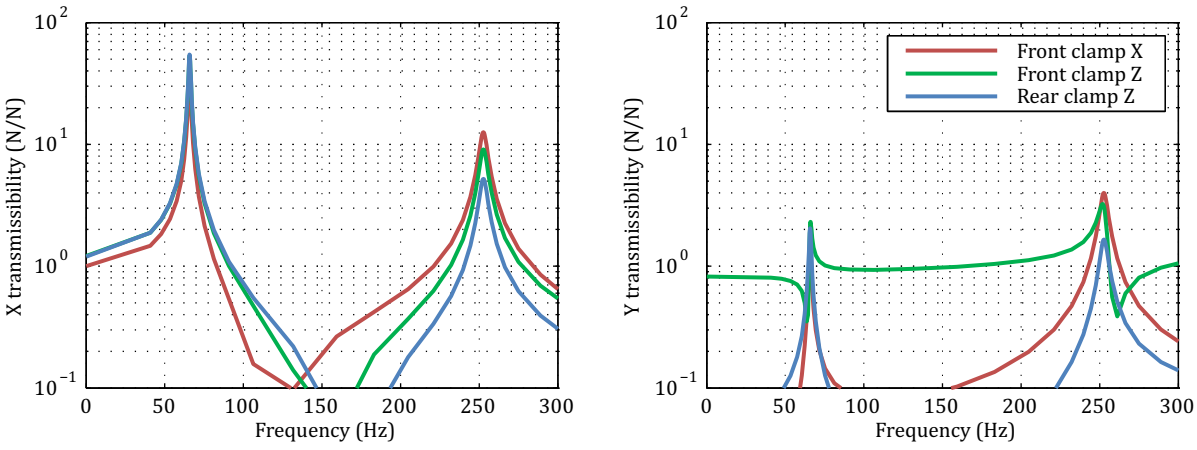

Figure 7.3. Transmissibility of the control arm in two orthogonal directions

Figure 7.3 shows the most relevant transmissibilities simulated for the control arm. A frequency range of 0-300 Hz has been chosen, since most vibration-related problems in midsize vehicles occur in this range. It can be noticed that, when a dynamic force of 1 N is applied at the wheel in the X direction, the force at the rear clamp in the Z direction is equal to 53 N at around 63 Hz. With the same input force, an amplified effort appears at the front clamp in the X direction, in this case 13 N at around 250 Hz.

The next step is to perform a modal analysis to identify the mode shape of the two most important transmission modes. **Figure 7.4** shows the deformed mode shapes of the first two modes. Mode 1 is at 63 Hz and represents a movement of the wheel point in the X direction and a bending in the Z direction of the UD layers between the wheel and rear points. Mode 2 is at 250 Hz and represents a movement of the wheel point in the X direction together with a bending in the X direction of the UD layers between the wheel and front points.

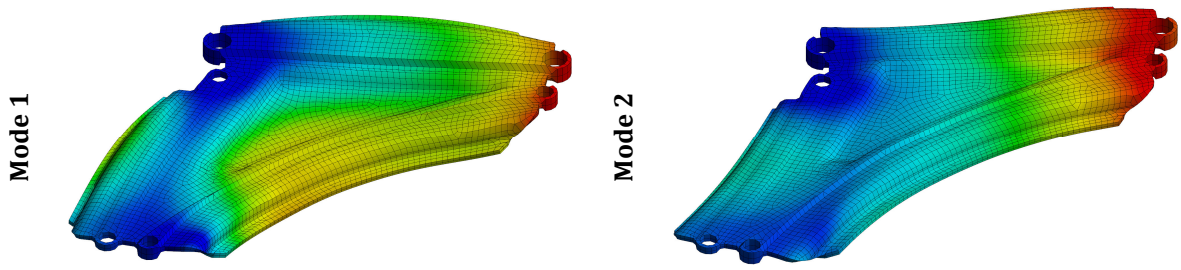

Figure 7.4. Mode shapes of the control arm

7.3 Fiber-reinforced piezoelectric module

Integrating piezoceramic transducers in this complex-shaped structure revealed to be a major challenge. Since the laminate does not have flat areas large enough for the integration of plate transducers, a major geometric redesign would be required. Moreover, integrating piezoceramics inside the final laminate structure would demand substantial changes in the manufacturing process, as this would require more stacking steps or even a new mold, which was not desirable in this prototype phase. Since the control arm is highly relevant for vehicle safety, the integrity of the part has to be checked during manufacturing and a long lifetime has to be assured. In the case of a mass production, this would mean high costs for durability and quality tests.

Moreover, when trying to apply shunt damping techniques to stiff structures like the control arm, the optimization of the GEMCC results in large piezoceramic plates, often several millimeters thick, which is intended to counteract the stiffness of the structure. If integrated between two plies, a thick piezoceramic plate would increase the ply drop-off in the composite and therefore increase stress concentration.

Preliminary simulations have shown that applying the piezoceramic transducers externally to the structure can be highly beneficial. In the case of bending modes, since the piezoceramic material is far away from the neutral axis, the capability of the transducer to generate bending moments is increased and therefore the GEMCC is improved.

In the case of a monolithic piezoceramic plate, if it is to be applied onto an irregular surface, customized shapes are necessary and, if manufacturing is possible, tooling costs for the ceramics are too high. Furthermore, it is known that thick monolithic plates generate very high voltages. A workaround consists in dividing the plate in thin ceramic layers and bonding them together, which reduces the generated voltage while maintaining the mechanical stiffness. This is the principle used in multi-layer piezoceramic actuators.

Considering these aspects and taking benefit from the layered structure of a laminate composite, a fiber-reinforced piezoelectric module has been developed and a patent application has been filed. The idea is to have an external component that can be easily applied to any structure. In the context of composite materials, the idea of having bonded patches is not new and is already used to repair structural failures [134]. **Figure 7.5** shows the cutaway drawing of the rectangular module used for the proof of principle. It consists of alternated composite material, in this case UD glass fiber to avoid isolation problems, oriented in the 90° direction, and very thin piezoceramic plates, to reduce ply drop-off. Five piezoceramic plates of dimensions 50 x 30 x 0,2 mm are included. The thickness of the plies and the plates are identical. Other than presenting the aforementioned advantages, the composite material protects the transducers from harsh environment conditions, therefore increasing their durability.

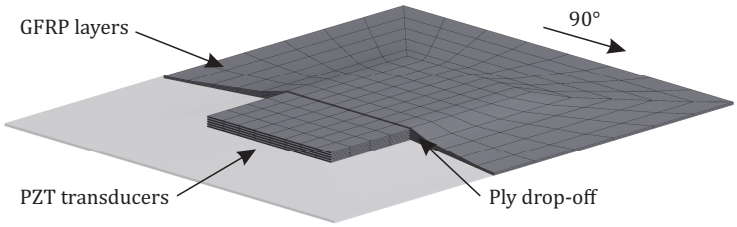

Figure 7.5. Fiber-reinforced piezoelectric module

In order to show the benefits of this piezoelectric module, it has been compared to a PIC151 monolithic piezoceramic plate of 1,0 mm thickness, which represents the same amount of active material. A clamped-clamped steel beam of dimensions 400 x 50 x 2,2 mm has been used as the host structure for the proof of principle. Its first eigenfrequency corresponds to a bending mode and is equal to 72 Hz. The maximum strain in the longitudinal direction is found near the clamps, as depicted in **Figure 7.6**, and is the position used to apply either the piezoceramic plate or module.

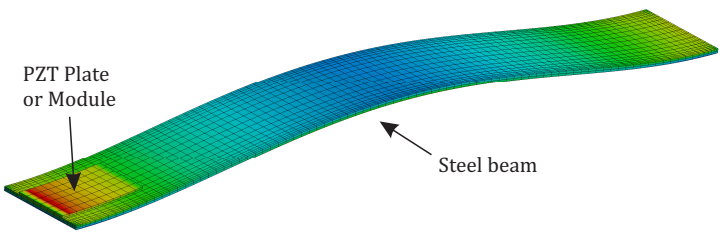

Figure 7.6. Strain distribution in the host structure used for the proof of principle

Initially, the piezoceramic plate has been applied to the host structure. In this case, the calculated K_{31}^2 is equal to 1,829 %. When applying the new piezoelectric module, the calculated K_{31}^2 is equal to 2,459 %, which represents an improvement of +35 % in energy conversion. The voltage generated by the monolithic plate is equal to 169 V per unit displacement in the center of the beam, in contrast to 38 V in the case of the piezoelectric module, which represents a level almost five times smaller. This shows that the concept of stacking thin piezoceramic plates inside a laminate composite has the potential to substitute monolithic plates in lightweight applications and to reduce the need for high-voltage electronics.

To show the potential of the fiber-reinforced piezoelectric module in a more realistic structure, the same concept has been applied to the CFRP control arm. Since the first mode has the highest transmissibility, it is crucial to reduce its contribution to improve the vibration performance of the part. In the context of shunt damping, it is also important to know where to position the piezoceramic transducers. In this sense, the modal analysis allowed to identify locations in the part where the strain is concentrated, i.e. possible candidate areas for the application of the piezoelectric module.

Figure 7.7 shows the normal strain distribution in the X direction of a local coordinate system. It can be noticed that, since the first mode is a bending vibration, the area with the highest strain is located between the rear and wheel points, in the top layer of the laminate. Therefore, the piezoelectric module has been applied onto this area.

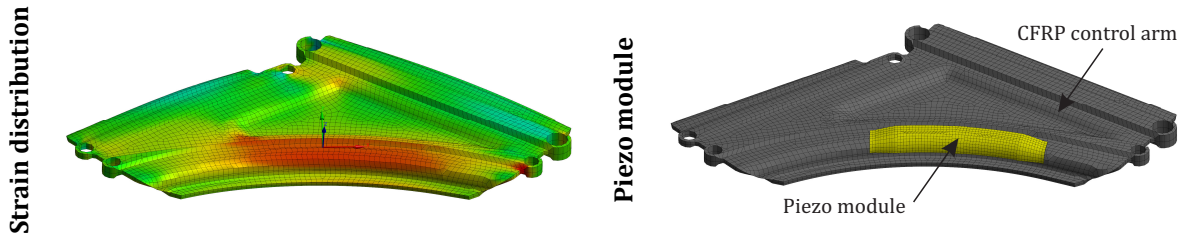

Figure 7.7. Area of application of the piezoelectric module on the control arm

This version of the piezoelectric module consists of glass fiber layers and several piezoceramic transducers divided into 2 stacks next to each other. Its longitudinal cross-section can be viewed in **Figure 7.8**.

A sensitivity analysis showed that, in order to maximize the GEMCC, it is important to reduce the stiffness of areas that act in parallel to the transducer and increase the stiffness of areas that act in series. This means that the fibers should be oriented in the longitudinal direction where they touch the sides of the plate and in the transverse direction where they touch the top and bottom surfaces of the plate. It is also important to see that the spread distribution of the glass fiber layers on the sides reduces the ply drop-off. A further advantage is that the surface of the structure is directly connected to the upper piezoceramic transducers, increasing the strain transmission and potentially the GEMCC.

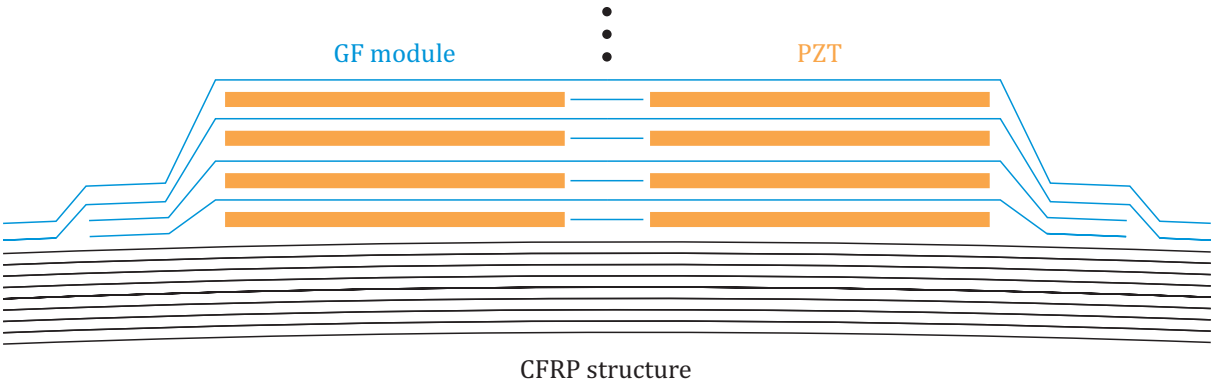

Figure 7.8. Cross-section of the piezoelectric module applied to the control arm

The number of piezoceramic elements inside the module has been chosen in order to maximize the GEMCC. The best value has been found when having a total of 20 piezoceramic transducers applied to the control arm.

In addition to applying the piezoelectric module onto the surface of the control arm, an optimization of its design has been carried out. Since the piezoelectric module is supposed to increase the resultant stiffness of the structure, an adjustment of the plies in the laminate of the control arm has to be made. Reducing the number of layers and optimizing the stacking sequence guarantees that the same static stiffness of the original control arm is maintained. Moreover, by removing layers from the laminate, it is potentially possible to compensate the additional mass brought by the piezoelectric module. The application of this module allowed the removal of 4 layers in the composite, which reduces the weight of the structure in 0,1 kg compared to the original configuration. When the piezoelectric module is taken into account, there is a 0,05 kg mass saving compared to the original passive structure, with the further advantage that the new configuration allows smart functionalities. The optimized stacking sequence is [-35/35/65/-70/75/70/-35/-20/-60] symmetric, which maintains the static stiffness of the original structure.

Table 7.2. Control arm characteristics along the design optimization process

	Original laminate	Optimized laminate	Smart structure
Lateral stiffness Y (kN/mm)	219,9	182,0	186,2
Longitudinal stiffness X (kN/mm)	9,906	8,400	9,979
Eigenfrequency (Hz)	62,95	57,92	62,98
Mass (kg)	0,644	0,540	0,600

Table 7.2 summarizes the main characteristics of the CFRP control arm step-by-step in the optimization process, from the original laminate to the smart structure. It can be noticed that the optimized laminate, together with the piezoelectric module, was only capable of maintaining the stiffness in the longitudinal direction, with an error smaller than 1 %, whereas the stiffness

in the lateral direction has been reduced in 15 %. The final eigenfrequency has been maintained almost constant. In this case, the piezoelectric module is responsible for 19 % of the total static stiffness. Finally, the simultaneous optimization not only fits the target stiffness, but also represents a further mass saving, which in this case has been reduced in 7 %. The optimized calculated K_{31}^2 is equal to 0,464 %.

7.4 Tuned mass damper

Large vibration amplitudes of a single degree of freedom system occur if the excitation frequency is near the resonance. When an additional mass-spring-damper system is attached to the vibrating body, if correctly designed, the resulting two degrees of freedom system presents natural frequencies that are away from the excitation. This so-called tuned mass damper absorbs the vibration of the main body and limits the amplitude of the movement. Its schematic representation is depicted in **Figure 7.9**.

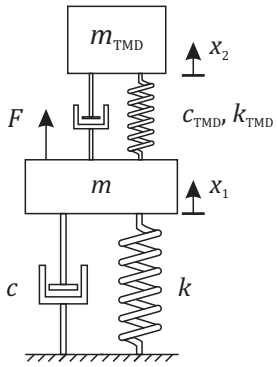

Figure 7.9. Principle of a tuned mass damper

To correctly tune this vibration absorber, optimal parameters have to be chosen. Analytical equations are well established in the literature [135] and a slightly modified tuned mass damper has been presented in [136]. Initially, the mass m_{TMD} of the tuned mass damper has to be chosen in terms of the mass m of the main body, through the ratio r_{m} (usually smaller than 0,2), as shown in Eq. (7.1):

$$m_{\mathrm{TMD}} = r_{\mathrm{m}} m \tag{7.1}$$

The stiffness k_{TMD} of the absorber also has to be chosen in terms of the stiffness k of the main body, as shown in Eq. (7.2):

$$k_{\mathrm{TMD}} = r_{\mathrm{c}} k \tag{7.2}$$

using the optimized ratio r_{c}, as calculated in Eq. (7.3):

$$r_{\mathrm{c}} = \frac{r_{\mathrm{m}}}{(1 + r_{\mathrm{m}})^2} \tag{7.3}$$

The optimal damping ratio ζ_{opt} of the tuned mass damper is obtained using Eq. (7.4):

$$\zeta_{\text{opt}} = \sqrt{\frac{3r_{\text{m}}}{8(1+r_{\text{m}})^3}} \tag{7.4}$$

leading to the damping coefficient c_{TMD}, calculated as in Eq. (7.5):

$$c_{\text{TMD}} = 2\zeta_{\text{opt}}\sqrt{k_{\text{TMD}}m_{\text{TMD}}} \tag{7.5}$$

Among all possible solutions to attenuate vibrations in the control arm, the tuned mass damper is the most traditional and will be used as a reference for the evaluation of the performance of an *RLC*-shunt connected to the fiber-reinforced piezoelectric module.

To find the optimal position for the tuned mass damper in the control arm, the effective modal mass of the first eigenfrequency has been calculated. Since an important tip mass is attached to the wheel point, the maximum displacement occurs in this location, more specifically in the X direction, so a tuned mass damper in the same direction has been attached to this point. To tune the mass damper, the control arm in its original laminate configuration without the piezoelectric module is considered. In this case, two different mass ratios r_{m} will be used for the tuning, 0,1 and 0,2. A structural damping ratio of 1,0 % is assumed.

In the case of the *RLC*-shunt, the effective modal mass is recalculated with the optimized design of the control arm, together with the piezoelectric module. To prove the effectiveness of the shunt damping technique, two different safety margins are used, 0,90 and 0,97.

Table 7.3 shows the main dynamic characteristics of the control arm, together with all optimal parameters calculated for both tuned mass dampers and *RLC*-shunts. It is important to notice that, considering the first eigenfrequency, the additional mass of either tuned mass dampers is very high compared to the 0,06 kg brought by the piezoelectric module. Furthermore, if the shunt damping solution is simultaneously designed with the structure, the optimal solution is even lighter than the original passive structure. Even if the weight of the necessary electronics and cables is taken into account, the mass balance is in favor of the shunt damping technique.

Table 7.3. Optimal characteristics of TMD and *RLC*-shunt applied to the control arm

Control arm	**Tuned mass damper**	***RLC*-shunt**	
	(r_{m} = 0,1)	**(β = 0,90)**	**(β = 0,97)**
$m = 16{,}86$ kg	$m_{\text{TMD}} = 1{,}686$ kg	$L_{\text{sh}} = 0{,}408$ H	$L_{\text{sh}} = 0{,}127$ H
$f_{\text{open}} = 62{,}98$ Hz	$k_{\text{TMD}} = 0{,}218$ kN/mm	$R_{\text{sh}} = 48{,}61\ \Omega$	$R_{\text{sh}} = 28{,}53\ \Omega$
$K_{31}^2 = 0{,}464$ %	$c_{\text{TMD}} = 203{,}6$ N·s/m	$R_1 = 0{,}886$ kΩ	$R_1 = 0{,}961$ kΩ
$C_{\text{p}} = 1{,}692$ µF	**(r_{m} = 0,2)**	$R_2 = 1{,}000$ kΩ	$R_2 = 1{,}000$ kΩ
	$m_{\text{TMD}} = 3{,}372$ kg	$\hat{R} = 6{,}695$ MΩ	$\hat{R} = 9{,}610$ MΩ
	$k_{\text{TMD}} = 0{,}366$ kN/mm	$C = 1{,}692$ µF	$C = 1{,}692$ µF
	$c_{\text{TMD}} = 463{,}2$ N·s/m		

Figure 7.10 shows the simulated responses of the control arm. The acceleration per unit force applied in the X direction is shown. The response of the original laminate without any vibration reduction measure is compared with the optimal tuned mass dampers and *RLC*-shunts.

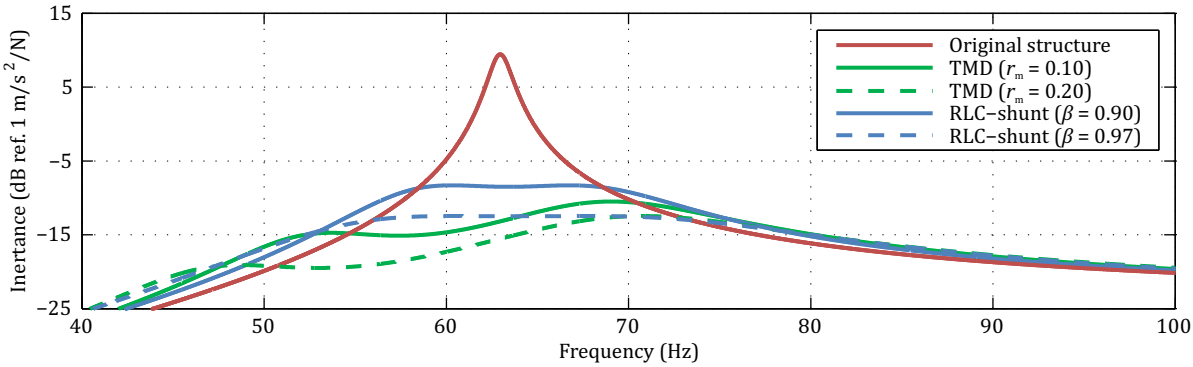

Figure 7.10. Comparison of different vibration reduction techniques in the control arm

When an optimal tuned mass damper is used, the maximum vibration reduction is equal to -19,9 dB or -21,9 dB, when the mass ratios of 0,1 and 0,2 are used, respectively. It can be noticed that the amplitude is a little unbalanced, since the analytical equations are derived for optimal displacement instead of acceleration, so a further improvement could be possible.

When the *RLC*-shunt is used together with the piezoelectric module, the optimal vibration reduction is equal to -17,7 dB or -21,9 dB, when the safety margins of 0,90 and 0,97 are used, respectively. This result shows that, even for a low GEMCC, the *RLC*-shunt is capable of strongly reducing the vibration amplitude of the control arm.

The frequency response function also highlights the benefit of the shunt technique in comparison to the classical tuned mass damper regarding the additional mass. If a low safety margin is used, a tuned mass damper with a low mass ratio shows better vibration attenuation, but an additional mass is anyway necessary. If a high safety margin is used, only a tuned mass damper with a high mass ratio is capable of attaining the same vibration attenuation.

In terms of practical feasibility of the *RLC*-shunt technique, the generated voltage in the circuit is extremely important, since it dictates the power consumption and therefore the size of components and ultimately the weight. In the simulated scenarios, the output voltage in the op-amp has been calculated. A value of 12,4 V per unit force has been calculated in the case of β = 0,90, and 14,5 V when β = 0,97. Thanks to the layered characteristic of the module and to the increased capacitance, the generated voltage is low and low-voltage electronics can be used in the case of vehicle implementation. Moreover, these values also show the advantage of choosing the working point of the negative capacitance far away from the stability limit, where a lower voltage is necessary but the vibration attenuation is still considerably high.

7.5 Conclusions

In this final chapter, a technical application of the methods developed previously has been investigated. A carbon fiber control arm has been redesigned using the simultaneous design approach and piezoceramic transducers. Additionally, the main contribution of this chapter was the development of a fiber-reinforced piezoelectric module, which consists of alternated composite and active materials. This allowed the integration of the transducers in the design process and the final application of the shunt damping technique to this complex-shaped structure.

Moreover, the effectiveness of this new smart design has been compared to a classical vibration suppression measure. It has been shown that the piezoelectric module, together with an *RLC*-shunt, is able to attenuate the mechanical response of the control arm as efficiently as a tuned mass damper. However, the additional weight brought by the tuned mass damper is much higher than the piezoelectric module and, if simultaneously designed, the smart structure can be even lighter than the original structure. Considering both host structure and piezoceramic transducers early in the design process also allows finding a better compromise between absolute weight and static stiffness. Finally, the mass reduction is followed by a further advantage that the structure now has an integrated function.

8 Summary and conclusions

This thesis has investigated shunted piezoceramics applied to composite structures and has shown the implications for their optimal design. Within the scope of vibration reduction, the work was targeted at embedded transducers and a resonant negative capacitance circuit. After an overview of the state-of-the-art techniques, the fundamentals of piezoelectric shunt damping have been presented. Then, the modeling and optimization techniques have been described.

In the first main part, a thorough analysis of the physical integration of piezoceramic transducers in FRPs has been conducted. The effectiveness of embedded piezoceramics has been evaluated through test coupons in regard to their longitudinal extensional vibration. Different integration patterns have been conceived for two types of materials, glass and carbon fiber. Numerical analyses using a finite element model have shown that the generalized electromechanical coupling coefficient (GEMCC) was present, as desirable for shunt damping applications, and that it is possible to maximize its value by changing the composite stacking sequence. The coupons have been then manufactured using DuraAct patch transducers. Experimental analyses have allowed a comparison with the numerical models and an evaluation of the importance of the integration pattern in the GEMCC. Tests have shown that the numerical model can be fitted to the experimental results, although a correction coefficient might be necessary for the coupling coefficient. This is mainly explained by the so-called shear lag effect, which results from the finite stiffness of the bonding between transducer and epoxy resin. Even though the coupling coefficient had been maximized in the simulation of the carbon fiber coupon, a large difference was not observed in comparison to non-optimized glass fiber coupons, so the applicability of this method can be questioned. Finally, a measurement has confirmed the lower strain level in the composite where the piezoceramic is integrated, which proves the load carrying role of the piezoceramic.

The second core part of this thesis has brought the integration of piezoceramics to the next level: The integration in the design process. The main contribution here was to develop and validate a new methodology to optimize the composite structure, the piezoceramic transducers and the shunt circuit in one single loop. Initially, a set of technical requirements has been defined based on a scale model of a control arm. Prior to the actual simultaneous optimization, the initial structure has been designed according to the traditional serial approach. This has allowed an experimental validation using a first prototype, in order to update the numerical model and verify the characteristics of the shunt circuit. Nonetheless, the classical approach alone was not capable of designing a smart structure that meets all the requirements at the same time. It has been suggested that the use of embedded instead of surface-bonded transducers could help to meet the requirements. In the simultaneous optimization, when designing the structure with the piezoceramics, the structure itself is compelled to have a lower stiffness than the requirement, but when the optimal piezoceramics are considered, the total stiffness attains the desired value. An optimization has been carried out with the novel design approach using a smart carbon fiber I-beam. During this phase, its mass, static and dynamic behaviors, the electromechanical coupling and electrical characteristics are among the main technical requirements. For the host structure, the stacking sequence and the part geometry are the main design variables, whereas for the transducers, its dimensions are crucial. To perform vibration reduction, a special attention was given to the *RLC*-shunt with a negative capacitance. The individual components of the shunt circuit are chosen not only to minimize the vibration amplitude, but also to respect the voltage limit across the op-amp. Even though the real

excitation spectrum was unknown, which is required for an accurate design, simulations have shown that the safety margin is a good instrument to reduce the maximum output voltage, to the detriment of vibration attenuation. The smart structure was manufactured, but the measured electromechanical coupling coefficient was not as high as expected. This can be mainly explained by the manufacturing process and the shear lag effect. Moreover, the measured inherent resistance of the piezoceramics was higher than expected, so the maximum damping predicted by the simulation could not be performed. Nevertheless, vibration attenuation and tuning with the negative capacitance have been successfully achieved.

In the third part, a novel tuning method for shunt damping has been proposed. It is based on the measured electromechanical impedance of the smart structure, which is represented through an equivalent electrical. The shunt circuit is then connected to the electrical network. Since the structure is represented in the electrical domain, the Norton equivalent impedance is obtained at the terminals that represent a mechanical mode of interest. Finally, the shunt circuit is numerically optimized by minimizing this equivalent impedance. Experimental results have shown that this method is very effective, especially with systems with high modal density. Moreover, it can be applied to arbitrary structures without the need of complicated mechanical tests. In the case of a single-mode vibration, the new method slightly outperformed the classical analytical method, which may not justify the high optimization effort. Nevertheless, the greatest advantage of this new technique is the integration of a real negative capacitance circuit that takes into account all the components in the circuit.

In the last part, the developed methods have been applied to a realistic case study of a carbon fiber control arm. The original laminate has been numerically investigated in order to identify its static stiffness and transmissibility. A modal analysis has allowed the shape identification of the most relevant eigenfrequencies. Vibration attenuation for this complex-shaped structure revealed to be a great challenge, which led to the development of the fiber-reinforced piezoelectric module. It consists of a layered patch with alternated composite material and thin piezoceramic plates. Once applied to a mechanical structure, it improves the coupling coefficient and facilitates the application of shunt damping techniques. The control arm has been then redesigned with the piezoelectric module. This allowed reducing the number of layers of the laminate and optimizing the stacking sequence, so as to maintain the static stiffness of the original part, which also represented a mass saving: The final structure was 7 % lighter than the original control arm, with the further advantage that this configuration allows smart functionalities. Finally, the effectiveness of this new design has been compared to a classical tuned mass damper, which adds much more weight to the structure for the same vibration attenuation. These final results indicate that laminate composites, combined with embedded transducers, offer state-of-the-art design possibilities that can significantly improve vibration behavior and simultaneously reduce structural weight.

9 Outlook

The approach presented in this work has tried to exploit the numerous advantages brought by shunted piezoceramics in lightweight composites. Some of the ideas could only be validated using academic examples, but for others, the conclusions remain unambiguous. Most importantly, these are significant results that serve as base for further investigations. The next steps of this research could hence concentrate on the following topics to encourage the successful use of smart structures and shunt damping techniques in commercial applications.

Since the coupling between the transducer and the composite structure is made through an elastic interlayer, the GEMCC is reduced. The stiffness coefficient factor used in this study was not enough to predict its value in the simulation. A possible improvement would be to take into account the shear lag effect, which is a non-uniform bonding over the surface of the transducers.

In spite of the extensive investigation of different integration patterns, the risk of delamination when the ply is discontinuous is real. The numerical simulations have given initial clues about the static strength of the different coupons. Nevertheless, a durability study still has to be carried out to assess the lifetime of the composite material under cyclic mechanical loads. Moreover, given the new function of the piezoceramics as a load carrying element, its durability also has to be examined.

It has been discovered in the experimental analyses that the inherent resistance of the piezoceramics plays a major role in defining the optimality of the shunt circuit afterwards. At present, no technique has been used to predict this value in the simulations. If it would be available during the simultaneous optimization, a more accurate damping could be calculated, together with the real component values and the maximum output voltage of the op-amp.

Further improvements could also include other important technical requirements in the optimization loop, such as the maximum power dissipation in the op-amp and the maximum electric field in the piezoceramics when the maximum mechanical load is applied. For this, however, a more complete model of the op-amp would be required, using e.g. SPICE, so that its output current can be correctly calculated. Nevertheless, precaution must be taken and simulation results must be experimentally validated. Furthermore, the real spectrum of the excitation force applied to the smart structure must be evaluated prior to the design. This usually requires expensive tests that are only carried out later in the design process.

Moreover, the simultaneous optimization could be implemented using other techniques. Instead of using the design of experiment approach to perform a parametric optimization, a full or reduced analytical model of the host structure could be used. In this case, a multiple degree of freedom system could also be envisaged. Besides, other objects of study can be investigated and optimized using similar modeling techniques as the ones presented in this study. This can include the use of other types of actuators such as piezoceramic stacks or different shunt circuits such as the gyrator, the high-voltage negative capacitance or even switching techniques. In addition, not only shunt damping techniques can be aimed at, but also energy harvesting, vibration isolation and precision control. The results provided here broaden the horizon of smart structures, which can reduce the weight of mobile systems, improve comfort and ultimately enhance energy efficiency.

Bibliography

[1] I. Chopra and J. Sirohi, Smart Structures Theory, 1st. ed., Cambridge University Press, 2014.

[2] T. Tanimoto, "A new vibration damping CFRP material with interlayers of dispersed piezoelectric ceramic particles," *Composites Science and Technology,* vol. 67, no. 2, p. 213–221, 2007.

[3] R. I. Wright and M. R. F. Kidner, "Vibration Absorbers: A Review of Applications in Interior Noise Control of Propeller Aircraft," *Journal of Vibration and Control,* vol. 10, no. 8, 2004.

[4] A. Preumont, Vibration Control of Active Structures, An Introduction, Springer, 2011.

[5] N. W. Hagood and A. von Flotow, "Damping of structural vibrations with piezoelectric materials and passive electrical networks," *Journal of Sound and Vibration,* vol. 146, no. 2, pp. 243-268, 22 April 1991.

[6] S. Behrens, A. J. Fleming and S. O. R. Moheimani, "A broadband controller for shunt piezoelectric damping of structural vibration," *Smart Materials and Structures,* vol. 12, p. 18–28, 2003.

[7] S.-M. Kim, S. Wang and M. J. Brennan, "Dynamic analysis and optimal design of a passive and an active piezo-electrical dynamic vibration absorber," *Journal of Sound and Vibration,* vol. 330, no. 4, p. 603–614, 2011.

[8] B. de Marneffe and A. Preumont, "Vibration damping with negative capacitance shunts: theory and experiment," *Smart Materials and Structures,* vol. 17, 2008.

[9] B. Beck and N. Schiller, "Experimental Comparison of two Active Vibration Control Approaches: Velocity Feedback and Negative Capacitance Shunt Damping," in *Noise-Con*, Denver, CO, USA, 2013.

[10] J. J. Hollkamp, "Multimodal Passive Vibration Suppression with Piezoelectric Materials and Resonant Shunts," *Journal of Intelligent Material Systems and Structures,* vol. 5, January 1994.

[11] R. L. Forward, "Electronic damping of vibrations in optical structures," *Applied Optics,* vol. 18, no. 5, pp. 690-697, 1979.

[12] D. Niederberger, "Smart Damping Materials using Shunt Control," *Ph.D. dissertation, ETH Zürich,* 2005.

[13] M. Neubauer, R. Oleskiewicz, K. Popp and T. Krzyzynski, "Optimization of damping and absorbing performance of shunted piezo elements utilizing negative capacitance," *Journal of Sound and Vibration,* vol. 298, no. 1–2, pp. 84-107, 22 November 2006.

[14] M. Neubauer and J. Wallaschek, "Vibration damping with shunted piezoceramics: Fundamentals and technical applications," *Mechanical Systems and Signal Processing,* vol. 36, no. 1, pp. 36-52, March 2013.

[15] A. J. Fleming and S. O. R. Moheimani, "Adaptive piezoelectric shunt damping," *Smart Materials and Structures,* vol. 12, p. 36–48, 2003.

[16] J.-Y. Jeon, "Passive vibration damping enhancement of piezoelectric shunt damping system using optimization approach," *Journal of Mechanical Science and Technology,* vol. 23, pp. 1435-1445, 2009.

[17] I. Giorgio, A. Culla and D. Del Vescovo, "Multimode vibration control using several piezoelectric transducers shunted with a multiterminal network," *Archive of Applied Mechanics,* vol. 79, no. 9, 2009.

[18] R. L. Forward, "Electromechanical transducer-coupled mechanical structure with negative capacitance compensation circuit". Patent US 4158787 A, 1979.

[19] J. Tang and K. W. Wang, "Active-passive hybrid piezoelectric networks for vibration control: comparisons and improvement," *Smart Materials and Structures,* vol. 10, no. 4, pp. 794-806, 2001.

[20] C. H. Park and A. Baz, "Vibration Control of Beams with Negative Capacitive Shunting of Interdigital Electrode Piezoceramics," *Journal of Vibration and Control,* vol. 11, no. 3, pp. 331-346, 2005.

[21] M. Neubauer, R. Oleskiewicz and K. Popp, "Comparison of Damping Performance of Tuned Mass Dampers and Shunted Piezo Elements," *Proceedings in Applied Mathematics and Mechanics,* vol. 5, p. 117–118, 2005.

[22] E. Fukada, M. Date, K. Kimura, T. Okubo, H. Kodama, P. Mokry and K. Yamamoto, "Sound isolation by piezoelectric polymer films connected to negative capacitance circuits," *IEEE Transactions on Dielectrics and Electrical Insulation,* vol. 11, no. 2, pp. 328-332, April 2004.

[23] O. O. Lazarev, K. V. Ogorodnik, R. Y. Chehmestruk and M. A. Filyniuk., "Investigation of circuit implementations of C-negatrons on the basis of negative-resistance converters," *Radioelectronics and Radioelectronic Equipment Design,* no. 4, 2011.

[24] S. Manzoni, S. Moschini, M. Redaelli and M. Vanali, "Vibration attenuation by means of piezoelectric transducer shunted to synthetic negative capacitance," *Journal of Sound and Vibration,* vol. 331, no. 21, pp. 4644-4657, 8 October 2012.

[25] B. S. Beck, "Negative capacitance shunting of piezoelectric patches for vibration control of continuous systems," *Ph.D. dissertation, Georgia Institute of Technology,* 2012.

[26] B. S. Beck, K. A. Cunefare and M. Collet, "Response-based tuning of a negative capacitance shunt for vibration control," *Journal of Intelligent Material Systems and Structures,* 7 November 2013 .

[27] B. S. Beck, K. A. Cunefare and M. Collet, "The power output and efficiency of a negative capacitance shunt for vibration control of a flexural system," *Smart Materials and Structures,* vol. 22, no. 6, 2013.

[28] M. Pohl , "Negative capacitance shunt damping system with optimized characteristics for use with piezoelectric transducers," in *SPIE*, San Diego, California, USA, 2014.

[29] N. W. Hagood and E. F. Crawley, "Experimental investigation into passive damping enhancement for space structures," *Journal of Guidance, Control, and Dynamics,* vol. 14, no. 6, 1991.

[30] B. Seba, J. Ni and B. Lohmann, "Vibration attenuation using a piezoelectric shunt circuit based on finite element method analysis," *Smart Materials and Structures,* vol. 15, no. 2, 2006.

[31] B. Mokrani, R. Bastaits, M. Horodinca, I. Romanescu, I. Burda, R. Viguié and A. Preumont, "Parallel Piezoelectric Shunt Damping of Rotationally Periodic Structures," *Advances in Materials Science and Engineering,* 2015.

[32] S. Raja, G. Prathap and P. K. Sinha, "Active vibration control of composite sandwich beams with piezoelectric extension-bending and shear actuators," *Smart Materials and Structures,* vol. 11, no. 1, 2002.

[33] A. Schubert, V. Wittstock, H.-J. Koriath, S. F. Jahn, S. Peter, B. Müller and M. Müller, "Smart metal sheets by direct functional integration of piezoceramic fibers in microformed structures," *Microsystem Technologies,* vol. 20, no. 6, pp. 1131-1140, 2014.

[34] E. F. Crawley and J. de Luis, "Use of Piezoelectric Actuators as Elements of Intelligent Structures," *AIAA Journal,* vol. 25, no. 10, 1987.

[35] V. Krajenski, G. Mook, H. Hanselka, T. Melz, P. Wierach and D. Sachau, "Active Composites with Integrated Piezoceramics," in *European Conference on Spacecraft Structures, Materials and Mechanical Testing*, Braunschweig, Germany, 1999.

[36] J. K. Dürr, U. Herold-Schmidt, H. W. Zaglauer and F. J. Arendts, "On the Integration of Piezoceramic Actuators in Composite Structures for Aerospace Applications," *Journal of Intelligent Material Systems and Structures,* vol. 10, no. 11, 1999.

[37] J. P. Hansen and A. J. Vizzini, "Fatigue Response of a Host Structure with Interlaced Embedded Devices," *Journal of Intelligent Material Systems and Structures,* vol. 11, no. 11, pp. 902-909, 2000.

[38] S. Mall, "Integrity of graphite/epoxy laminate embedded with piezoelectric sensor/actuator under monotonic and fatigue loads," *Smart Materials and Structures,* vol. 11, no. 4, 2002.

[39] M. Lin and F.-K. Chang, "The manufacture of composite structures with a built-in network of piezoceramics," *Composites Science and Technology,* vol. 62, no. 7-8, p. 919–939, 2002.

[40] K. Wu, A. Schwinn and H. Janocha, "Active Vibration Control Using Embedded Piezoceramics as both Actuators and Sensors," in *European Conference on Noise Control Euronoise*, Naples, Italy, 2003.

[41] P. Konstanzer, M. Grünewald, P. Jänker and S. Storm, "Piezo tunable vibration absorber system for aircraft interior noise reduction," in *European Conference on Noise Control Euronoise*, Tampere, Finland, 2006.

[42] P. Konstanzer, P. Jänker and S. Storm, "A piezo inertial force generator optimized for high force and low frequency," *Smart Materials and Structures,* vol. 16, no. 4, 2007.

[43] Y. K. Yong and A. J. Fleming, "Piezoelectric Actuators With Integrated High-Voltage Power Electronics," *IEEE/ASME Transactions on Mechatronics,* vol. 20, no. 2, 2015.

[44] K. B. Lazarus, M. E. Lundstrom, J. W. Moore and E. F. Crawley, "Packaged strain actuator". Patent US 5656882 A, 1997.

[45] P. Wierach, "Electromechanical functional module and associated process". Patent US 6930439 B2, 2005.

[46] P. Wierach, "Entwicklung Multifunktionaler Werkstoffsysteme mit piezokeramischen Folien im Leitprojekt Adaptronik," in *Adaptronic Congress*, Wolfsburg, Germany, 2003.

[47] P. Wierach and A. Schönecker, "Bauweisen und Anwendungen von Piezokompositen in der Adaptronik," in *Adaptronic Congress*, Göttingen, Germany, 2005.

[48] W. Hufenbach, M. Gude and T. Heber, "Embedding versus adhesive bonding of adapted piezoceramic modules for function-integrative thermoplastic composite structures," *Composites Science and Technology,* vol. 71, no. 8, p. 1132–1137, 2011.

[49] W. A. Hufenbach, N. Modler, A. Winkler, J. Ilg and S. J. Rupitsch, "Fibre-reinforced composite structures based on thermoplastic matrices with embedded piezoceramic modules," *Smart Materials and Structures,* vol. 23, no. 2, 2014.

[50] A. Weder, S. Geller, A. Heinig, T. Tyczynski, W. Hufenbach and W.-J. Fischer, "Integration of Piezoceramic Sensor Elements and Electronic Components in Glass Fibre Reinforced Polyurethane Composite Structures," *Procedia Engineering,* vol. 47, 2012.

[51] F. Bachmann, "Integration of Monolithic Piezoelectric Damping Devices into Adaptive Composite Structures," *Ph.D. dissertation, ETH Zürich,* 2012.

[52] T. Delpero, "Design of adaptive structures with piezoelectric materials," *Ph.D. dissertation, ETH Zürich,* 2014.

[53] V. Gupta, M. Sharma and N. Thakur, "Optimization Criteria for Optimal Placement of Piezoelectric Sensors and Actuators on a Smart Structure: A Technical Review," *Journal of Intelligent Material Systems and Structures,* vol. 21, no. 12, 2010.

[54] G. A. Lesieutre, G. K. Ottman and H. F. Hofmann, "Damping as a result of piezoelectric energy harvesting," *Journal of Sound and Vibration,* vol. 269, no. 3–5, pp. 991-1001, 22 January 2004.

[55] T. Bein, J. Bös, S. Herold, D. Mayer, T. Melz and M. Thomaier, "Smart interfaces and semi-active vibration absorber for noise reduction in vehicle structures," *Aerospace Science and Technology,* vol. 12, no. 1, 2008.

[56] T. C. de Godoy and M. A. Trindade, "Modeling and analysis of laminate composite plates with embedded active-passive piezoelectric networks," *Journal of Sound and Vibration,* vol. 330, 2011.

[57] J. Ducarne, O. Thomas and J.-F. Deü, "Placement and dimension optimization of shunted piezoelectric patches for vibration reduction," *Journal of Sound and Vibration,* vol. 331, no. 14, 2012.

[58] M. A. Trindade and A. Benjeddou, "Parametric analysis of effective material properties of thickness-shear piezoelectric macro-fibre composites," *J. Braz. Soc. Mech. Sci. & Eng.,* vol. 34, 2012.

[59] A. L. Araújo, J. F. A. Madeira, C. M. M. Soares and C. A. M. Soares, "Optimal design for active damping in sandwich structures using the Direct MultiSearch method," *Composite Structures,* vol. 105, 2013.

[60] M. Neubauer, "Optimal design of piezoelectric actuators for shunt damping techniques," *Archives of Acoustics,* vol. 39, no. 4, 2014.

[61] T. Delpero, A. Bergamini and P. Ermanni, "Concurrent Design of Adaptively Damped Structures," in *International Conference on Adaptive Structures and Technologies, ICAST*, The Hague, The Netherlands, 2014.

[62] M. I. Frecker, "Recent advances in optimization of smart structures and actuators," *Journal of Intelligent Material Systems and Structures,* vol. 14, pp. 207-216, 2003.

[63] D. S. Bodden and J. L. Junkins, "Eigenvalue optimization algorithms for structure/controller design iterations," *Journal of Guidance, Control, and Dynamics,* vol. 8, no. 6, 1985.

[64] W.-S. Hwang and H. C. Park, "Finite element modeling of piezoelectric sensors and actuators," *AIAA Journal,* vol. 31, no. 5, 1993.

[65] X. Liu and D. W. Begg, "On simultaneous optimisation of smart structures – Part I: Theory," *Computer Methods in Applied Mechanics and Engineering,* vol. 184, no. 1, 2000.

[66] D. W. Begg and X. Liu, "On simultaneous optimization of smart structures – Part II: Algorithms and examples," *Computer Methods in Applied Mechanics and Engineering,* vol. 184, no. 1, 2000.

[67] M. J. Buehler, B. Bettig and G. G. Parker, "Topology Optimization of Smart Structures Using a Homogenization Approach," *Journal of Intelligent Material Systems and Structures,* vol. 15, August 2004.

[68] M. Kögl and E. C. N. Silva, "Topology optimization of smart structures: design of piezoelectric plate and shell actuators," *Smart Materials and Structures,* vol. 14, no. 2, 2005.

[69] Z. Kang and X. Wang, "Topology optimization of bending actuators with multilayer piezoelectric material," *Smart Materials and Structures,* vol. 19, no. 7, 2010.

[70] J. Y. Noh and G. H. Yoon, "Topology optimization of piezoelectric energy harvesting devices considering static and harmonic dynamic loads," *Advances in Engineering Software,* vol. 53, 2012.

[71] J. M. S. Moita, V. M. F. Correia, P. G. Martins, C. M. M. Soares and C. A. M. Soares, "Optimal design in vibration control of adaptive structures using a simulated annealing algorithm," *Composite Structures,* vol. 75, no. 1-4, 2006.

[72] B. Xu, J. P. Ou and J. S. Jiang, "Integrated optimization of structural topology and control for piezoelectric smart plate based on genetic algorithm," *Finite Elements in Analysis and Design,* vol. 64, pp. 1-12, February 2013.

[73] B. Besselink, U. Tabak, A. Lutowska, N. van de Wouw, H. Nijmeijer, D. J. Rixen, M. E. Hochstenbach and W. H. A. Schilders, "A comparison of model reduction techniques from structural dynamics, numerical mathematics and systems and control," *Journal of Sound and Vibration,* vol. 332, no. 19, 2013.

[74] Y. Zhu, J. Qiu, J. Tani, Y. Urushiyama and Y. Hontani, "Simultaneous Optimization of Structure and Control for Vibration Suppression," *Journal of Vibration and Acoustics,* vol. 121, 1999.

[75] W. P. Li and H. Huang, "Integrated optimization of actuator placement and vibration control for piezoelectric adaptive trusses," *Journal of Sound and Vibration,* vol. 332, no. 1, 2013.

[76] J. He and X. Chen, "Integrated Topology Optimization of Structure/Vibration Control for Piezoelectric Cylindrical Shell Based on the Genetic Algorithm," *Shock and Vibration,* 2015.

[77] G. Genta and L. Morello, "Comfort Performance," in *The Automotive Chassis Volume 2: System Design*, Springer, 2009.

[78] H. Janocha, Adaptronics and Smart Structures – Basics, Materials, Design and Applications, Springer, 2007.

[79] W. D. Callister Jr., Fundamentals of Materials Science and Engineering, John Wiley & Sons, Inc., 2001.

[80] K. Friedrich and A. A. Almajid, "Manufacturing Aspects of Advanced Polymer Composites for Automotive Applications," *Applied Composite Materials,* vol. 20, no. 2, pp. 107-128, 2013.

[81] S. K. Mazumdar, Composites Manufacturing - Materials, Product, and Process Engineering, CRC Press, 2002.

[82] Hexcel, "HexPly® Prepreg Technology," 2013.

[83] R. M. Jones, Mechanics of composite materials, CRC Press, 1999.

[84] A. Puck and H. Schürmann, "Failure analysis of FRP laminates by means of physically based phenomenological models," *Composites Science and Technology,* vol. 58, 1998.

[85] A. Puck and H. Schürmann, "Failure analysis of FRP laminates by means of physically based phenomenological models," *Composites Science and Technology,* vol. 62, no. 12-13, pp. 1633-1662, 2002.

[86] J. Degrieck and W. V. Paepegem, "Fatigue damage modeling of fibre-reinforced composite materials: Review," *Applied Mechanics Reviews,* vol. 54, no. 4, 2001.

[87] *IEEE Standard on Piezoelectricity,* ANSI/IEEE Std 176-1987.

[88] S. R. Moheimani and A. J. Fleming, Piezoelectric Transducers for Vibration Control and Damping, Springer, 2006.

[89] Physik Instrumente GmbH, "Piezoelectrics in Positioning, Tutorial on Piezotechnology in Nanopositioning Applications," 2008.

[90] B. de Marneffe, "Active and Passive Vibration Isolation and Damping via Shunted Transducers," *Ph.D. dissertation, Université Libre de Bruxelles,* 2007.

[91] S. Sherrit, H. D. Wiederick, B. K. Mukherjee and M. Sayer, "An accurate equivalent circuit for the unloaded piezoelectric vibrator in the thickness mode," *Journal of Physics D: Applied Physics,* vol. 30, no. 16, 1997.

[92] J. Kim, B. L. Grisso, J. K. Kim, D. S. Ha and D. J. Inman, "Electrical Modeling of Piezoelectric Ceramics for Analysis and Evaluation of Sensory Systems," in *IEEE Sensors Applications Symposium*, 2008.

[93] G. Genta, Vibration Dynamic and Control, Springer, 2009, pp. 263-320.

[94] C. H. Park, "On the Circuit Model of Piezoceramics," *Journal of Intelligent Material Systems and Structures,* vol. 12, no. 7, pp. 515-522, 2001.

[95] M. Guan and W.-H. Liao, "Studies on the circuit models of piezoelectric ceramics," in *Proceedings of International Conference on Information Acquisition*, 2004.

[96] A. Preumont, Mechatronics - Dynamics of Electromechanical and Piezoelectric Systems, Springer, 2006.

[97] A. J. Fleming, S. Behrens and S. O. R. Moheimani, "Synthetic impedance for implementation of piezoelectric shunt-damping circuits," *Electronics Letters,* vol. 36, no. 18, 2000.

[98] C. L. Davis and G. A. Lesieutre, "An Actively Tuned Solid-State Vibration Absorber Using Capacitive Shunting of Piezoelectric Stiffness," *Journal of Sound and Vibration,* vol. 232, no. 3, pp. 601-617, 2000.

[99] M. Date, M. Kutani and S. Sakai, "Electrically controlled elasticity utilizing piezoelectric coupling," *Journal of Applied Physics,* vol. 87, no. 2, 2000.

[100] B. K. Jones, J. Santana and M. McPherson, "Negative capacitance effects in semiconductor diodes," *Solid State Communications,* vol. 107, no. 2, p. 47–50, 1998.

[101] D. H. Sheingold, "Impedance & Admittance Transformations using Operational Amplifiers," *The Lightning Empiricist,* vol. 12, no. 1, 1964.

[102] George A. Philbrick Researches, Inc., Applications Manual for Computing Amplifiers for Modeling, Measuring, Manipulating & Much Else, 1966, p. 97.

[103] Texas Instruments Inc., "A Comprehensive Study of the Howland Current Pump (AN1515)," 2013.

[104] G. Gonzalez, "Theory of Oscillators," in *Foundations of Oscillator Circuit Design*, Artech House, 2006.

[105] P. Horowitz and W. Hill, The Art of Electronics, 2. ed., Cambridge University Press, 1989, pp. 175-262.

[106] Texas Instruments Inc., "Understanding Op Amp Parameters," in *Op Amps for Everyone*, 2002.

[107] Microchip Technology Inc., "Driving Capacitive Loads With Op Amps (AN884)," 2008.

[108] Apex Microtechnology Inc., "Driving Capacitive Loads (AN25)," 2012.

[109] Apex Microtechnology Inc., "Optimizing Output Power (AN08)," 2012.

[110] Apex Microtechnology Inc., "General Operating Considerations (AN01)," 2012.

[111] Texas Instruments Inc., "Stability Analysis of Voltage-Feedback Op Amps (SLOA020A)," 2001.

[112] Apex Microtechnology Inc., "Stability for Power Operational Amplifiers (AN19)," 2013.

[113] J.-Y. Plesseria , P. Rochus and J. M. Defise, "Effective modal masses," in *5éme Congrès National de Mécanique Théorique et Appliquée*, Louvain-la-Neuve, Belgium, 2000.

[114] C. Kyriazoglou and F. Guild, "Finite element prediction of damping of composite GFRP and CFRP laminates – a hybrid formulation – vibration damping experiments and Rayleigh damping," *Composites Science and Technology,* vol. 67, no. 11–12, pp. 2643-2654, September 2007.

[115] B. Wu, "A correction of the half-power bandwidth method for estimating damping," *Archive of Applied Mechanics,* vol. 85, no. 2, pp. 315-320, 2015.

[116] R. Oleskiewicz, M. Neubauer, T. Krzyzynski and K. Popp, "Synthetic Impedance Circuits in Semi-Passive Vibration Control with Piezo-Ceramics - Efficiency and Limitations," *Proceedings in Applied Mathematics and Mechanics,* vol. 5, no. 1, pp. 121-122, 2005.

[117] S. Leary, A. Bhaskar and A. Keane, "Optimal orthogonal-array-based latin hypercubes," *Journal of Applied Statistics,* vol. 30, no. 5, 2003.

[118] W. Härdle, Applied Nonparametric Regression, Cambridge University Press, 1992.

[119] A. Gosavi, "Parametric Optimization: Response Surfaces and Neural Networks," in *Simulation-Based Optimization*, 2003.

[120] A. Konak, D. W. Coit and A. E. Smith, "Multi-objective optimization using genetic algorithms: A tutorial," *Reliability Engineering & System Safety,* vol. 91, no. 9, 2006.

[121] R. Messer, "Integration of piezoelectric actuators inside composite structures," *Master's thesis, Technische Universität Darmstadt,* 2015.

[122] N. Jalili, Piezoelectric-Based Vibration Control, Springer, 2010.

[123] I. Kido and S. Ueyama, "Coupled Vibration Analysis of Tire and Wheel for Road Noise Improvement," *SAE Technical Paper 2005-01-2525,* 2005.

[124] F. Min, W. Wen, L. Zhao, X. Yu and J. Xu, "Shimmy Identification Caused by Self-Excitation Components at Vehicle High Speed," in *FISITA World Automotive Congress*, Beijing, China, 2012.

[125] T. Bein, "The ENLIGHT Project - Enhanced Lightweight Design," 2013. [Online]. Available: http://www.project-enlight.eu/.

[126] J. W. Meschke, "The ALIVE Project - Advanced High Volume Affordable Lightweighting for Future Electric Vehicles," 2012. [Online]. Available: http://www.project-alive.eu/.

[127] D. Lupascu and J. Rödel, "Fatigue In Bulk Lead Zirconate Titanate Actuator Materials," *Advanced Engineering Materials,* vol. 7, no. 10, 2005.

[128] T. Fett, D. Munz and G. Thun, "Tensile and bending strength of piezoelectric ceramics," *Journal of Materials Science Letters,* vol. 18, no. 23, pp. 1899-1902, 1999.

[129] F.-X. Irisarri, A. Lasseigne, F.-H. Leroy and R. Le Riche, "Optimal design of laminated composite structures with ply drops using stacking sequence tables," *Composite*

Structures, vol. 107, pp. 559-569, January 2014.

[130] Physik Instrumente GmbH, "Piezoelectric Actuators - Components, Technologies, Operation," 2014.

[131] J. Kim, Y.-H. Ryu and S.-B. Choi, "New shunting parameter tuning method for piezoelectric damping based on measured electrical impedance," *Smart Materials and Structures,* vol. 9, no. 6, 2000.

[132] G. Fox Lang and D. Snyder, "Understanding the Physics of Electrodynamic Shaker Performance," *Dynamic Testing Reference Issue, Sound and Vibration,* 2001.

[133] P. Töws, "Konstruktion und Herstellung eines Leichtbauquerlenkers aus einem Kohlenstofffaser-Epoxid-Verbund," *Master's thesis, Hochschule Darmstadt,* 2014.

[134] C. Soutis and F. Z. Hu, "Design and performance of bonded patch repairs of composite structures," *Proceedings of the Institution of Mechanical Engineers, Part G: Journal of Aerospace Engineering,* vol. 211, no. 4, 1997.

[135] S. G. Kelly, Fundamentals of Mechanical Vibrations, 2. ed., McGraw-Hill, 2000.

[136] The Association of German Engineers, *VDI-Standard: VDI 3833 Blatt 2 Dynamic damper and dynamic vibration absorber - Dynamic vibration absorber and dynamic vibration absorption,* 2006.

Own publications

Journal papers

[1] O. Heuss, R. Salloum, D. Mayer and T. Melz, “Tuning of a vibration absorber with shunted piezoelectric transducers,” *Archive of Applied Mechanics*, 2014.

Conference contributions

[2] R. Salloum, O. Heuss and D. Mayer, “Simultaneous optimization of composite structures with shunted piezoceramics,” *International Conference on Engineering Vibration ICoEV*, 2015.

[3] R. Salloum, O. Heuss, B. Götz and D. Mayer, “Optimally tuned resonant negative capacitance for piezoelectric shunt damping based on measured electromechanical impedance,” *SPIE Smart Structures*, 2015.

[4] R. Salloum, O. Heuss and D. Mayer, “Design of smart lightweight structures: Simultaneous optimization of mechanical and shunt circuit parameters,” *25th International Conference on Adaptive Structures and Technologies ICAST*, 2014.

[5] R. Salloum, O. Heuss and D. Mayer, “Global optimization of smart lightweight structures,” *International Conference on Noise and Vibration Engineering ISMA*, 2014.

[6] O. Heuss, B. Götz, R. Salloum and D. Mayer, “Technical limits of resonant shunted damping techniques for lightweight design,” *6th World Conference on Structural Control and Monitoring 6WCSCM*, 2014.

[7] R. Salloum, O. Heuss and D. Mayer, “Tuning of a Vibration Absorber with Shunted Piezoelectric Transducers,” *10th International Workshop on Piezoelectric Materials and Applications in Actuators IWPMA*, 2013.

Patents

[8] D. Mayer and R. Salloum, “Anordnung und Verfahren zur Beeinflussung und/oder Detektion einer dynamischen oder statischen Eigenschaft einer Tragstruktur,” *Deutsche Patentanmeldung 10 2015 216 846.8*, 2015.

Appendix A

RLC-shunt real circuit implementation

For the inductive part, an inductance decade (L3–250, COSINUS Messtechnik GmbH) has been used and is shown in **Figure A.1**. It provides adjustable values in the range 1 µH – 11,11111 H with an accuracy of 2,5 %.

The NIC has been built using the basic layout presented in **Figure 2.11**, where all resistors were built as adjustable potentiometers. A prototype of the NIC was built in order to allow an easy measurement of the resistances with a multimeter, as shown in **Figure A.1**. The high-voltage PAD183 op-amp from PowerAmp Design was used. It allows a maximum supply voltage V_S of ±175 V, a maximum output current of 1,5 A and power of 35 W. In order to avoid saturation, a special attention must be given to the voltage swing. In the case of the PAD183, its maximum value is equal to $\mp$10 V, i.e. when a supply voltage V_S of ±150 V is used, the maximum allowable voltage at the output terminal is equal to ±140 V, otherwise saturation occurs. This value however depends on the output current and the frequency of operation. A capacitor of value 150 pF has been externally connected for phase compensation and the resultant slew rate is equal to 15 V/µs. Finally, diodes for the protection of the op-amp and capacitors for the bypass of the power supply have been added to the design, as shown in **Figure A.2**.

Figure A.1. Inductance decade (left) and NIC prototype (right)

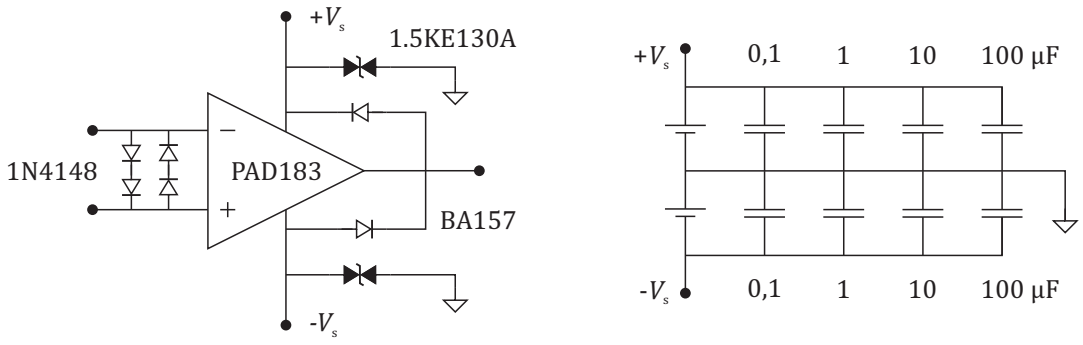

Figure A.2. Op-amp protection (left) and power supply bypass (right)

A symmetric power supply of ±150 V has been built connecting several DC/DC converters in series. The model TEN 5-1223 from TRACO Power was chosen. It has an input voltage of +12 V and an output voltage of ±15 V. It allows a maximum output current of ±200 mA, which can be sufficient for shunt damping applications. All converters have been protected in the output level with a transient voltage suppressor BZW04. The schematic layout of the symmetric power supply can be seen in **Figure A.3** and the built prototype in **Figure A.4**.

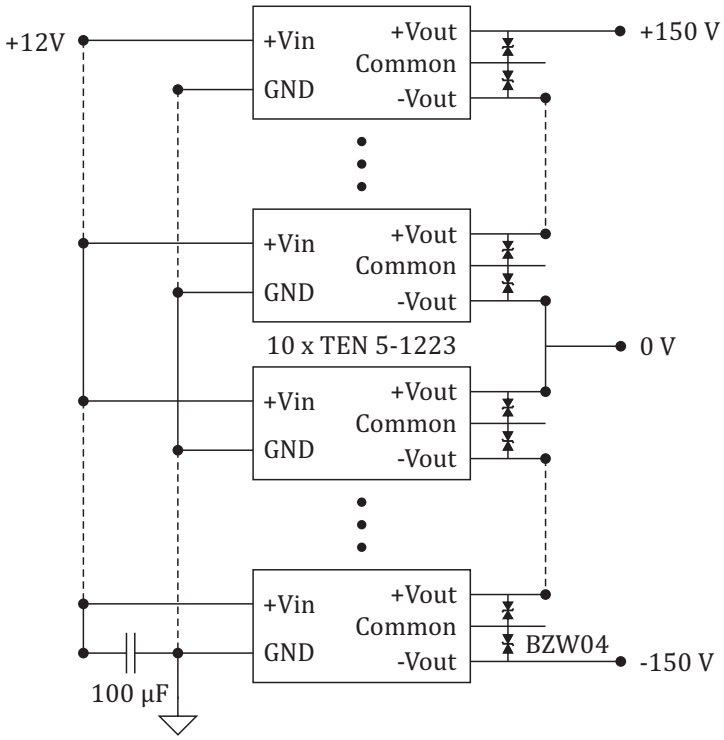

Figure A.3. High-voltage symmetric power supply: Schematic layout

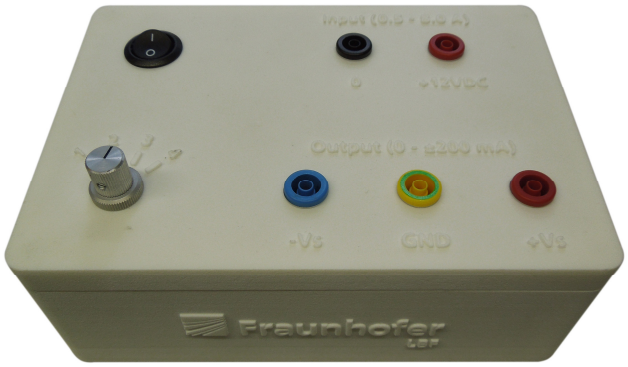

Figure A.4. High-voltage symmetric power supply: The prototype

The electrical connection of the *RLC*-shunt circuit to the piezoceramics is also important. When a NIC is used together with an inductor, it is recommendable that the piezoceramic

transducer do not be grounded and be electrically isolated from the mechanical structure, as shown in **Figure A.5**. In this case, if the electrical isolation of the piezoceramics is not sufficient, e.g. if there is a low resistance between transducer and ground, the optimality of the shunt cannot be guaranteed and even instability problems can occur. Moreover, if a gyrator is to be used instead of a real inductor, the depicted layout is mandatory, since both NIC and gyrator demand an electrical ground connection.

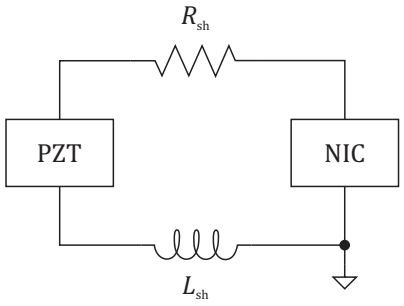

Figure A.5. Electrical connection of the *RLC*-shunt to the piezoceramics

Appendix B

Fiber-reinforced plastics material characteristics (CFRP and GFRP)

The carbon or glass fiber prepregs were supplied by the company "SGL TECHNOLOGIES GmbH". They are pre-impregnated with epoxy resin and contain unidirectional fibers in the X direction. Test coupons were manufactured using either a vacuum bag (P = 1 bar) or by hot pressing (P = 3 bars) and cured at a temperature of T = 80°C during 12 hours. The material parameters used in the finite element model were adjusted to fit the first six eigenfrequencies obtained in an experimental analysis of the coupons.

Table B.1. Fiber-reinforced plastics material characteristics

Description	CFRP	GFRP	GFRP	Unit
Manufacturing	Vacuum bag	Vacuum bag	Hot pressing	—
Fiber volume	55,0	54,5	60,0	%
Ply thickness	0,24	0,22	0,20	mm
Density	1530	1920	2000	kg/m^3
E_x	119167	40909	45843	MPa
E_y	7640	9383	11087	MPa
E_z	7640	9383	11087	MPa
ν_{xy}	0,27	0,30	0,26	—
ν_{yz}	0,42	0,40	0,40	—
ν_{xz}	0,27	0,30	0,26	—
G_{xy}	4874	4643	6233	MPa
G_{yz}	3021	3603	3846	MPa
G_{xz}	4874	4643	6233	MPa

Appendix C

Piezoelectric material characteristics (PIC151 and PIC255)

Manufacturer information (PI Ceramic GmbH): The data was determined using test bodies with geometries and dimensions in accordance with the European Standard EN 50324-2.

Table C.1. Material density

Coefficient	PIC151	PIC255	Unit
ρ	7760	7800	kg/m^3

I) Representation in compliance form:

Table C.2. Compliance matrix at constant electric field E ("short circuit")

Coefficient	PIC151	PIC255	Unit
S_{11}^E	1,683 × 10^{-11}	1,590 × 10^{-11}	m^2/N
S_{12}^E	-5,656 × 10^{-12}	-5,699 × 10^{-12}	m^2/N
S_{13}^E	-7,107 × 10^{-12}	-7,376 × 10^{-12}	m^2/N
S_{33}^E	1,900 × 10^{-11}	2,097 × 10^{-11}	m^2/N
S_{44}^E	5,096 × 10^{-11}	4,492 × 10^{-11}	m^2/N

Table C.3. Compliance matrix at constant dielectric displacement D ("open electrodes")

Coefficient	PIC151	PIC255	Unit
S_{11}^D	1,436 × 10^{-11}	1,393 × 10^{-11}	m^2/N
S_{12}^D	-8,112 × 10^{-12}	-7,660 × 10^{-12}	m^2/N
S_{13}^D	-2,250 × 10^{-12}	-2,945 × 10^{-12}	m^2/N
S_{33}^D	9,750 × 10^{-12}	1,096 × 10^{-11}	m^2/N
S_{44}^D	2,924 × 10^{-11}	2,532 × 10^{-11}	m^2/N

Table C.4. Piezoelectric strain matrix coefficients

Coefficient	PIC151	PIC255	Unit
d_{31}	-2,140 × 10^{-10}	-1,740 × 10^{-10}	m/V
d_{33}	4,230 × 10^{-10}	3,940 × 10^{-10}	m/V
d_{15}	6,100 × 10^{-10}	5,350 × 10^{-10}	m/V

Table C.5. Relative permittivity at constant mechanical stress T ("mechanically free")

Coefficient	PIC151	PIC255	Unit
ε_{11}^{T}	1936	1649	—
ε_{33}^{T}	2109	1750	—

II) Representation in stiffness form:

Table C.6. Stiffness matrix at constant electric field E ("short circuit")

Coefficient	PIC151	PIC255	Unit
C_{11}^{E}	$1{,}076 \times 10^{11}$	$1{,}230 \times 10^{11}$	N/m^2
C_{12}^{E}	$6{,}312 \times 10^{10}$	$7{,}670 \times 10^{10}$	N/m^2
C_{13}^{E}	$6{,}385 \times 10^{10}$	$7{,}025 \times 10^{10}$	N/m^2
C_{33}^{E}	$1{,}004 \times 10^{11}$	$9{,}711 \times 10^{10}$	N/m^2
C_{44}^{E}	$1{,}962 \times 10^{10}$	$2{,}226 \times 10^{10}$	N/m^2

Table C.7. Stiffness matrix at constant dielectric displacement D ("open electrodes")

Coefficient	PIC151	PIC255	Unit
C_{11}^{D}	$1{,}183 \times 10^{11}$	$1{,}298 \times 10^{11}$	N/m^2
C_{12}^{D}	$7{,}376 \times 10^{10}$	$8{,}345 \times 10^{10}$	N/m^2
C_{13}^{D}	$4{,}436 \times 10^{10}$	$5{,}729 \times 10^{10}$	N/m^2
C_{33}^{D}	$1{,}392 \times 10^{11}$	$1{,}220 \times 10^{11}$	N/m^2
C_{44}^{D}	$3{,}420 \times 10^{10}$	$3{,}949 \times 10^{10}$	N/m^2

Table C.8. Piezoelectric stress matrix coefficients

Coefficient	PIC151	PIC255	Unit
e_{31}	-9,60	-7,15	N/Vm
e_{33}	15,10	13,70	N/Vm
e_{15}	12,00	11,90	N/Vm

Table C.9. Relative permittivity at constant mechanical strain S ("mechanically clamped")

Coefficient	PIC151	PIC255	Unit
ε_{11}^{S}	1110	930	—
ε_{33}^{S}	852	857	—

Appendix D

Simultaneous *vs.* traditional design approach: Simulation results

The cross-section geometry in real scale of the optimized passive structure is depicted in **Figure D.1**. The optimized dimensions of the piezoceramics are 70 x 15 x 2,5 mm each.

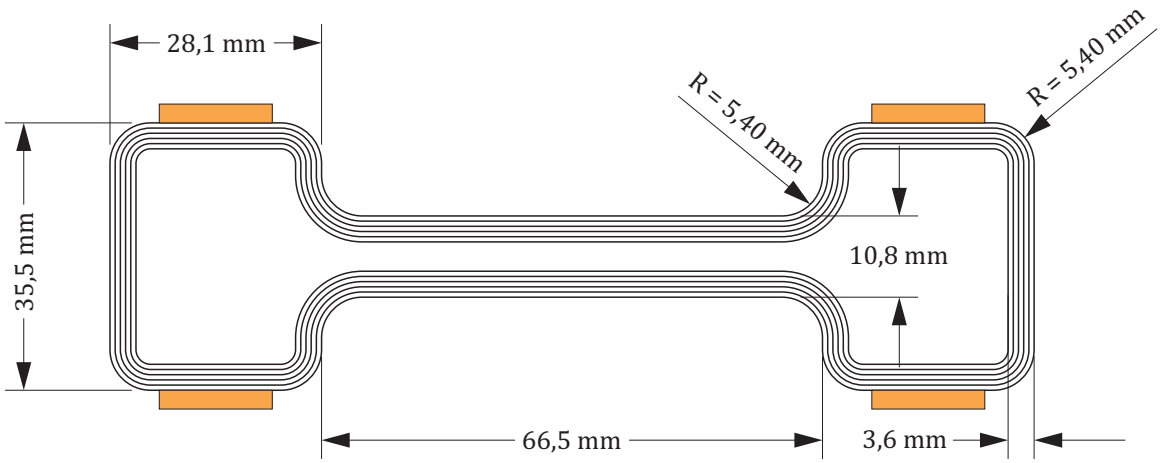

Figure D.1. Detdetailed geometry of the cross-section of the cantilever CFRP I-beam

The cross-section geometry in real scale of the optimized smart structure is depicted in **Figure D.2**. The optimized dimensions of the piezoceramics are 50 x 15 x 0,27 mm each.

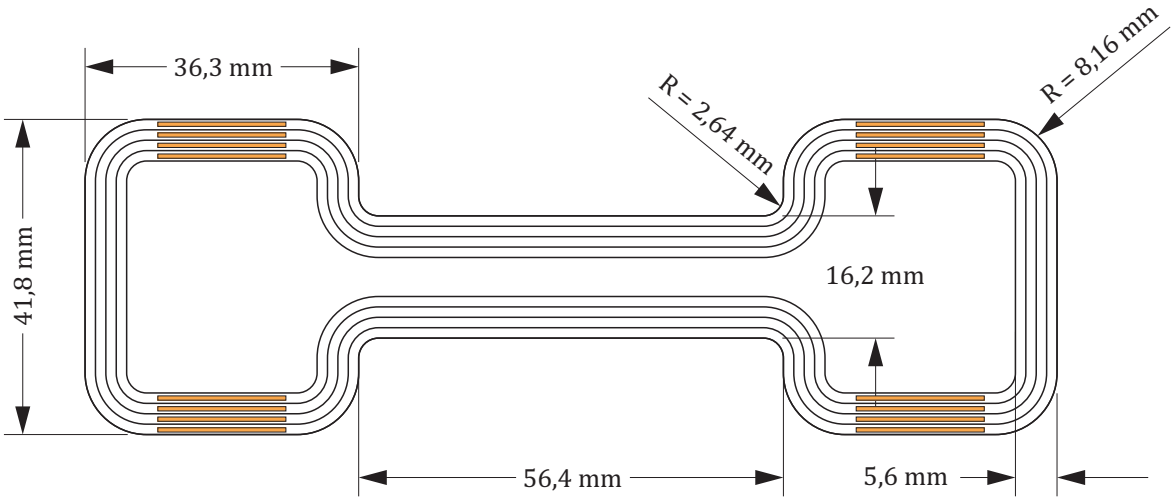

Figure D.2. Detailed geometry of the cross-section of the final smart structure

The main characteristics of the passive and smart structures, obtained with the traditional and simultaneous approach, can be seen in **Table D.1**. The *RLC*-shunt circuits that minimize the inertance response are described in **Table D.2**. The values that meet the technical requirements are marked in **green** and the ones that don't, in **red**.

Table D.1. Traditional *vs.* simultaneous design results of the smart structure

Sub-system	Description	Symbol	Traditional approach	Simultaneous approach	Unit
Passive structure	I-beam total mass	—	0,580	0,911	kg
	Stiffness	k	0,275	0,329	kN/mm
	Eigenfrequency	—	53,56	58,85	Hz
	Modal damping ratio	—	0,502	—	%
Smart structure	I-beam total mass	—	**0,661**	**0,936**	kg
	Effective modal mass	m	1,999	2,167	kg
	Stiffness	$k + k_{\mathrm{p}}$	**0,330**	**0,377**	kN/mm
	S.C. eigenfrequency	f_{short}	62,08	62,90	Hz
	O.C. eigenfrequency	f_{open}	62,52	63,50	Hz
	Coupling coefficient	K_{31}^2	**1,408**	**1,914**	%
	PZT capacitance	C_{p}	36,47	565,9	nF
	PZT normal stress	T_1	**145,0**	**92,67**	MPa
	Puck reserve factor	—	**3,430**	**1,050**	—
	Modal damping ratio	ζ	0,927	0,719	%

Table D.2. Optimal *RLC*-shunt characteristics

Variable	Traditional approach	Simultaneous approach		Unit
β	0,975	1,000	0,900	—
R_{sh}	1,788	0,168	0,316	kΩ
L_{sh}	7,938	0,309	1,347	H
R_1	0,939	0,952	0,858	kΩ
R_2	1,000	1,000	1,000	kΩ
$\hat{R}$	13,46	10,00	10,00	MΩ
C	36,37	565,9	565,9	nF
$\max(V_{\mathrm{out}})$	**213,0**	**44,90**	**36,00**	V/N